REMARKS

Favorable reconsideration and allowance of the claims of the present application are respectfully requested.

Before addressing the merits of the Official Action, applicants would like to express appreciation to Examiner Shawquia Young for granting an interview conducted on March 3, 2008.

In the Official Action, Claims 13-15, 17, 20, 23, 25, 27 and 28 stand objected as allegedly containing non-elected subject matter. Moreover, Claims 27 and 28 stand rejected under 35 U.S.C. §112, first paragraph, as allegedly failing to comply with the enablement requirement.

In response, applicants have amended Claims in a manner as indicated above. Support for the amendment can be found at page 2, lines 14-26, and page 4, lines 24-28 of the specification. Since the aforesaid amendment does not introduce any new matter into the originally filed application, entry thereof is respectfully requested.

With respect to the objection on the ground of containing non-elected subject matter, applicants believe that the above-described amendment complies with the restriction requirement. Therefore, applicants submit that the instant objection has been obviated, and withdrawal of the same is respectfully requested.

Regarding the rejection to Claim 28 on the ground of lacking enablement, applicants have deleted Claim 28, without prejudice. Therefore, applicants respectfully submit that the instant rejection should be withdrawn.

As far as the rejection to Claim 27 on the ground of lacking enablement is concerned, applicants respectfully submit the specification provides sufficient support to enable a person skilled in the art to make and/or use the subject matter recited in the amended Claim 27.

Specifically, the specification describes that the malfunctioning of protein kinases (PKs) is the hallmark of numerous diseases. More specifically, the specification describes that a large share of the oncogenes and proto-oncogenes involved in human cancers code for PKs. The enhanced activities of PKs are also implicated in many non-malignant diseases such as benign prostate hyperplasia, familial adenomatosis, polyposis, neuro-fibromatosis, psoriasis, vascular smooth cell proliferation associated with atherosclerosis, pulmonary fibrosis, arthritis glomerulonephritis and post-surgical stenosis and restenosis. See page 1, lines 15-24. In this regard, the specification further refers to a scientific publication, see page 1, lines 25-26. Furthermore, the specification teaches that the compounds recited in the present application are protein kinase inhibitors, see page 1, line 9-10, and page 2, lines 4-7. Therefore, in view of the key role of PKs in the regulation of celluar proliferation, particularly in cancer formation, development and control; and the presently claimed compounds are active protein kinase inhibitors, a person skilled in the art would readily understand that the compounds presently claimed can be used in anticancer therapy. In other words, the specification establishes a link between the mechanism of action of the compounds presently claimed and the diseases intended to be treated.

Second, applicants submit *in vitro* biological data of representative compounds as presently claimed and the corresponding biological test description (enclosed as Exhibit A). In this regard, applicants direct the Examiner's attention to the fact that the tested kinases are among the listed kinases specified at page 3, lines 11-16, for example, Met, Aurora 1, Aurora 2,

PLK, PDGF-R, IGF-R, VEGF-R, and CDK2/CYCA. Therefore, applicants submit that the above-described biological data, together with the pharmacological information described at page 29 to page 37, provides more than adequate enablement for a person skilled in the art to understand and be able to practice the subject matter recited in the amended Claim 27.

Third, in order to further illustrate that the presently claimed compounds can be used in anti-cancer treatment, applicants submit the following findings which establishes the link between the tested kinases and the diseases intended to be treated. For example, "the Polo-like kinase-1 (PLK1) [is] the principal protein kinase that carried out B23 phosphorylation at this site. Inhibition of PLK1 is predicted to block the reproduction of cancer cells indicating its potential as a promising cancer drug target." See http://www.drugresearcher.com/news/ng.asp?n=53915-plk-a-cancer. For Aurora kinase, applicants submit that the following scientific publications (enclosed) further support that Aurora kinase inhibitors can be used to treat cancer.

Specifically, *Mol Cancer Ther. 2007 :6(12), pp 3147-57* (enclosed as Exhibit B), describes that a wide range of cancers could respond therapeutically to Aurora kinase inhibitors. Moreover, it describes that Aurora kinase inhibitors can exhibit antiproliferative activity and induce tumor regression (see the last paragraph of page 3147 and the first paragraph of page 3148). Furthermore, it provides detailed description of anticancer activity of CCT129202, an Aurora kinase inhibitor (see Abstract at page 3147).

Clin Cancer Res. 2007 Jun 15;13(12):3682-8 (enclosed as Exhibit C), describes that Aurora kinase inhibitors have been developed as anticancer agents (see the second to last paragraph at page 3682). It further describes AZD1152, an Aurora kinase inhibitor, can inhibit the growth of human colon, ling, and hematologic tumor xenografts in immunodeficient mice (see the Abstract at page 3682).

Clin Cancer Res. 2006 Jul 1;12(13):4080-9 (enclosed as Exhibit D), describes that Aurora kinases are attractive targets for anticancer therapy (see the third paragraph at page 4081). It further provides description of PHA-680632, an Aurora kinase inhibitor, with potent antitumoral activity. (see Abstract at page 4080).

Nat Med. 2004 Mar;10(3):262-7 (enclosed as Exhibit E), describes that Aurora kinases are essential for the regulation of chromosome segregation and cytokinesis during mitosis, and it further reports that the in vivo data of VX-680, an Aurora kinase inhibitor, provide compelling evidence that inhibition of the Aurora kinase family represents a new approach to the pharmacological intervention in oncology (see the first paragraph at page 263).

Cancer Res. 2005; 65: (19):9038-46 (enclosed as Exhibit F), describes that Aurora kinase inhibitors should prevent the continuous, proliferative growth of cancer cells and provide a way of controlling abnormal mitosis, which would be applicable to a wide range of tumor types (see the third paragraph on the right column of page 9038). It further reports that JNJ-7706621, an Aurora kinase inhibitor, is a promising antineoplastic agent (see the last paragraph at page 9045).

In view of the above remarks, applicants submit that the specification provides sufficient support to enable a person skilled in the art to make and/or use the subject matter claimed in amended Claim 27. Therefore, applicants submit that the instant rejection has been obviated, and withdrawal of the same is respectfully requested.

Thus, in view of the foregoing amendments and remarks, it is firmly believed that the present case is in condition for allowance, which action is earnestly solicited.

Respectfully submitted,

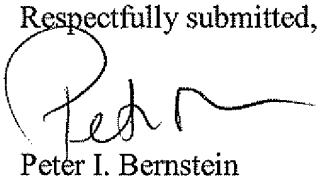

Peter I. Bernstein
Registration No. 43,497

Scully, Scott, Murphy & Presser, P.C.
400 Garden City Plaza, Suite 300
Garden City, New York 11530
(516) 742-4343
Enclosure: Exhibits A-F
PIB/AZ:dg

EXHIBIT A

Robotized Kinase-Glo assay

This assay was set up for the measurement of kinase activity and/or inhibition. It is homogeneous, suitable for all type of protein kinases, quick and radioactivity-free.
We established the assay in 384 well-plates: the test mix consisted of:

1) 3x Enzyme mix (done in Kinase Buffer 3X), 5 µl/well

2) 3x substrate and ATP mix (done in ddH2O), 5 µl/well

3) 3x test compounds (diluted into ddH2O – 3% DMSO) – 5 µl/well

As an outcome, the percentage of inhibition at 10 µM was evaluated for each compound tested: see below for compound dilution and assay scheme. Each enzyme had its own buffer constitution, substrate type and concentration, enzyme concentration.
Incubation time instead was 90 min for all targets.

Dilution of compounds

Test compounds were received as a 1 mM solution in 100% DMSO into 96 well plates.
The plates were diluted to 30 µM in ddH_2O, 3% DMSO; 4 plates are reorganized in 384 well plate by dispensing 5 µl of each 96wp into the four quadrants of a 384wp.
In well P23 and P24 the internal standard inhibitor staurosporine was added

Assay scheme
Test plates were first added with 5 µl of the compound dilution (30 µM, corresponding to 3X dilution) and then loaded onto a robotized station together with one reservoir for the Enzyme mix (3X) and one for the ATP mix (3X), specific for each target under study.
To start the assay, the robot aspirated 5 µl of ATP/Substrate mix, made an air gap inside the tips (5 µl) and aspirated 5 µl of Enzyme mix. The successive dispensation into the test plates allowed the kinase reaction to start after 3 cycles of mixing, done by the robot itself by up and down pipetting. At this point, the correct concentration was restored for all reagents.

The robot incubated the plates for 90 minutes at room temperature, and then stopped the reaction by pipetting 15 µl of Kinase-Glo reagent into the reaction mix. Three cycles of mixing were done immediately after the addition of the reagent.
The principle of the Kinase-Glo technique is the presence in the reagent mixture of oxygen, luciferin and luciferase enzyme: in the presence of ATP, remaining from the kinase reaction, oxi-luciferin is produced with the emission of light, directly dependent on the amount of ATP. To have best performances of this technique, the kinase reaction should utilize at least 15-20% of the available ATP.
After another 60 minutes of incubation to stabilize the luminescent signal, the plates were read on a ViewLux instrument.
Data were analyzed using a customized version of the software package "Assay Explorer" that provided % inhibition data.

Chemical formula	AUR1	AUR2	CDK2/CYCA	IGFR1
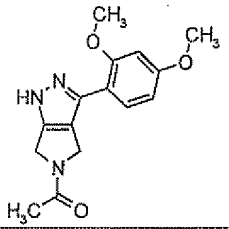				65.5
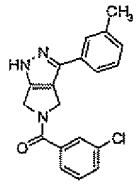				81.3
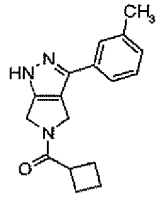				66.9
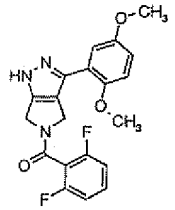		53.6	63.1	
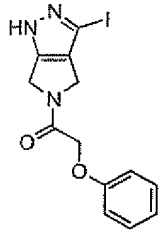	103.7			64.9

Chemical Formula	MET	NEK6	PDGFR	PLK1	VEGFR2
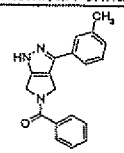					69.5
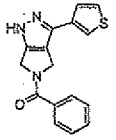			71.0		103.5
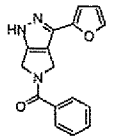					83.9
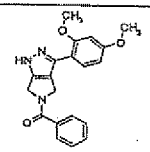				71.4	79.0
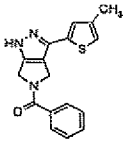			64.0	61.1	106.7
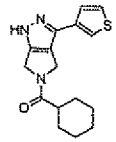				51.9	98.1
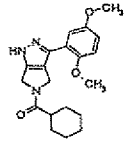				57.8	
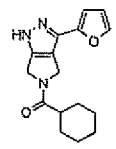				61.8	84.6

Chemical Formula	MET	NEK6	PDGFR	PLK1	VEGFR2
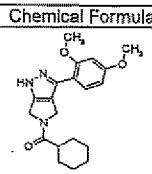				52.9	57.7
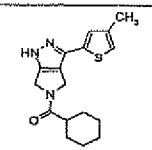				72.4	
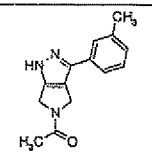					87.1
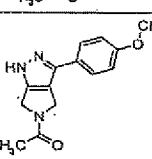					87.8
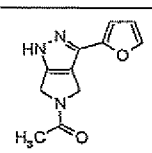					76.2
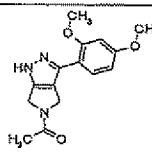			80.9		106.4
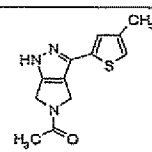					116.6
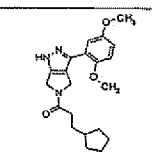				80.5	

Chemical Formula	MET	NEK6	PDGFR	PLK1	VEGFR2
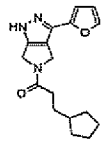	53.1			60.2	67.4
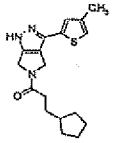				57.7	
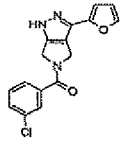				72.5	64.9
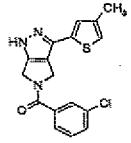				76.4	85.1
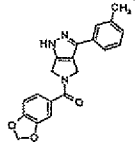				51.6	
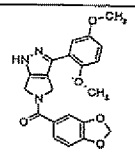				97.8	
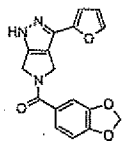				55.3	92.2
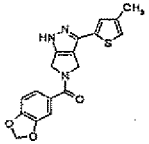				69.9	96.7

Chemical Formula	MET	NEK6	PDGFR	PLK1	VEGFR2
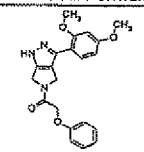					56.0
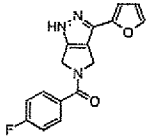					80.4
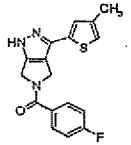				56.9	92.3
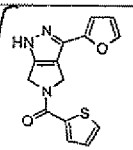				55.6	67.9	103.3
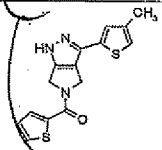				52.9	59.3	
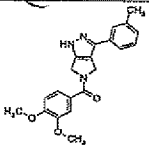					51.3
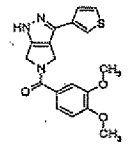					95.4
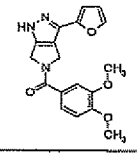					88.0

Chemical Formula	MET	NEK6	PDGFR	PLK1	VEGFR2
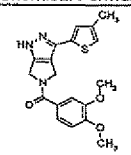					61.6
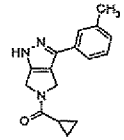			50.0		
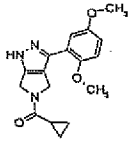			91.9		79.7
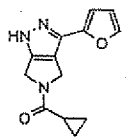					71.8
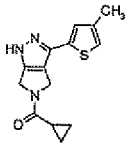					74.3
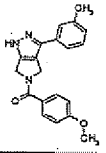					79.7
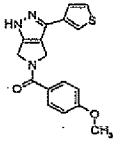			51.2		69.8
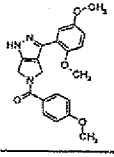				91.8	

Chemical Formula	MET	NEK6	PDGFR	PLK1	VEGFR2
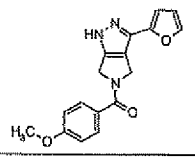				56.3	97.4
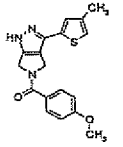					
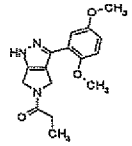			79.6		110.3
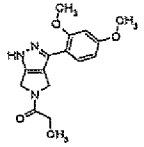			60.0		103.8
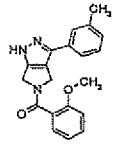				55.8	
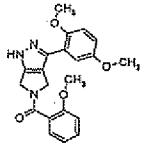				51.9	
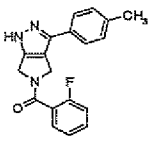			63.1		89.1
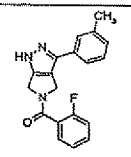			75.9	79.3	100.8

Chemical Formula	MET	NEK6	PDGFR	PLK1	VEGFR2
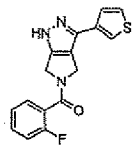			66.8	54.4	106.7
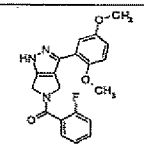				79.3	
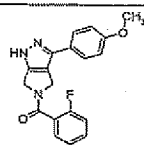			54.7		
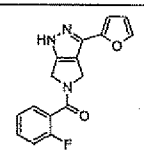				60.2	99.7
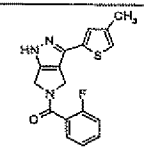			85.1	75.9	99.3
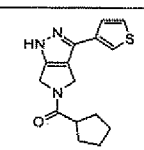					98.4
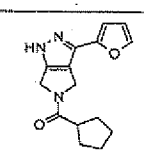				54.0	81.4
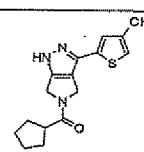					56.9

Chemical Formula	MET	NEK6	PDGFR	PLK1	VEGFR2
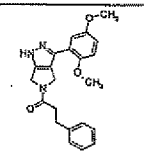				63.8	73.4
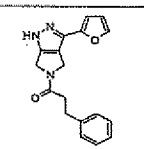				63.6	60.9
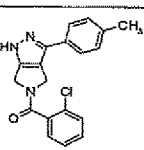					92.2
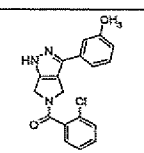			75.6	85.8	100.6
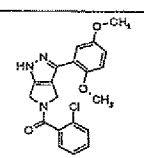				89.1	60.2
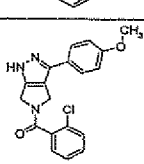			59.8		98.8
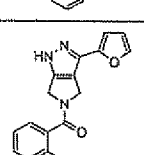			54.0	67.1	103.5
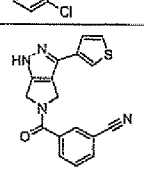					81.9

Chemical Formula	MET	NEK6	PDGFR	PLK1	VEGFR2
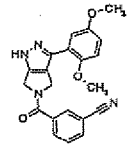				89.7	
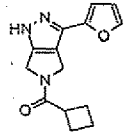				52.9	74.6
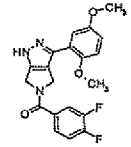				74.4	
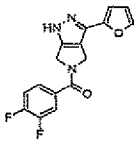					54.3
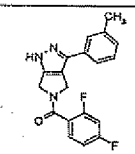					91.7
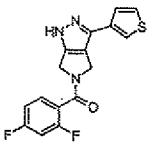			57.4		100.0
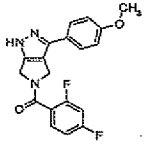			56.8	69.0	96.6
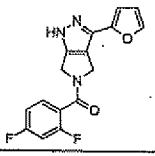				56.7	88.3

Chemical Formula	MET	NEK6	PDGFR	PLK1	VEGFR2
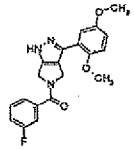				88.4	
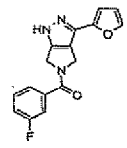				54.3	
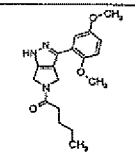					
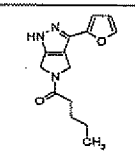				67.2	50.9
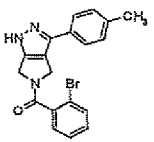					53.8
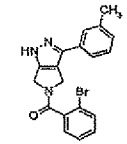					79.4
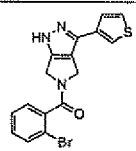					57.1
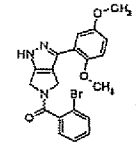				80.0	67.7

Chemical Formula	MET	NEK6	PDGFR	PLK1	VEGFR2
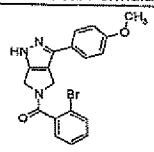					63.9
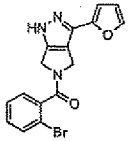				54.7	67.3
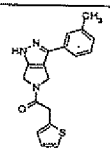				59.4	
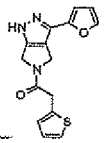				63.9	
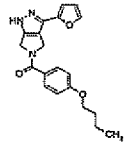					54.9
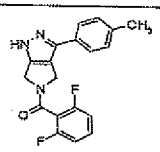			70.0	60.3	74.3
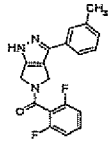			79.9	98.9	104.3
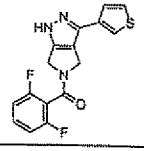			70.6	78.7	108.7

Chemical Formula	MET	NEK6	PDGFR	PLK1	VEGFR2
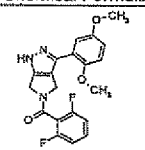				103.8	51.1
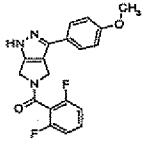			72.7	89.4	99.6
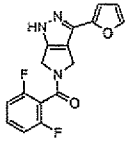			83.0	100.8	103.8
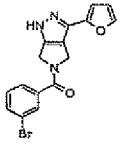				86.3	57.9
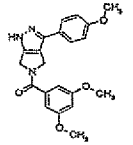					75.4
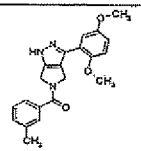				83.4	
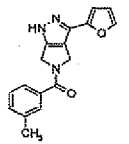				81.5	83.6
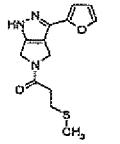					57.8

Chemical Formula	MET	NEK6	PDGFR	PLK1	VEGFR2
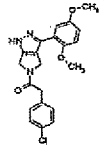				76.2	
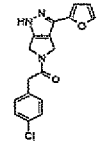					55.2
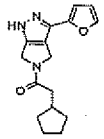				59.5	
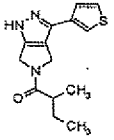					54.9
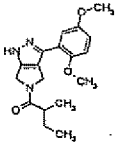				51.0	
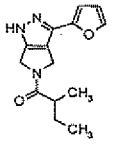				66.9	66.6
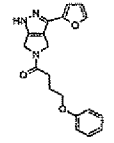					52.5
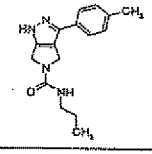					59.6

Chemical Formula	MET	NEK6	PDGFR	PLK1	VEGFR2
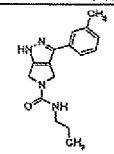					60.6
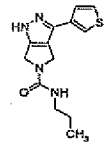			57.7		100.5
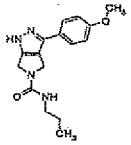			63.3		73.1
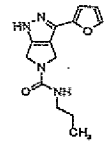					93.6
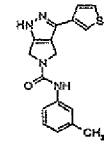			55.1		92.6
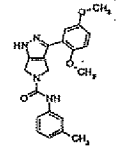			68.9		
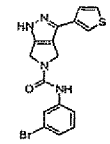					66.0
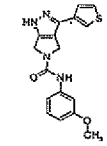			65.5		104.3

Chemical Formula	MET	NEK6	PDGFR	PLK1	VEGFR2
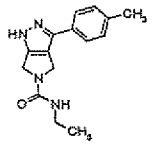					62.8
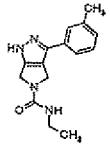					68.5
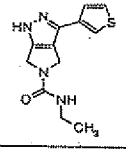				56.6	100.5
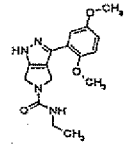				64.9	
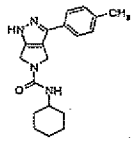					53.2
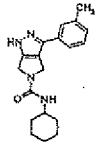					65.0
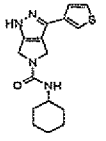					100.4
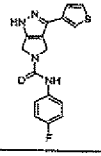					94.1

Chemical Formula	MET	NEK6	PDGFR	PLK1	VEGFR2
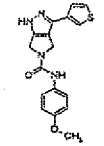					92.7
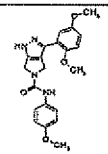					56.7
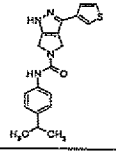					99.3
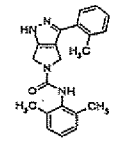				81.8	
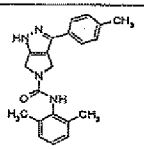				68.0	
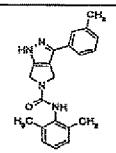				90.5	
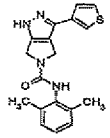				54.0	
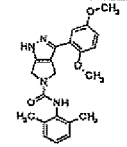				104.4	

Chemical Formula	MET	NEK6	PDGFR	PLK1	VEGFR2
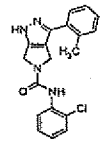			68.2		
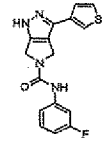					89.4
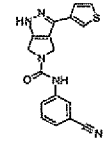					79.5
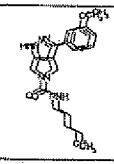			51.9		
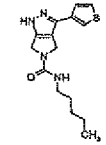			61.3		100.4
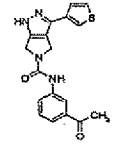			82.1		117.1
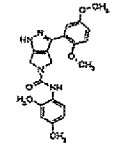			103.0		
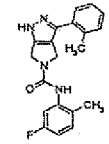			81.4		

Chemical Formula	MET	NEK6	PDGFR	PLK1	VEGFR2
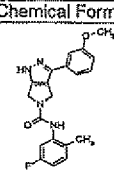			78.9		
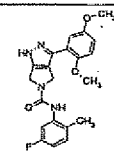			98.5		
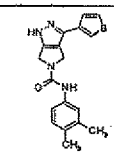					96.3
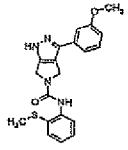			51.1		
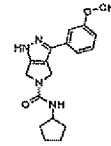					89.6
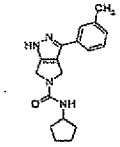					62.2
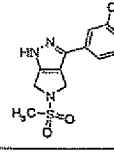					90.9
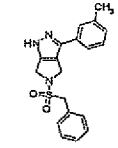			54.2		60.9

Chemical Formula	MET	NEK6	PDGFR	PLK1	VEGFR2
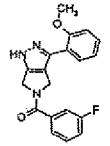			51.1	70.3	58.7
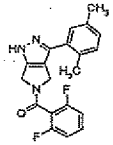				75.9	55.1
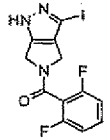				59.5	
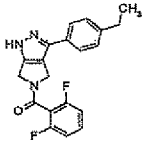			55.2		92.1
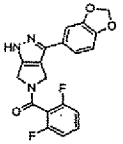			54.2	72.4	101.6
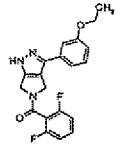				81.5	83.6
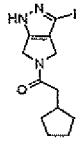					51.3
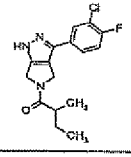				57.3	

Chemical Formula	MET	NEK6	PDGFR	PLK1	VEGFR2
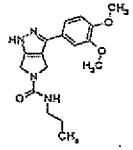					54.9
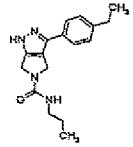					65.8
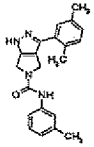					59.5
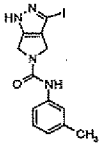					56.2
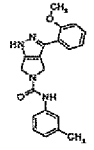					59.6
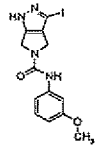					52.2
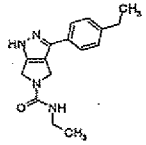			53.5		72.1
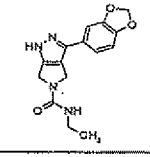			59.2		110.7

Chemical Formula	MET	NEK6	PDGFR	PLK1	VEGFR2
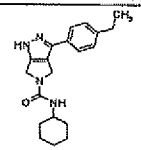					64.6
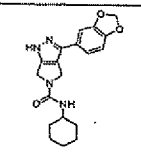					74.2
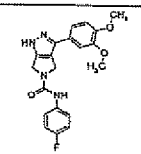					57.7
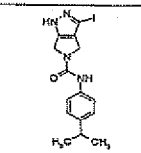					51.3
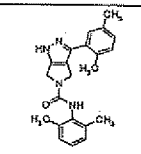			94.5		
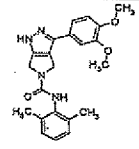			95.8		
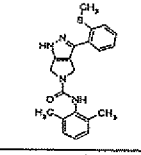			84.0		
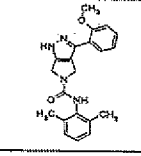			97.8		

Chemical Formula	MET	NEK6	PDGFR	PLK1	VEGFR2
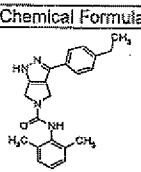			89.5		
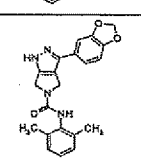			66.4		
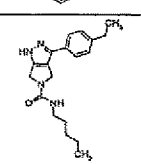			61.6		
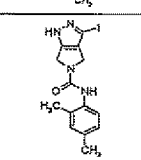				57.1	
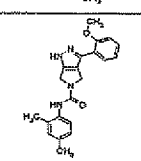			102.7		50.0
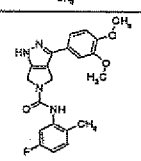			99.1		
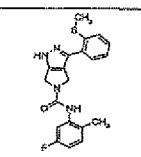			85.6		
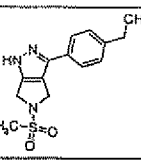					68.7

Chemical Formula	MET	NEK6	PDGFR	PLK1	VEGFR2
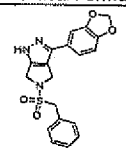					81.1
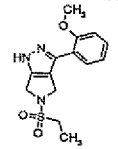			71.0		
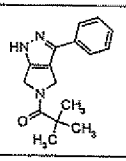					72.0
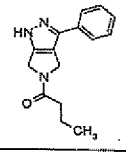					118.1
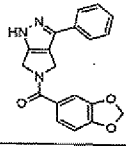			52.5	57.0	100.5
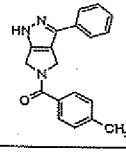			54.9		81.0
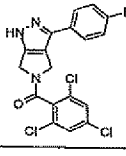					122.1
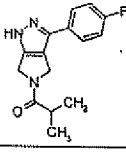			51.5		

Chemical Formula	MET	NEK6	PDGFR	PLK1	VEGFR2
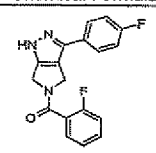			73.4	64.4	102.9
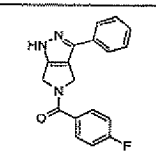			52.9		90.7
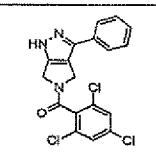					98.4
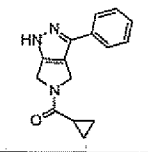			69.1		117.3
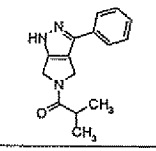					92.5
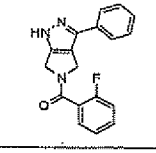			71.8	63.7	101.6
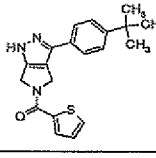					66.6
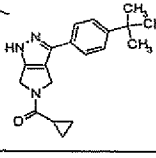					57.0

Chemical Formula	MET	NEK6	PDGFR	PLK1	VEGFR2
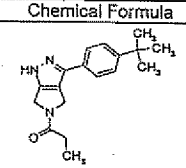					62.3
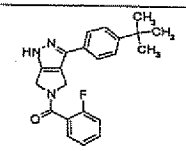					103.4
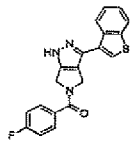					73.9
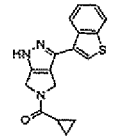		72.4	76.1		
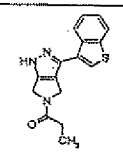		56.6			55.7
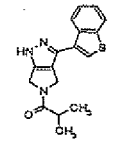		51.0			
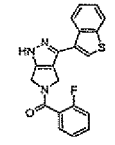				61.0	79.6
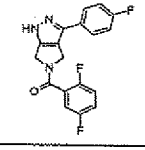				59.9	61.9

Chemical Formula	MET	NEK6	PDGFR	PLK1	VEGFR2
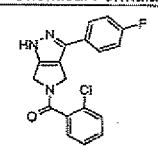					123.5
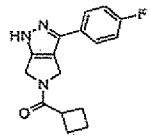			58.1		79.2
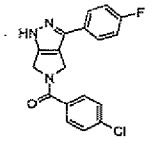					71.7
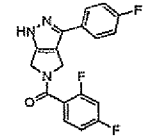			58.9		85.6
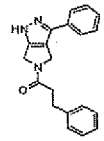					64.6
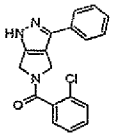					96.9
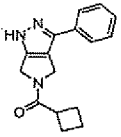			52.1		93.8
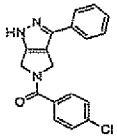					103.5

Chemical Formula	MET	NEK6	PDGFR	PLK1	VEGFR2
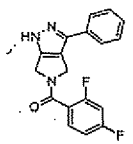			60.6		97.6
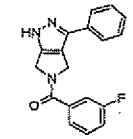					55.8
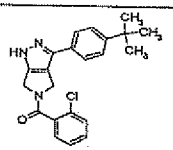					81.2
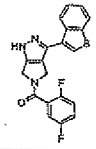				67.8	50.4
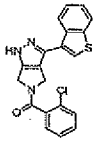			50.4	58.0	89.8
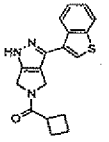			52.6	51.0	50.7
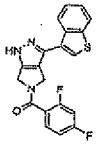					76.3
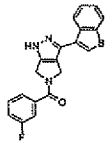				57.8	

Chemical Formula	MET	NEK6	PDGFR	PLK1	VEGFR2
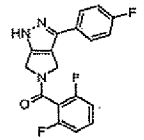			72.7	90.1	105.2
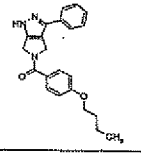					50.5
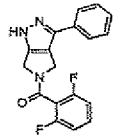			67.9	77.9	122.3
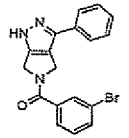					60.0
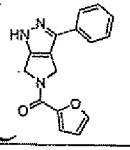			84.8		107.5
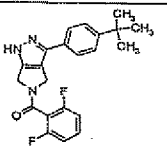					96.4
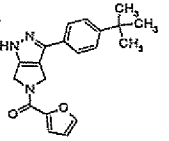					81.4
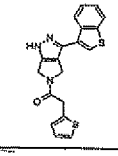			54.3		

Chemical Formula	MET	NEK6	PDGFR	PLK1	VEGFR2
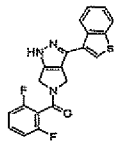			64.8	88.8	89.6
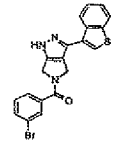				67.6	50.0
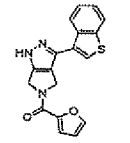			73.4		80.3
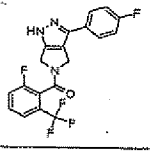					67.5
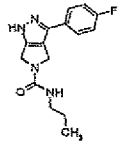			78.2		97.3
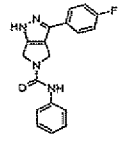					67.3
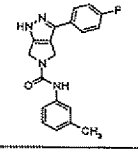					53.7
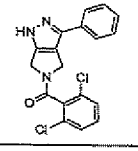					96.9

Chemical Formula	MET	NEK6	PDGFR	PLK1	VEGFR2
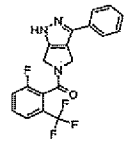					80.2
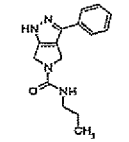			68.2		109.1
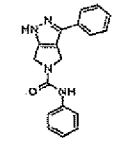			74.0		98.3
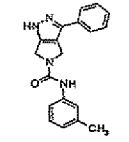			66.0		91.3
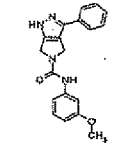			68.6		115.0
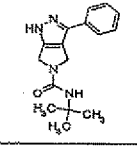					108.3
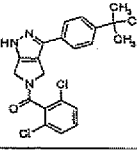					65.3
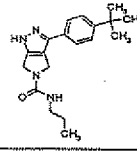					99.5

Chemical Formula	MET	NEK6	PDGFR	PLK1	VEGFR2
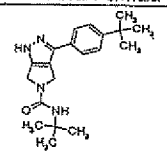					58.4
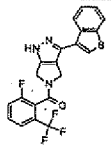				62.9	
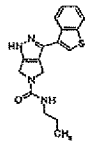			50.9		70.0
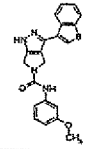					55.0
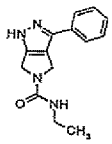			65.0		86.3
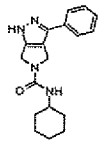			57.6		95.4
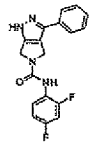					64.6
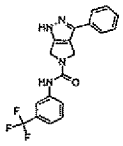			50.8		84.1

Chemical Formula	MET	NEK6	PDGFR	PLK1	VEGFR2
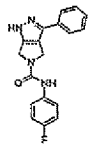					84.2
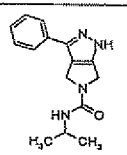			66.6		104.8
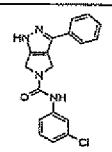			54.7		102.1
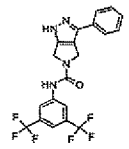					74.1
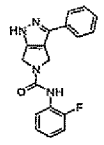					78.4
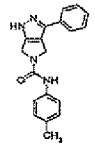					90.3
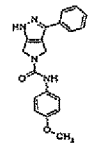			57.7		103.9
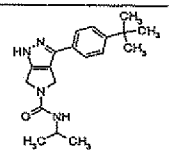					99.8

Chemical Formula	MET	NEK6	PDGFR	PLK1	VEGFR2
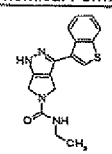			74.5		66.2
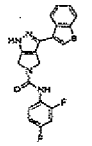			72.5		
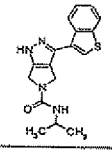			65.0		72.6
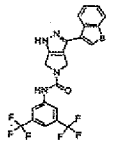			52.1		
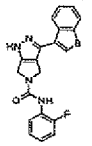			92.6		52.6
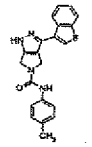			57.2		
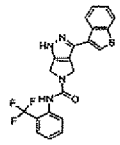				57.5	
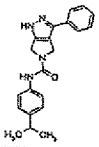					88.7

Chemical Formula	MET	NEK6	PDGFR	PLK1	VEGFR2
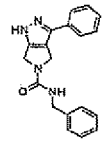			85.2		120.9
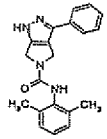			83.7		97.6
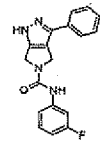					104.6
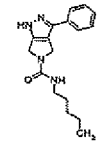			77.1		95.2
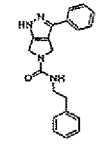			66.1		126.1
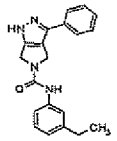			62.9		105.9
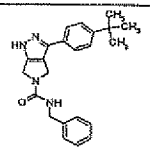			66.6		104.6
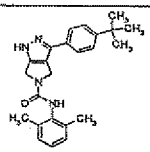			79.8		

Chemical Formula	MET	NEK6	PDGFR	PLK1	VEGFR2
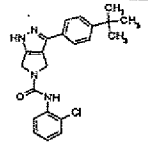			78.1		91.7
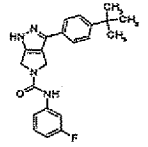			69.4		92.0
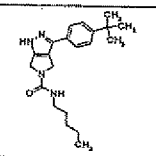					70.6
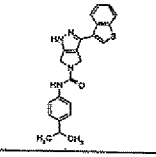			56.6		64.3
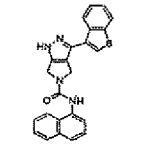					60.5
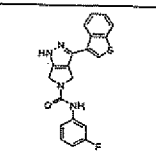			58.3		66.5
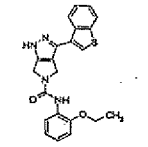			56.5		58.8
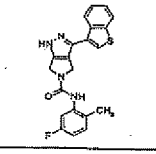			100.4		

Chemical Formula	MET	NEK6	PDGFR	PLK1	VEGFR2
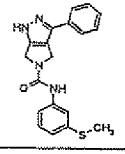			75.8		96.3
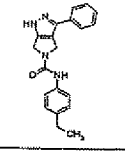			51.3		100.2
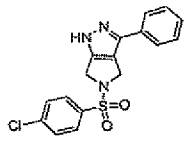					65.6
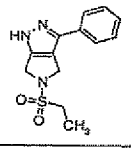					52.3
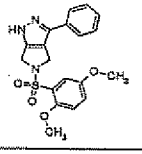					51.8

EXHIBIT B

Mechanism of action of the Aurora kinase inhibitor CCT129202 and *in vivo* quantification of biological activity

Florence Chan,[1] Chongbo Sun,[1] Meg Perumal,[2] Quang-De Nguyen,[2] Vassilios Bavetsias,[1] Edward McDonald,[1] Vanessa Martins,[1] Nicola E. Wilsher,[1] Florence I. Raynaud,[1] Melanie Valenti,[1] Sue Eccles,[1] Robert te Poele,[1] Paul Workman,[1] Eric O. Aboagye,[2] and Spiros Linardopoulos[1,3]

[1]Cancer Research UK, Centre for Cancer Therapeutics, The Institute of Cancer Research, Belmont, Surrey, United Kingdom; [2]Molecular Therapy, Imperial College London, Faculty of Medicine Hammersmith Hospital, and [3]Breakthrough Breast Cancer Research Centre, The Institute of Cancer Research, London, United Kingdom

Abstract

The Aurora family of serine/threonine kinases is important for the regulation of centrosome maturation, chromosome segregation, and cytokinesis during mitosis. Overexpression of Aurora kinases in mammalian cells leads to genetic instability and transformation. Increased levels of Aurora kinases have also been linked to a broad range of human tumors. Here, we describe the properties of CCT129202, a representative of a structurally novel series of imidazopyridine small-molecule inhibitors of Aurora kinase activity. This compound showed high selectivity for the Aurora kinases over a panel of other kinases tested and inhibits proliferation in multiple cultured human tumor cell lines. CCT129202 causes the accumulation of human tumor cells with ≥4*N* DNA content, leading to apoptosis. CCT120202-treated human tumor cells showed a delay in mitosis, abrogation of nocodazole-induced mitotic arrest, and spindle defects. Growth of HCT116 xenografts in nude mice was inhibited after i.p. administration of CCT129202. We show that p21, the cyclin-dependent kinase inhibitor, is induced by CCT129202. Up-regulation of p21 by CCT129202 in HCT116 cells led to Rb hypophosphorylation and E2F inhibition, contributing to a decrease in thymidine kinase 1 transcription. This has facilitated the use of 3′-deoxy-3′[^{18}F]fluorothymidine-positron emission tomography to measure noninvasively the biological activity of the Aurora kinase inhibitor CCT129202 *in vivo*. [Mol Cancer Ther 2007;6(12):3147–57]

Introduction

The Aurora kinase family is a group of cell cycle–regulated serine/threonine kinases that are important for mitosis (1–4). The activity of all three Aurora kinases peaks at G_2 and during mitosis, whereas their expression is low in resting cells (5, 6). Aurora A is a centrosome-associated kinase (7), whereas Aurora B is a "chromosome passenger" kinase that is essential for chromosome segregation and cytokinesis (2, 8). Aurora C is a centrosome-associated kinase, predominantly restricted to germ cells (6), the function of which remains unclear. A variety of Aurora substrates have been identified, of which the most well characterized for Aurora A are p53, TPX2, Ajuba, XIEg5, and D-TACC (9, 10). Aurora B has been reported to be present in a complex with the inner centromere protein and survivin (11, 12). The most well-characterized substrate for Aurora B is histone H3, a structural component of chromatin (13). Overexpression of Aurora A induces abnormal spindle formation, leading to prolonged mitosis and polyploidy (14). Aurora A was first described in human cancer cell lines, but has subsequently been found to be overexpressed in a broad range of human tumors, including primary colorectal carcinoma, gliomas, breast, ovarian, and pancreatic cancers (5, 15–18). Aurora B is also overexpressed in human tumors such as gliomas, thyroid carcinoma, seminoma, and colon cancer (19–21). A polymorphism in the *Aurora A* gene has been identified that shows preferential amplification associated with increased aneuploidy in colon cancer (22). We have shown recently that Aurora A mediates phosphorylation of IκBα that induces nuclear factor-κB activation, a novel function of Aurora A, that could potentially lead to carcinogenesis and drug resistance (23, 24).

The overexpression of the Aurora kinases and the association with genetic instability in tumors suggest that a wide range of cancers could respond therapeutically to inhibitors of the Aurora kinases. During the past 3 years, the first generation of Aurora kinase inhibitors, including ZM447439 (25), Hesperadin (26), VX-680 (27; also known as MK-0457), and more recently, PHA-680632 (28) and the specific Aurora A inhibitor MLN8054 (29) have been described. Inhibitors of Aurora kinases kill proliferating cells through apoptosis after accumulation of tetraploid

Received 10/2/07; accepted 11/1/07.

Grant support: Programme grants from Cancer Research UK (C309/A8274 and C2536/A5708) and Breakthrough Breast Cancer.

The costs of publication of this article were defrayed in part by the payment of page charges. This article must therefore be hereby marked *advertisement* in accordance with 18 U.S.C. Section 1734 solely to indicate this fact.

Requests for reprints: Spiros Linardopoulos, Centre for Cancer Therapeutics, The Institute of Cancer Research, Cancer Research UK, 15 Cotswold Road, Belmont, Surrey SM2 5NG, United Kingdom. Phone: 44-208-722-4133; Fax: 44-207-153-5340. E-mail: spiros.linardopoulos@icr.ac.uk

doi:10.1158/1535-7163.MCT-07-2156

cells generated by the inhibition of cytokinesis and blocking of mitotic histone H3 phosphorylation (25–27). VX-680 and PHA-680632 inhibit all three Aurora kinases, exhibit antiproliferative activity, and induce tumor regression in animal models (28, 29), providing a strong support for developing inhibitors against this target. With respect to biomarkers of drug activity in preclinical studies, Aurora kinase inhibitors have been assessed mainly by measuring histone H3 phosphorylation (27, 28). Noninvasive imaging methods can be very advantageous for cancer drug development (30). It is, therefore, desirable to develop and validate noninvasive imaging methods that measure the biochemical effect of Aurora kinase inhibition. Imaging biomarker assays such as [^{18}F]fluorothymidine-positron emission tomography ([^{18}F]FLT-PET) have previously been used successfully to monitor the biological activity of targeted therapies (31).

In this report, we describe the characterization of a representative of a novel class of highly selective Aurora kinase inhibitors CCT129202, which is active on a wide range of human cancer cell lines *in vitro* and in human xenografts in athymic mice. The molecular mechanism of action of CCT129202 is consistent with the inhibition of Aurora A and Aurora B, as has been shown by monitoring phosphorylation of histone H3 and p53 protein stabilization. We found that CCT129202 induces p21, resulting in the down-regulation of thymidine kinase 1 (TK1) via the Rb pathway. This decrease in TK1 activity provides the opportunity to use [^{18}F]FLT-PET for measuring the biological activity of Aurora inhibitors, and we describe the utility of this approach with CCT129202 *in vivo*.

Materials and Methods

Chemistry

CCT129202, a derivative of the piperazinyl imidazo[4,5-*b*] pyridine scaffold, was synthesized as discussed elsewhere (32).

In vitro Aurora A Kinase Assays

NH_2-terminal glutathione *S*-transferase (GST)-fusion recombinant human Aurora A (aa 118–403), Aurora B (full length), and Aurora C (full length) were expressed in baculovirus, purified, and used in kinase inhibition assays as previously described (32, 33). The selectivity of the compound was tested in a series of *in vitro* kinase assays using a selected panel of protein kinases (Invitrogen).

Cell Culture, Immunoblotting, and Cell Cycle Analysis

Human colon cancer cell lines (HCT116, Colo205, SW620, HT29, KW12), ovarian tumor cell lines (A2780, OVCAR8), a breast tumor cell line MDA-MB-157, and HeLa cervical tumor cells were maintained in DMEM with 10% FCS, penicillin, streptomycin, and glutamine, whereas the B-myelomonocytic leukemia cell line (MV4-11; American Type Culture Collection) was maintained in Iscove's modified Dulbecco's medium with 4 mmol/L L-glutamine supplemented with 10% FCS, penicillin, and streptomycin at 37°C and 5% CO_2. Immunoblotting was assessed as previously described (23). For cell cycle analysis, cells were treated with inhibitors for 24 h in the absence or presence of amphidicolin (1 μg/mL) or nocodazole (50 ng/mL) and harvested with 5 mmol/L EDTA-PBS, then fixed in 85% ice-cold ethanol overnight and stained with propidium iodide (Sigma), and analyzed on Beckman Coulter Cytomics FC500. Antibodies used were IAK1 (Aurora A; BD Bioscience), α-tubulin (Sigma), poly(ADP-ribose) polymerase (PARP; Cell Signaling Technology), p53 (Oncogene), ezrin (gift from Prof. C. Isacke, The Breakthrough Breast Cancer Research Centre, London, United Kingdom), MPM2 and Ser^{10} phosphorylated histone H3 (Upstate Biotechnology), total histone H3 and TK1 (Abcam), p21, total and hypo-phosphorylated Rb (BD Bioscience), and glyceraldehyde-3-phosphate dehydrogenase (GAPDH; Chemicon International).

Histone Extraction

Cells were harvested and resuspended in lysis buffer [10 mmol/L Tris (pH, 7.4), 50 mmol/L sodium bisulfite, 1% Triton ×100, 10 mmol/L $MgCl_2$, and 8.6% sucrose] and then dounce homogenized for 1 min. Cell nuclei were pelleted at 1,500 × *g* for 10 min at 4°C. Nuclei were washed 3× in lysis buffer and once in wash buffer [10 mmol/L Tris (pH 7.5), 13 mmol/L EDTA]. The nuclei were then resuspended in ice-cold distilled water and 0.4 N sulfuric acid and incubated on ice for 1 h. Samples were pelleted at 20,000 × *g* for 10 min at 4°C. The resulting supernatant was added to acetone, incubated overnight at −20°C, pelleted at 20,000 × *g* for 10 min at 4°C, and air dried, and the extracted histone were resuspended in 50 μL distilled water. The proteins were quantified using Bio-Rad Bradford dye and ran on SDS-PAGE gels.

Cell Viability Assay

The effects of CCT129202 on cell proliferation were analyzed with the colorimetric 3-(4,5-dimethylthiazol-2-yl)-2,5-diphenyltetrazolium bromide (MTT) assay (Sigma) according to the manufacturer's instructions. Cells were plated in 96-well plates at 2,500 per well and were treated with a range of 0 to 50 μmol/L of CCT129202 for 72 h. The absorbance was measured at 570 nm using the Wallac VICTOR$^2_{TM}$ 1420 Multilabel Counter (PerkinElmer).

Cell-based Enzyme-Linked Immunosorbent Assay (CELISA)

Cells were seeded at 8,000 cells per well in sterile 96-well plates 24 h before the addition of inhibitors. Cells were harvested at the indicated times and fixed in 3% paraformaldehyde/0.25% glutaradehyde/0.25% Triton X-100 for 30 min at 37°C, followed by blocking with 5% nonfat milk for 30 min at 37°C. Cells were incubated with anti–phospho-histone H3 Ser^{10} antibody (Upstate Biotechnology) or anti-p53 antibody (Merck Chemicals Ltd.) for 1 h at 37°C, then with Eu-labeled secondary antibody (PerkinElmer) for 1 h at 37°C. DELFIA enhancement solution was added, and plate was read at 615 nmol/L on Wallac VICTOR$^2_{TM}$ 1420 Multilabel Counter (PerkinElmer).

Immunofluorescence Microscopy

Cells were grown overnight on coverslips and treated with inhibitors for 24 h. Cells were washed with PBS and fixed with 4% paraformaldehyde for 1 h at 37°C and

permeabilized with 0.5% Triton ×100, followed by 1 h incubation with anti–α-tubulin antibody at room temperature and 1 h incubation with FITC-labeled anti-mouse antibody at room temperature. DNA was stained with TO-PRO-3 (Invitrogen). Coverslips were mounted on microscope slides and fluorescence visualized with Leica SP1 confocal microscope.

Gene Expression cDNA Microarrays

RNA was harvested using the ABI PRISM 6100 Nucleic Acid PrepStation (Applied Biosystems). The quantity was determined with the NanoDrop ND-1000 Spectrophotometer (NanoDrop Technologies). The CyScribe Post-Labeling Kit (GE Healthcare) was used to label 5 μg of total RNA, according to the manufacturer's recommendations, except that the reverse transcription reaction was carried out overnight. The control samples (untreated cell lines) were labeled with Cy3, and the test samples (treated with CCT129202) were labeled with Cy5. cDNA microarrays were done according to the procedure outlined in ref. (34) (Supplementary Materials and Methods).[4]

In vivo Pharmacokinetics

Mice (female Balb/C, ages 6–8 weeks) received an i.v. dose of CCT129202·3HCl (5 mg kg^{-1}) in 10% DMSO, 5% Tween 20 in saline. After administration, mice were killed at 5, 15, and 30 min and 1, 2, 4, 6, and 24 h. Blood was removed by cardiac puncture and centrifuged to obtain plasma samples. Plasma samples (100 μL) were added to the analytic internal standard (CCT129127, a 6-H analogue of CCT129202; IS), followed by protein precipitation with 300 μL acetonitrile. Following centrifugation (1,200 × *g*, 20 min, 4°C), the resulting supernatants were analyzed for CCT129202 levels by LCMS using a reverse-phase Synergi Max-RP (Phenomenex, 50 × 2.1 mm) analytic column and positive ion mode ESI MRM on a Waters 2795 liquid chromatography system coupled to a Quattro Ultima triple quadrupole mass spectrometer (Micromass Ltd.). *In vitro* metabolic stability was assessed by the incubation of CCT129202 (1 μmol/L) with male CD1 mouse liver microsomes (1 mg/mL) protein in the presence of NADPH (2 mmol/L), NADH (2 mmol/L), and $MgCl_2$ (10 mmol/L) in PBS (10 mmol/L) at 37°C. Samples were taken from the incubation mixture at 0, 15, and 30 min and added directly to 3× v/v acetonitrile containing IS. Samples were centrifuged as described for plasma samples before analysis on a Thermo Finnigan LC system consisting of an online degassing system (Alltech Associates), P4000 pump, AS3000 autosampler, and SN4000 system controller interface (SpectraSystems, Thermo Separation Products) coupled to an iontrap MS (LCQ Classic) with Xcalibur data handling system (version 1.1). Control incubations were generated by the omission of NADPH and NADH from the incubation reaction. The percentage compound remaining was determined after analysis by liquid chromatography–mass spectrometry (LCMS).

Animal Efficacy Studies

For efficacy studies, human HCT116 colon carcinoma xenografts were established from the inoculation of 2×10^6 cells in the bilateral flanks of female NCr athymic mice, 6 to 8 weeks old. CCT129202 was dissolved in DMSO and injected i.p in vehicle, which comprised 10% DMSO, 5% Tween 20, and 85% sterile saline at 0.1 mL/10 g body weight. Dosing with CCT129202 commenced when tumors were well established (~5 mm mean diameter); control animals received an equivalent volume of vehicle. Mouse body weights and condition were monitored throughout the study. Tumors were measured thrice weekly across two perpendicular diameters and tumor volume (V) was calculated using the formula $V = 4/3\pi\ [(d_1 + d_2)/4]^3$ (35). At the end of the study, tumors were excised, weighed, and snap frozen in liquid nitrogen for pharmacokinetic and pharmacodynamic analyses. Serum and tumor samples were collected at 2, 4, and 6 h after the final dose.

Molecular Biomarker Analysis

The levels of total histone H3 and phosphorylated histone H3 were determined using an electrochemiluminescent immunoassay (Meso Scale Discovery, MSD system). Tumor xenografts were homogenized with the PreCellys 24 (Bertin Technologies) in xenograft lysis buffer [1% NP40, 1% sodium deoxycholate, 0.1% SDS, 50 mmol/L Tris (pH, 7.5), 1 mmol/L EDTA, 150 mmol/L NaCl, 1 mmol/L β-glycerophosphate, 2 mmol/L phenylmethylsulfonyl fluoride, 10 mmol/L NaF, mini complete protease inhibitor (Roche)]. Homogenates were pelletted, and the resulting supernatant was used for the analysis. Standard 96-well single-spot MA6000 MSD plates were pre-coated overnight with pan-histone antibody (Chemicon) at 4°C, followed by 1 h incubation with 3% MSD Blocker A at room temperature on shaker and 2 h incubation with 10 μg per well of tumor sample at room temperature also on shaker. MSD plates were then incubated with anti-total histone H3 antibody (Abcam) or anti–phospho-histone H3 Ser^{10} antibody (Upstate Biotechnology) for 2 h at room temperature on a shaker, followed by MSD anti-rabbit sulfo-tagged detection antibody for 1 h at room temperature also on a shaker. MSD read buffer was added, and the fluorescence was read immediately on a MSD Sector 6000. The amount of phosphorylated histone H3 was normalized to the total amount of histone H3 to obtain the relative histone H3 phosphorylation.

PET Imaging

[^{18}F]FLT was synthesized and characterized as previously reported (31). Before imaging studies, size-matched tumor-bearing mice were randomized into four cohorts (day 2 vehicle and CCT129202-treated groups, and day 7 vehicle and CCT129202-treated groups) and given daily doses of CCT129202 at 100 mg/kg body weight or vehicle i.p. for 2 (three doses) or 7 days (eight doses). The last drug dose was injected 2 h before imaging. The scanning procedure and the image analysis have been described previously (31). Tumor radioactivity uptake normalized that of heart at 60 min post-injection (NUV_{60}) was used for comparison. The area under the nTAC (AUC) was

[4] Supplementary material for this article is available at Molecular Cancer Therapeutics Online (http://mct.aacrjournals.org/).

calculated as the integral from 0 to 60 min. The fractional retention of tracer (FRT) at 60 min relative to that at 1.5 min was also calculated.

All procedures involving animals were done in accordance with National Home Office regulations under the Animals (Scientific Procedures) Act 1986 and within guidelines set out by the Institute's Animal Ethics Committee and the United Kingdom Coordinating Committee for Cancer Research's Ad hoc Committee on the Welfare of Animals in Experimental Neoplasia (36).

Results

Identification and Characterization of CCT129202: A Representative of a Novel Class of Potent and Selective of Aurora Kinase Inhibitors

It is valuable to develop a range of Aurora inhibitors based on different chemical backbones. We have previously described the development of an assay for Aurora A activity suitable for high-throughput screening (33). The assay was successfully used for screening of ~70,000 compounds for Aurora A inhibition. One identified inhibitor was further modified to produce the imidazopyridine inhibitor CCT129202 (ref. 32; Fig. 1A). In *in vitro* kinase assays using purified recombinant proteins, CCT129202 inhibited Aurora A, Aurora B, and Aurora C, with IC_{50} values of 0.042 ± 0.022, 0.198 ± 0.05, and 0.227 ± 0.064 μmol/L, respectively. To define the biochemical mechanism of action of CCT129202, we examined the effect of increasing concentration of ATP on the inhibitory activity of the compound using steady-state analysis. The results showed that the CCT129202 is an ATP-competitive inhibitor of recombinant Aurora A kinase with a K_i of 49.8 nmol/L (data not shown). The compound was tested in a series of *in vitro* kinase assays using different recombinant kinases. CCT129202 showed high selectivity for the Aurora kinases over a broad range of 13 other kinases tested at 1 μmol/L concentration (Fig. 1B). We evaluated the activity of CCT129202 against different human tumor cell lines, and this compound was found to induce apoptosis with half-maximal growth inhibition (GI_{50}) values that ranged between 0.08 and 1.7 μmol/L (Fig. 1C). All cell lines tested showed increased expression levels of Aurora A and Aurora B in comparison with the expression levels of the two proteins in normal tissue controls (refs. 5, 28, and data not shown). Aurora A and Aurora B levels were affected only at very high concentrations of the inhibitor (>5× GI_{50}) possibly due to cell toxicity (data not shown). We did not find an obvious relationship between the sensitivity of cells in the growth inhibition assay and the protein levels of the Aurora kinases within the cell lines analyzed. Differences in sensitivity might rather be associated with different genetic backgrounds of the cell lines, such as lack of proteins associated with Aurora kinases (28).

CCT129202 Induces Aberrant Mitosis that Leads to Apoptosis

It was of interest to test the effect of CCT129202 on the cell cycle progression, growth, and viability of human tumor cells. We examined the effects of CCT129202 on the cell cycle profile of the HCT116 human colon tumor cell line by flow cytometry. CCT129202 caused the accumulation of HCT116 cells with ≥4*N* DNA content (Fig. 2A). Furthermore, a sub-G_1 cell population can be seen at 24 h after CCT129202 treatment, which is indicative of apoptosis (Fig. 2A). These results were confirmed by an increase in cleaved PARP in treated cells (Fig. 2B).

It has been reported that the inhibition of Aurora A results in G_2-M accumulation and spindle defects (29), whereas inhibition of Aurora B abrogates the mitotic

A

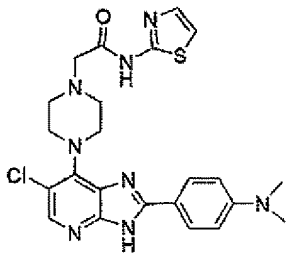

CCT129202

B

Kinase	CCT129202 (% inhibition at 1 μM)
Aurora-A	92
Aurora-B	60
ABL1	8
AKT1	2
CDK2/cyclinA	9
CHK1	7
CK2α1	7
EGFR	4
FGFR3	27
GSK3β	15
IKKβ	8
MAPK14	10
PDGFRβ	22
PKA	3
CRAF	0

C

Cell Line	GI_{50} (μM)
Colo205	0.46
SW620	0.7
HCT116	0.35
HT29	0.5
KW12	1.2
HeLa	0.2
A2780	0.3
OVCAR8	1
MDA-MB-157	1.7
MV4-11	0.08

Figure 1. CCT129202 is a selective Aurora kinase inhibitor that inhibits proliferation of several human tumor cell lines. **A**, chemical structure of CCT129202 [2-(4-(6-chloro-2-(4-(dimethylamino)phenyl)-3*H*-imidazo[4,5-*b*]pyridin-7-yl)piperazin-1-yl)-*N*-(thiazol-2-yl)acetamide], a derivative of the piperazinyl imidazo[4,5-*b*]pyridine scaffold. **B**, activity of the CCT129202, against a panel of protein kinases at a concentration of 1 μmol/L. **C**, cell growth inhibition assays of CCT129202 in a panel of human tumor cell lines.

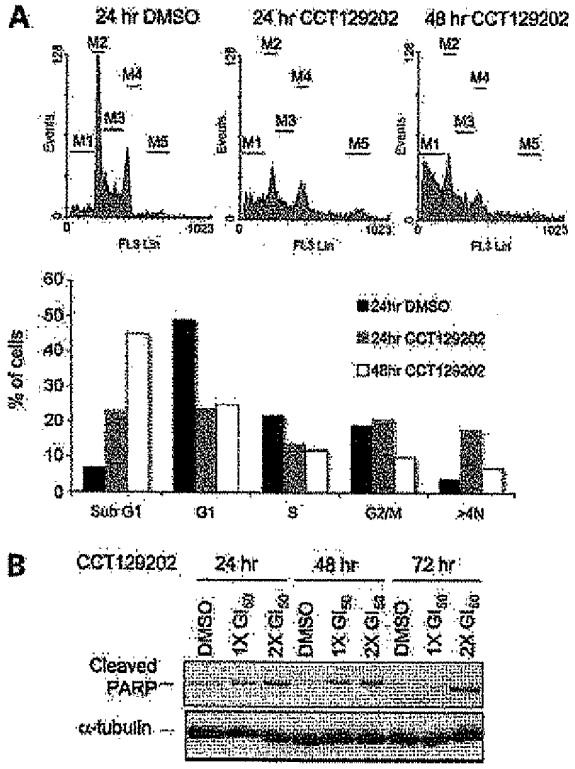

Figure 2. CCT129202 induces accumulation of cells with ≥4*N* DNA and apoptosis. **A,** HCT116 cells were treated with 700 nmol/L (2 × GI_{50}) of CCT129202 for 24 and 48 h or 0.1% DMSO vehicle control. DNA content was assessed by flow-cytometric analysis of cells labeled with propidium iodine (*FL3Lin*; *top*). Percentage of HCT116 cells in the sub-G_1, G_1, S, G_2-M, and >4*N* DNA following treatment with 700 nmol/L of CCT129202 for 24 and 48 h or 0.1% DMSO vehicle (*bottom*). *M1*, sub-G_1; *M2*, G_1; *M3*, S; *M4*, G_2-M; *M5*, >4*N* DNA. **B,** detection of apoptosis in HCT116 cells with cleaved PARP was assessed by immunoblotting. Tubulin was used as a loading control. *GI*, growth inhibition.

checkpoint leading to aneuploidy due to cytokinesis failure (25). We examined the effects of CCT129202 on the cell cycle status of aphidicolin-synchronized cells by determining DNA content by flow cytometry. Figure 3A shows the DNA content of cells in each phase of the cell cycle. Approximately 28% of CCT129202-treated HCT116 cells remain temporarily in G_2-M 12 h after the release from aphidicolin compared with 16% in G_2-M in the untreated cells (P = 0.0009; Fig. 3B). Moreover, HCT116 cells treated with CCT129202 showed abrogation of nocodazole arrest 2 to 4 h earlier than untreated cells (Fig. 3C), consistent with Aurora B inhibition (25). Similar results were obtained with paclitaxel-arrested HCT116 cells (data not shown). CCT129202 abrogated paclitaxel-induced arrest of HCT116 cells 6 h earlier than nontreated cells.

Aurora A and Aurora B play an important role in centrosome maturation, spindle formation, and cytokinesis (7). Therefore, inhibition of Aurora kinases disturbs the progression of cells through normal mitosis, resulting in aberrant mitotic spindles. To determine the effects of CCT129202 on spindle formation, HCT116 or HeLa cells were incubated with DMSO or CCT129202 for 24 h, and the morphology of mitotic spindles was examined by immunofluorescence microscopy. As expected, in DMSO-treated cells, normal metaphase and anaphase spindles were readily apparent, as shown using an α-tubulin antibody (Fig. 3D). CCT129202-treated HCT116 (Fig. 3D) and HeLa cells (data not shown) induced the formation of abnormal mitotic spindles, with various degrees of chromosome alignment defects. This phenotype is consistent with the inhibition of Aurora kinase activity as shown by the use of small interfering RNA (siRNA) and other Aurora kinase inhibitors (25, 29).

CCT129202 Decreases Histone H3 Phosphorylation and Causes p53 Stabilization

Aurora B has been shown to phosphorylate histone H3 at Ser^{10} (13). Inhibition of histone H3 phosphorylation by CCT129202 was confirmed in several human tumor cell lines (data not shown). Using a Ser^{10} phospho-specific α-histone H3 antibody, we have developed an assay (CELISA), in which we measure the inhibition of H3 phosphorylation after inhibitor treatment. Time course experiments in HCT116 cells treated with CCT129202 showed that the inhibitory effect on the phosphorylation of the histone H3 occurred as early as 15 min after treatment (Fig. 4A). These results are consistent with the inhibition of Aurora B by CCT129202.

We next looked for molecular evidence that CCT129202 targets Aurora A in cells. It has been reported that Aurora A phosphorylates p53 at Ser^{315} (37). This phosphorylation leads to p53 degradation in an MDM2-dependent manner. We used this information to test if CCT129202 also inhibited Aurora A in cells. Using the DO1 antibody against p53 protein, we have developed a CELISA assay in which p53 stabilization can be measured after inhibitor treatment. HCT116 cells treated for 24 h with CCT129202 or the previously described Aurora kinase inhibitor VX-680 (27) showed p53 stabilization compared with the DMSO-treated control HCT116 cells (Fig. 4B). These results are consistent with the inhibition of Aurora A by CCT129202.

CCT129202 Inhibits Phosphorylation of Histone H3 in HCT116 Tumor Xenografts in Athymic Mice and Causes Tumor Growth Inhibition

Before investigating the therapeutic activity of CCT129202 in HCT116 human tumor xenografts in athymic mice, the pharmacokinetic properties of the compound were first assessed in non–tumor-bearing mice. Following i.v. administration of 5 mg/kg of CCT129202 to mice, the compound had a reasonable half-life of 0.94 h and a low clearance (0.07 L/h). The volume of distribution was 0.053 L, and the plasma concentrations were above IC_{50} for up to 3 h. *In vitro* metabolism studies showed that CCT129202 was metabolically stable, with only a ~25% decrease in parent compound following incubation with mouse liver microsomes for 30 min. This was in good agreement with the clearance measured *in vivo*.

Tumor levels of CCT129202 were determined following a single dose of 100 mg/kg to athymic mice bearing s.c. HCT116 colon cancer xenografts. We examined the inhibition of histone H3 phosphorylation as a biomarker of Aurora B inhibition *in vivo*. Reduction of histone H3 phosphorylation by ~50% was observed in tumors 30 min following the administration of CCT129202 as measured by electroluminescent immunoassay (Fig. 4C), demonstrating the inhibition of Aurora B kinase. The effect started to disappear 2 h after treatment, compatible with the half-life of the compound.

Based on these promising pharmacokinetic-pharmacodynamic results, we next examined the effects of CCT129202 on the growth of HCT116 xenografts. CCT129202 was given i.p at 100 mg/kg once a day for a period of 9 days to HCT116 tumor-bearing athymic mice. Significant tumor growth inhibition was observed compared with the vehicle-treated mice (% treated versus control, 57.7; $P = 0.0355$, Mann Whitney U test; Fig. 4D). CCT129202 was well tolerated, with <5% body weight changes compared with vehicle controls.

CCT129202 Causes p21 Up-regulation, Rb Hypophosphorylation, and H2F-Dependent TK1 Down-regulation

To identify genes that are deregulated by the Aurora kinase inhibitor CCT129202 and that may be potential additional biomarkers, we did a gene expression microarray analysis in HCT116 human colon tumor cells. HCT116 cells were treated for different time periods with 1× GI_{50} CCT129202 or with vehicle (0.1% DMSO). cDNA microarrays of 28K cDNA clones were used to analyze gene expression changes. The complete list is supplied as supplementary data (Supplementary Table S1).[4] These comprise E2F-regulated genes, together with a group of genes that play a significant role in mitosis. A decrease in expression of mitotic checkpoint genes such as BUB1, BUB3, MAD2L1, and TTK was observed in response to CCT129202, most likely as a consequence of mitotic abrogation caused by the inhibition of Aurora B (Supplementary Table S1; Supplementary Fig. S1).[4] Among the genes we found to show expression changes in HCT116 cells treated with CCT129202 was the cyclin-dependent kinase (cdk) inhibitor *p21*, a regulator of the Rb/E2F pathway. The differential regulation of *p21* was confirmed at the protein level using immunoblot assays. A time-dependent up-regulation of p21 was observed following CCT129202 treatment (Fig. 5A). The specificity of the effect of CCT129202 on the p21 regulation was tested using the inactive analogue CCT129127 (2-(4-(2-(4-(dimethylamino)-phenyl)-3*H*-imidazo[4,5-*b*]pyridin-7-yl)piperazin-1-yl)-*N*-(thiazol-2-yl)acetamide). HCT116 cells were treated with

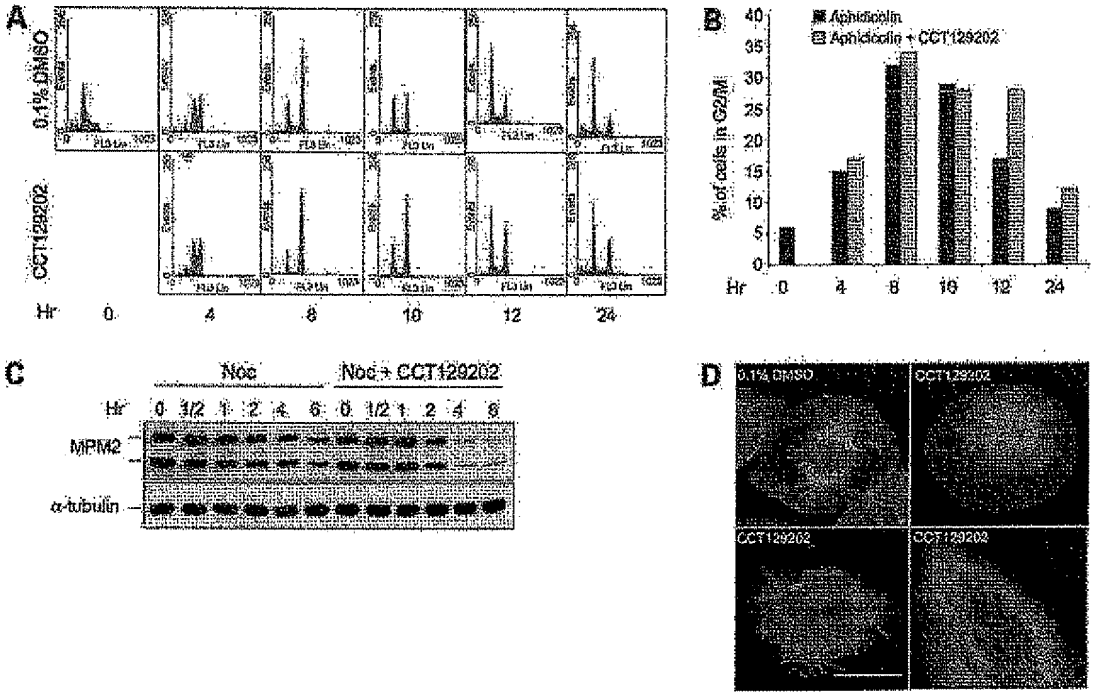

Figure 3. Effect of CCT129202 on cell cycle and cell morphology. **A**, HCT116 cells were released from aphidicolin-induced G_1-S block in the presence of 350 nmol/L (GI_{50}) of CCT129202 or DMSO vehicle. DNA content of cells collected at the indicated time points was assessed by flow cytometry analysis of cells labeled with propidium iodine. **B**, percent of HCT116 cells in G_2-M phase of the cell cycle ($P = 0.0009$). **C**, HCT116 cells were treated with nocodazole alone or in combination with 350 nmol/L CCT129202. At the indicated time points, cells were lysed, and the MPM2 phosphorylation was assessed by immunoblotting. Tubulin was used as a loading control. **D**, HCT116 cells were treated with CCT129202 or vehicle control (0.1% DMSO) for 24 h. α-Tubulin staining (*green*) was assessed by immunocytochemistry. 4′,6-Diamidino-2-phenylindole staining (*blue*) indicates the DNA content. *Bar*, 1 cm = 25 μm.

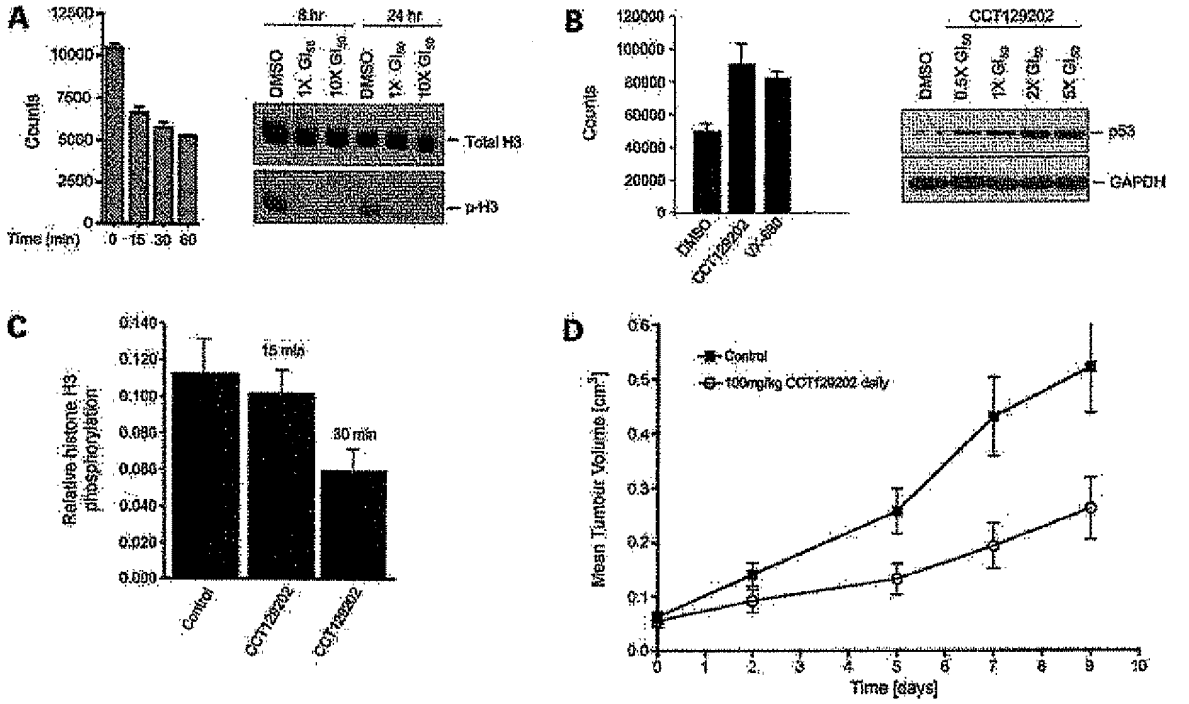

Figure 4. CCT129202 reduces phosphorylation of histone H3, stabilizes p53, and inhibits growth of HCT116 human colon cancer xenografts in athymic mice. **A,** HCT116 cells treated with CCT129202, and the relative levels of phosphorylated histone H3 was assessed at the indicated time points by CELISA (*left*). HCT116 cells were treated with different concentrations of CCT129202 or 0.1% DMSO for 8 and 24 h, and the levels of total histone H3 and phosphorylated histone H3 were assessed by immunoblotting after histone extraction (*right*). **B,** HCT116 cells were treated with 350 nmol/L CCT129202, 160 nmol/L VX-680, or 0.1% DMSO control for 24 h, and the levels of p53 were assessed by CELISA (*left*). HCT116 cells treated with different concentrations of CCT129202 or 0.1% DMSO control at 24 h and the levels of p53 were assessed by immunoblotting. GAPDH was used as a loading control (*right*). **C,** athymic mice bearing HCT116 human colon cancer xenografts were treated i.p. with a single dose of 100 mg/kg of CCT129202 or 0.1% DMSO vehicle control, and the phosphorylation of histone H3 was assessed in tumors at different time points by electrochemiluminescence immunoassay. **D,** athymic mice bearing established HCT116 tumors were treated i.p. with either vehicle control (■) or CCT129202 (○) at a dose of 100 mg/kg/day for 9 d. $n = 5$ per group. *Points,* mean tumor volumes; *bars,* SE. *GI,* growth inhibition.

equimolar concentrations of the active or inactive analogues. p21 up-regulation was only observed in the HCT116 cells treated with CCT129202 (Fig. 5B).

We next investigated whether p21 up-regulation by CCT129202 was also seen in cell lines with deregulated p53. In HT29 and HeLa cells, p53 is mutated or inactivated, respectively. HT29 and HeLa cells were treated with different concentrations of CCT129202 for 24 h. Although the overall p21 protein levels were less than in HCT116 cells, which has wild-type p53, up-regulation of p21 was seen in both cell lines, indicating that a minor p53-independent inhibition also takes place (Fig. 5C). Through its inhibitory effects on cdks, p21 decreases the phosphorylation of the Rb protein. When hypophosphorylated, Rb is in a complex with the transcription factor E2F and thereby inhibits the activity of E2F in regulating proteins that play a role in the S-phase entry. To examine the effect of CCT129202 on the p21/Rb pathway, we first examined the phosphorylation status of the Rb protein. Figure 5D shows that, in CCT129202-treated HCT116 cells, the Rb protein is hypophosphorylated in a concentration-dependent manner. One of the genes known to be regulated by E2F is that encoding TK1 (38). We therefore examined the effect of CCT129202 on TK1 levels in HCT116 cells. As shown in Fig. 5D, TK1 expression was decreased in a concentration-dependent manner in HCT116 cells. The down-regulation of TK1 levels was also confirmed in p53-mutant HT29 cells (Supplementary Fig. S2).[4] To further confirm that the deregulation of p21/Rb/E2F pathway was a consequence of Aurora inhibition, we also tested the known pan-Aurora inhibitor VX-680. HCT116 cells treated with this inhibitor showed similar kinetics of p21 up-regulation, Rb hypophosphorylation, and TK1 down-regulation, consistent with the view that this effect is due to Aurora inhibition (Supplementary Fig. S3).[4] The inactive analogue CCT129127 showed no effect on Rb phosphorylation or TK1 in HCT116 cells (data not shown). In summary, these data suggest that Aurora kinase inhibition affects the p21/Rb/E2F pathway, and that the effect on TK1 expression might be used as a biomarker of pathway inhibition downstream of Aurora inhibition by CCT129202.

CCT129202 Decreases [^{18}F]FLT Uptake

The alterations described above in p21, phosphorylation of Rb and TK1 levels that are mediated by CCT129202,

together with the data demonstrating that TK1 is required for [^{18}F]FLT uptake *in vivo* (39), led us to hypothesize that [^{18}F]FLT-PET might be used to monitor the biological activity of CCT129202 *in vivo*. [^{18}F]FLT-PET images of mice bearing HCT116 colon cancer xenografts are shown in Fig. 6A. The data illustrated are intensity-normalized images from vehicle control and CCT129202-treated mice. Whereas no obvious difference in image intensity was observed between CCT129202-treated and controls at the early time point (day 2), there was a marked difference at day 7. CCT129202 reduced the retention of [^{18}F]FLT-derived radioactivity at day 7, as illustrated by the quantitative normalized time versus radioactivity curves (nTACs; Fig. 6B), in keeping with a reduction in proliferation with treatment. All three parameters of [^{18}F]FLT retention (mean NUV60, FRT, and AUC) were unchanged on day 2 of CCT129202 treatment, but were significantly reduced at day 7 compared with control (Fig. 6C). Of note, NUV60, FRT, and AUC for tumor 15 shown in Fig. 6A (day 7, CT129202) were in the lower 50% of the respective mean day 7 CCT129202-treated values.

We investigated the effect of CCT129202 on tumor TK1 protein levels in HCT116 tumor xenografts in treated mice. Figure 6D shows TK1 protein levels in pretreatment tumors on day 7 vehicle- and CCT129202-treated HCT116 tumors. TK1 levels decreased after treatment with CCT129202. These findings are consistent with the reduction of the [^{18}F]FLT uptake as determined by PET.

Discussion

Because Aurora kinases are overexpressed in a variety of human tumors leading to deregulation of mitosis, they represent important targets for anticancer drug development. We have discovered the novel ATP-competitive imidazopyridine inhibitor CCT129202, a representative of a new class of small-molecule inhibitors with potent activity against Aurora kinases. The compound showed no substantial cross-reactivity with a panel of other kinases tested, indicating considerable selectivity. CCT129202 inhibited the growth of a range of human tumor cell lines. The sensitivity might be associated with the inhibition of all Aurora kinases, in particular Aurora A and Aurora B, in addition to a different genetic background among the cell lines. First, there is evidence that links Aurora A with p53 in carcinogenesis. It has been shown that Aurora A phosphorylates p53, leading to its inactivation either by degradation or by suppression of its transcriptional activity (37, 40). Our own results are consistent with these previous studies because we showed that inhibition of Aurora A by CCT129202 resulted in the stabilization of p53 levels in tumor cells. Second, Aurora B has been shown to phosphorylate histone H3 at Ser^{10}, and phosphorylation of histone H3 is associated with the induction of neoplastic transformation (41). Consistent with this, we showed that CCT129202 is a potent inhibitor of the phosphorylation of histone H3 in tumor cells. Antitumor activity was seen in human tumor xenografts at a dose of 100 mg/kg, with

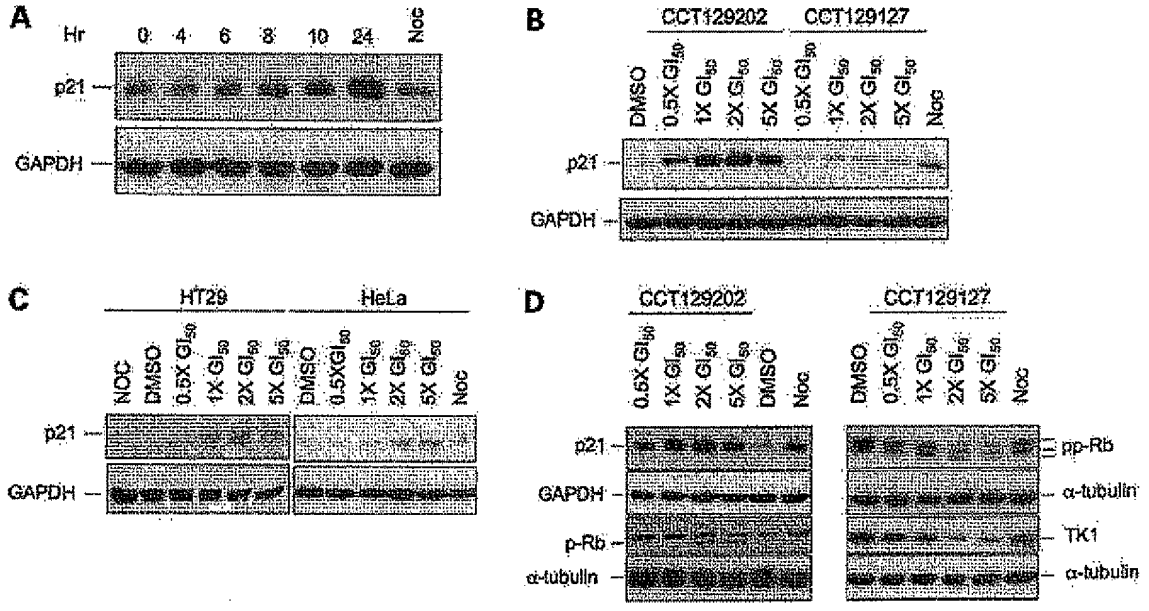

Figure 6. CCT129202 up-regulates p21, inhibits Rb phosphorylation, and decreases TK1 expression. **A**, HCT116 cells were treated with 350 nmol/L CCT129202 at different time points or 50 ng/mL nocodazole for 24 h, and p21 expression was assessed at the indicated time points by immunoblotting. **B**, HCT116 cells were treated with different concentrations of CCT129202, an equimolar concentration of the inactive analogue CCT129127, 50 ng/mL nocodazole, or 0.1% DMSO vehicle control for 24 h, and p21 expression was assessed by immunoblotting. **C**, HT29 and HeLa cells were treated with different concentrations of CCT129202, nocodazole, or 0.1% DMSO control for 24 h, and p21 expression was assessed by immunoblotting. **D**, HCT116 cells were treated with different concentrations of CCT129202, nocodazole, or 0.1% DMSO control for 24 h, and the p21, hypophosphorylated Rb (p-Rb), total Rb (pp-Rb), and TK1 expression levels were assessed by immunoblotting. GAPDH and tubulin were used as loading control. *GI*, growth inhibition.

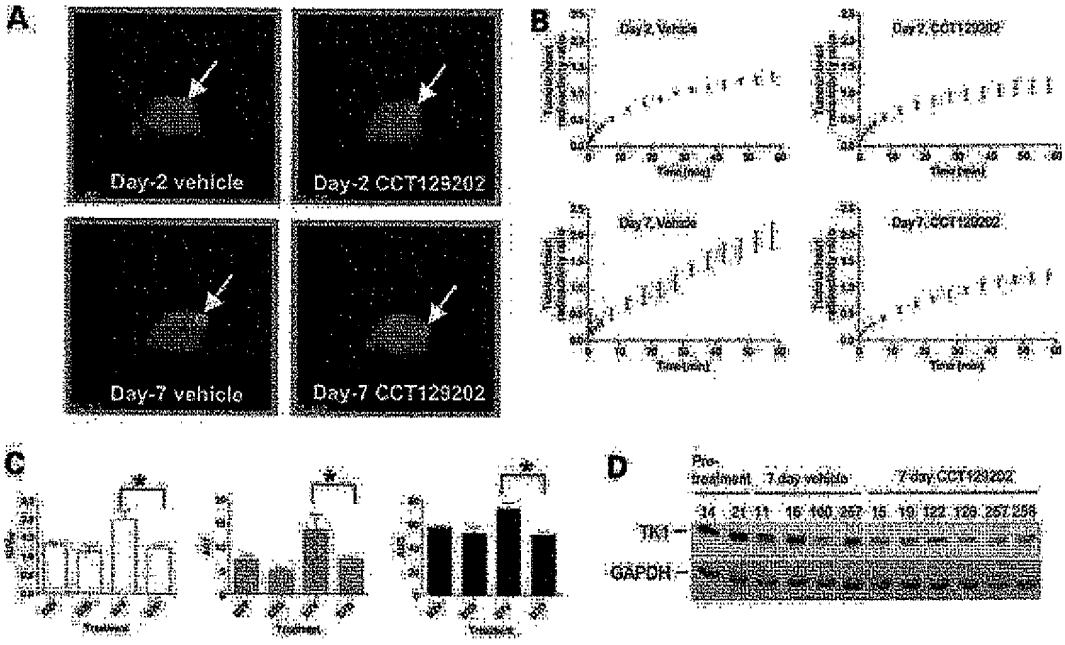

Figure 6. [^{18}F]FLT-PET studies of CCT129202. **A,** transverse (0.5 mm) PET images of vehicle and CCT129202-treated athymic mice bearing HCT116 human colon cancer xenografts on the days indicated. **B,** summary normalized time versus radioactivity curves in HCT116 tumors under the different treatment conditions. For each mouse, five image slices of tumor were averaged for each of the 19 time points and normalized to the mean activity from five slices of the heart region (blood volume). Data were mean ± SD for four to six mice. **C,** summary of kinetic parameters—NUV60, FRT, and AUC—determined as described in Materials and Methods for the different conditions of day 2 vehicle, day 2 CCT129202, day 7 vehicle, and day 7 CCT129202 (2V, 2D, 7V, and 7D, respectively). *Bar*, SD. *, $P < 0.02$ (Mann-Whitney test). **D,** athymic mice bearing HCT116 human colon cancer xenografts were treated i.p. with 100 mg/kg of CCT129202 or vehicle control at days 2 and 7, and the TK1 protein levels were assessed in tumors by immunoblotting on the days indicated. GAPDH was used as loading control.

evidence of Aurora inhibition provided by decreased phosphorylation of histone H3. Moreover, CCT129202-treated HCT116 or HeLa cells were able to abrogate both the temporarily induced mitotic arrest due to Aurora A inhibition or nocodazole-induced mitotic arrest. This abrogation was possibly due to the reduction in the expression of mitotic checkpoint proteins such as BubR1, Bub1 Mad2L1, and TTK that we observed upon treatment with CCT129202. When the mitotic checkpoint is compromised, cells can exit mitosis without undergoing cytokinesis with ≥4*N* DNA content. The observed abnormal mitotic spindles and multinucleation of tumor cells treated with CCT129202 resembles the phenotype induced in cells by inhibiting Aurora A and Aurora B using siRNA or other chemical inhibitors (25, 29).

Pharmacodynamic markers are essential for the rational development of molecular therapeutics (30, 42), including Aurora inhibitors. They can be used to show proof of concept for the proposed mechanism of drug action in phase I studies, as well as to help select the optimal dose schedule. Given the desirability of avoiding invasive methods, particularly involving tumor biopsies (30, 42), it would be of interest to develop noninvasive imaging methods to measure the biological activity of Aurora kinase inhibitors. Here, we have shown, using a molecular profiling approach, that p21 is induced in tumor cells by Aurora inhibitors. Although the p21 induction was more intense in cells with wild-type p53, human tumor cells with mutated or inactivated p53 also showed up-regulation of p21. This suggests that the effect is mainly p53 dependent, with a minor p53-independent component. Based on these findings, we examined the effect of CCT129202 on the pathway downstream of p21, in particular the Rb/E2F pathway, to identify potential end points. Of particular interest was that the TK1 protein was modulated by CCT129202. TK1 is required for [^{18}F]FLT uptake *in vivo* (39). Therefore, we hypothesized that we may be able to visualize a decrease in [^{18}F]FLT uptake using [^{18}F]FLT-PET following the inhibition of Aurora kinases by CCT129202. As predicted, a decrease in [^{18}F]FLT was shown. [^{18}F]FLT-PET is a validated preclinical and clinical noninvasive imaging approach commonly used to measure tumor cell proliferation (31). Taken together, these observations support the *in vivo* use of [^{18}F]FLT imaging for detecting the biological effects of CCT129202. CCT129202 was used *in vivo* at doses that were associated with the inhibition of phosphorylation of histone H3, up-regulation of p21, and reduction of tumor growth. In addition, the significant reduction of NUV60, FRT, and AUC at day 7, as measured by PET, mirrored the changes in TK1 protein levels.

Although more potent inhibitors of Aurora have been described (27), CCT129202 is representative of an imidazopyridine novel chemical series. Aurora inhibitors based on distinct chemical scaffolds could have potential advantages, for example, in term of selectivity and therapeutic index, and it is important that the different Aurora inhibitory chemotypes are advanced into the clinic. We are continuing to optimize this new series, in particular to improve *in vivo* potency. The biomarkers reported here will be used for this. In addition, this should be suitable for use with other Aurora inhibitors.

In conclusion, Aurora is now recognized as an important molecular target for anticancer drug discovery. In this study, we have shown that the imidazopyridine CCT129202 is a novel, potent, and selective Aurora kinase inhibitor *in vitro* and *in vivo*. Molecular and biochemical changes such as p21 induction, hypophosphorylation of pRB, reduction in TK1 protein, and histone H3 phosphorylation are associated with CCT129202 treatment of human tumor cells and xenografts. In addition, CCT129202 induces a reduction in tumor [^{18}F]FLT retention, detectable by noninvasive PET imaging. These favorable attributes of CCT129202 warrant further investigation of the imidazopyridine compound class as therapeutic agents. The molecular, biochemical, and imaging methods described in this report could form an integral part of the preclinical and early clinical evaluation of this and other classes of Aurora kinase inhibitors.

Acknowledgments

We thank Chroma Therapeutics (Oxford, United Kingdom) for providing the kinome profiling results, D. Moffat and A. Drummond from Chroma Therapeutics, A. Ashworth and C. Isacke from The Breakthrough Breast Cancer Research Centre, and all the members of the Cancer Drug Target Discovery Team, The Institute of Cancer Research, for critically reading and discussing the manuscript. We also thank Sharon Gowan for help with tumor sample processing.

References

1. Bischoff JR, Plowman GD. The Aurora/Ipl1p kinase family: regulators of chromosome segregation and cytokinesis. Trends Cell Biol 1999;9:454–9.

2. Carmena M, Earnshaw WC. The cellular geography of Aurora kinases. Nat Rev Mol Cell Biol 2003;4:842–54.

3. Giet R, Prigent C. Aurora/Ipl1p-related kinases, a new oncogenic family of mitotic serine-threonine kinases. J Cell Sci 1999;112:3591–601.

4. Nigg EA. Mitotic kinases as regulators of cell division and its checkpoints. Nat Rev Mol Cell Biol 2001;2:21–32.

5. Bischoff JR, Anderson L, Zhu Y, et al. A homologue of *Drosophila* Aurora kinase is oncogenic and amplified in human colorectal cancers. EMBO J 1998 1;17:3052–65.

6. Kimura M, Matsuda Y, Yoshioka T, Okano Y. Cell cycle-dependent expression and centrosome localization of a third human aurora/Ipl1-related protein kinase, AIK3. J Biol Chem 1999;274:7334–40.

7. Dutertre S, Descamps S, Prigent C. On the role of Aurora A in centrosome function. Oncogene 2002;2:6175–83.

8. Adams RR, Carmena M, Earnshaw WC. Chromosomal passengers and the (Aurora) ABCs of mitosis. Trends Cell Biol 2001;11:49–54.

9. Hirota T, Kunitoku N, Sasayama T, et al. Aurora A and an interacting activator, the LIM protein Ajuba, are required for mitotic commitment in human cells. Cell 2003;114:585–98.

10. Meraldi P, Honda R, Nigg EA. Aurora kinases link chromosome segregation and cell division to cancer susceptibility. Curr Opin Genet Dev 2004;14:29–36.

11. Bishop JD, Schumacher JM. Phosphorylation of the carboxyl terminus of inner centromere protein (INCENP) by the Aurora B kinase stimulates Aurora B kinase activity. J Biol Chem 2002;277:27577–80.

12. Honda R, Korner R, Nigg EA. Exploring the functional interactions between Aurora B, INCENP, survivin in mitosis. Mol Biol Cell 2003;14:3325–41.

13. Hsu JY, Sun ZW, Li X, et al. Mitotic phosphorylation of histone H3 is governed by Ipl1/Aurora kinase and Glc7/PP1 phosphatase in budding yeast and nematodes. Cell 2000;102:279–91.

14. Meraldi P, Honda R, Nigg EA. Aurora A overexpression reveals tetraploidization as a major route to centrosome amplification in p53$^{-/-}$ cells. EMBO J 2002;21:483–92.

15. Zhou H, Kuang J, Zhong L, et al. Tumour amplified kinase STK15/BTAK induces centrosome amplification, aneuploidy and transformation. Nat Genet 1998;20:189–93.

16. Gritsko TM, Coppola D, Paciga JE, et al. Activation and overexpression of centrosome kinase BTAK/Aurora A in human ovarian cancer. Clin Cancer Res 2003;9:1420–6.

17. Tanaka T, Kimura M, Matsunaga K, Fukada D, Mori H, Okano Y. Centrosomal kinase AIK1 is overexpressed in invasive ductal carcinoma of the breast. Cancer Res 1999;59:2041–4.

18. Reichardt W, Jung V, Brunner C, et al. The putative serine/threonine kinase gene STK15 on chromosome 20q13.2 is amplified in human gliomas. Oncol Rep 2003;10:1275–9.

19. Araki K, Nozaki K, Ueba T, Tatsuka M, Hashimoto N. High expression of Aurora B/Aurora and Ipli-like midbody-associated protein (AIM-1) in astrocytomas. J Neurooncol 2004;67:53–64.

20. Chieffi P, Troncone G, Caleo A, et al. Aurora B expression in normal testis and seminomas. J Endocrinol 2004;181:263–70.

21. Sorrentino R, Libertini S, Pallante PL, et al. Aurora B overexpression associates with the thyroid carcinoma undifferentiated phenotype and is required for thyroid carcinoma cell proliferation. J Clin Endocrinol Metab 2005;90:928–35.

22. Ewart-Toland A, Briassouli P, de Koning JP, et al. Identification of Stk6/STK15 as a candidate low-penetrance tumor-susceptibility gene in mouse and human. Nat Genet 2003;34:403–12.

23. Briassouli P, Chan F, Savage K, Reis-Filho JS, Linardopoulos S. Aurora A regulation of nuclear factor-κB signaling by phosphorylation of IκBα. Cancer Res 2007;67:1689–95.

24. Sun C, Chan F, Briassouli P, Linardopoulos S. Aurora kinase inhibition down-regulates NF-κB and sensitises tumour cells to chemotherapeutic agents. Biochem Biophys Res Commun 2007;352:220–5.

25. Ditchfield C, Johnson VL, Tighe A, et al. Aurora B couples chromosome alignment with anaphase by targeting BubR1, Mad2, and Cenp-E to kinetochores. J Cell Biol 2003;161:267–80.

26. Hauf S, Cole RW, LaTerra S, et al. The small molecule Hesperadin reveals a role for Aurora B in correcting kinetochore-microtubule attachment and in maintaining the spindle assembly checkpoint. J Cell Biol 2003;161:281–94.

27. Harrington EA, Bebbington D, Moore J, et al. VX-680, a potent and selective small-molecule inhibitor of the Aurora kinases, suppresses tumor growth *in vivo*. Nat Med 2004;10:262–7.

28. Soncini C, Carpinelli P, Gianellini L, et al. PHA-680632, a novel Aurora kinase inhibitor with potent antitumoral activity. Clin Cancer Res 2006;12:4080–9.

29. Manfredi MG, Ecsedy JA, Meetze KA, et al. Antitumor activity of MLN8054, an orally active small-molecule inhibitor of Aurora A kinase. Proc Natl Acad Sci U S A 2007;104:4106–11.

30. Workman P, Aboagye EO, Chung YL, et al. Minimally invasive pharmacokinetic and pharmacodynamic technologies in hypothesis-testing clinical trials of innovative therapies. J Natl Cancer Inst 2006;98:580–98.

31. Leyton J, Alao JP, Da Costa M, et al. *In vivo* biological activity of the histone deacetylase inhibitor LAQ824 is detectable with 3′-deoxy-3′-[^{18}F]fluorothymidine positron emission tomography. Cancer Res 2006;66:7621–9.

32. Bavetsias VME, Linardopoulos S, inventors; Chroma Therapeutics Ltd. Piperazinyl imidazopyridine Aurora inhibitors. International Publication Number WO 2007/072017 A2 June 28, 2007.

33. Sun C, Newbatt Y, Douglas L, Workman P, Aherne W, Linardopoulos S. High-throughput screening assay for identification of small molecule inhibitors of Aurora2/STK15 kinase. J Biomol Screen 2004;9:391–7.

34. Clarke PA, Hostein I, Banerji U, et al. Gene expression profiling of human colon cancer cells following inhibition of signal transduction by 17-allylamino-17-demethoxygeldanamycin, an inhibitor of the hsp90 molecular chaperone. Oncogene 2000;19:4125–33.

35. Eccles SA, Court WJ, Box GA, Dean CJ, Melton RG, Springer CJ. Regression of established breast carcinoma xenografts with antibody-directed enzyme prodrug therapy against c-erbB2 p185. Cancer Res 1994;54:5171–7.

36. Workman P TP, Balkwill F, et al. United Kingdom Coordinating Committee on Cancer Research guidelines for the welfare of animals in experimental neoplasia. Br J Cancer 1998;77:1–10.

37. Katayama H, Sasai K, Kawai H, et al. Phosphorylation by aurora kinase A induces Mdm2-mediated destabilization and inhibition of p53. Nat Genet 2004;36:55–62.

38. Johnson DG, Schwarz JK, Cress WD, Nevins JR. Expression of transcription factor E2F1 induces quiescent cells to enter S phase. Nature 1993;365:349–52.

39. Barthel H, Perumal M, Latigo J, et al. The uptake of 3′-deoxy-3′-[^{18}F]fluorothymidine into L5178Y tumours *in vivo* is dependent on thymidine kinase 1 protein levels. Eur J Nucl Med Mol Imaging 2005;32:257–63.

40. Liu Q, Kaneko S, Yang L, et al. Aurora A abrogation of p53 DNA binding and transactivation activity by phosphorylation of serine-215. J Biol Chem 2004;279:52175–82.

41. Choi HS, Choi BY, Cho YY, et al. Phosphorylation of histone H3 at serine 10 is indispensable for neoplastic cell transformation. Cancer Res 2005;65:5818–27.

42. Sarker D, Workman P. Pharmacodynamic biomarkers for molecular cancer therapeutics. Adv Cancer Res 2007;96:213–68.

EXHIBIT C

AZD1152, a Selective Inhibitor of Aurora B Kinase, Inhibits Human Tumor Xenograft Growth by Inducing Apoptosis

Robert W. Wilkinson,[1] Rajesh Odedra,[1] Simon P. Heaton,[1] Stephen R. Wedge,[1] Nicholas J. Keen,[2] Claire Crafter,[1] John R. Foster,[1] Madeleine C. Brady,[1] Alison Bigley,[1] Elaine Brown,[1] Kate F. Byth,[2] Nigel C. Barrass,[1] Kirsten E. Mundt,[1] Kevin M. Foote,[1] Nicola M. Heron,[1] Frederic H. Jung,[3] Andrew A. Mortlock,[1] F. Thomas Boyle,[1,†] and Stephen Green[1]

Abstract

Purpose: In the current study, we examined the *in vivo* effects of AZD1152, a novel and specific inhibitor of Aurora kinase activity (with selectivity for Aurora B).

Experimental Design: The pharmacodynamic effects and efficacy of AZD1152 were determined in a panel of human tumor xenograft models. AZD1152 was dosed via several parenteral (s.c. osmotic mini-pump, i.p., and i.v.) routes.

Results: AZD1152 potently inhibited the growth of human colon, lung, and hematologic tumor xenografts (mean tumor growth inhibition range, 86% to ≥100%; $P < 0.05$) in immunodeficient mice. Detailed pharmacodynamic analysis in colorectal SW620 tumor-bearing athymic rats treated i.v. with AZD1152 revealed a temporal sequence of phenotypic events in tumors: transient suppression of histone H3 phosphorylation followed by accumulation of 4N DNA in cells (2.4-fold higher compared with controls) and then an increased proportion of polyploid cells (>4N DNA, 2.3-fold higher compared with controls). Histologic analysis showed aberrant cell division that was concurrent with an increase in apoptosis in AZD1152-treated tumors. Bone marrow analyses revealed transient myelosuppression with the drug that was fully reversible following cessation of AZD1152 treatment.

Conclusions: These data suggest that selective targeting of Aurora B kinase may be a promising therapeutic approach for the treatment of a range of malignancies. In addition to the suppression of histone H3 phosphorylation, determination of tumor cell polyploidy and apoptosis may be useful biomarkers for this class of therapeutic agent. AZD1152 is currently in phase I trials.

The Aurora kinases play a critical role in mitosis and have been suggested as promising targets for cancer therapy due to their frequent overexpression in a variety of tumors (1). Compared with more established inhibitors of cell division, such as the anti-tubulins (2), novel agents that target mitotic enzymes have the potential to provide similar efficacy but with fewer side effects. Mammalian cells possess three forms of Aurora kinase (Aurora A, Aurora B, and Aurora C) that exhibit different subcellular localizations and have distinct roles (3, 4). However, it is still unclear which Aurora kinase represents the best target for anticancer therapy. Interestingly, inhibitors that target both Aurora A and Aurora B induce a failure in cell division and endoreduplication rather than a G_2-M arrest, effects that are indicative of Aurora B rather than Aurora A inhibition (5). Furthermore, it has been suggested that inhibition of Aurora B kinase overrides the effects of inhibition of Aurora A by abrogating the spindle checkpoint (6).

Several small-molecule inhibitors of Aurora kinases have been developed as anticancer agents, some of which have progressed to early clinical evaluation (7). ZM447439 (5), Hesperadin (8), and VX-680 (MK-0457; ref. 9) were the first to be described and have similar potency versus Aurora A, Aurora B, and Aurora C (reviewed in ref. 7). VX-680 also has activity versus Flt-3 and the imatinib-resistant T351I Bcr-Abl mutant kinase (10). More recently, PHA-680632, a more potent inhibitor of Aurora A (IC_{50}, 27 nmol/L) than Aurora B or Aurora C (IC_{50}, 135 and 120 nmol/L, respectively), has been described, although the phenotypic effects induced in tumor cells by this compound (i.e., decreased phosphorylation of histone H3 on Ser^{10} and polyploidy) are consistent with inhibition of Aurora B (11).

AZD1152 is a dihydrogen phosphate prodrug of a pyrazoloquinazoline Aurora kinase inhibitor [AZD1152–hydroxyquinazoline pyrazol anilide (HQPA)] and is converted rapidly to the active AZD1152-HQPA in plasma (12). AZD1152-HQPA is a highly potent and selective inhibitor of Aurora B

Authors' Affiliations: [1]AstraZeneca Pharmaceuticals, Macclesfield, Cheshire, United Kingdom; [2]Cancer and Infection Discovery, AstraZeneca Pharmaceuticals LP, Waltham, Massachusetts; and [3]AstraZeneca, Centre de Recherches, Reims, France

Received 12/15/06; revised 2/21/07; accepted 3/5/07.

The costs of publication of this article were defrayed in part by the payment of page charges. This article must therefore be hereby marked *advertisement* in accordance with 18 U.S.C. Section 1734 solely to indicate this fact.

† Deceased.

Note: This work is presented in memory of Tom Boyle.

Requests for reprints: Robert W. Wilkinson, AstraZeneca Pharmaceuticals, Alderley Park, Macclesfield, Cheshire SK10 4TG, United Kingdom. Phone: 44-1625-516661; E-mail: robert.wilkinson@astrazeneca.com.

doi:10.1158/1078-0432.CCR-06-2979

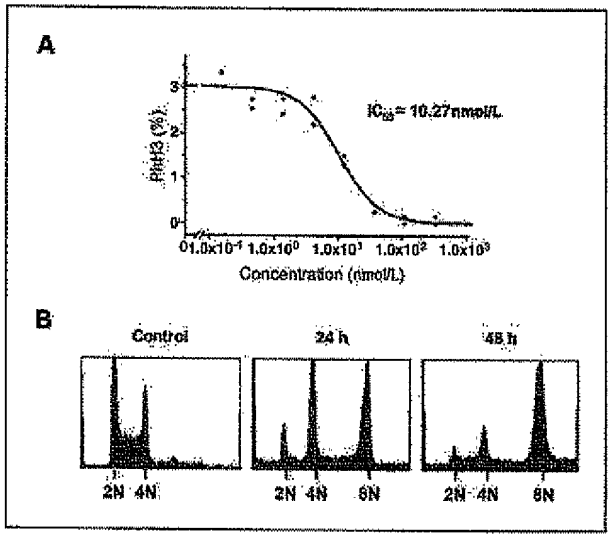

Fig. 1. AZD1152-HQPA inhibits histone H3 Ser^{10} phosphorylation and induces polyploidy *In vitro*. *A*, a typical dose-response curve showing inhibition of histone H3 phosphorylation in SW620 cells following 48-h exposure to AZD1152-HQPA. The cells were analyzed on an Array Scan II. Data are representative of at least six separate experiments. *B*, flow cytometric DNA content histograms of SW620 cells exposed to 300 nmol/L AZD1152-HQPA for 0, 24, and 48 h, showing that cells fail to divide in the presence of AZD1152-HQPA and become polyploid.

(K_i, 0.36 nmol/L) compared with Aurora A (K_i, 1,369 nmol/L) and has a high specificity versus a panel of 50 other kinases (13).[4] Consistent with inhibition of Aurora B kinase, addition of AZD1152-HQPA to tumor cells *in vitro* induces chromosome misalignment, prevents cell division, and consequently reduces cell viability and induces apoptosis (13).[4] The aim of the present study was to investigate the effects of AZD1152 administration in a panel of human tumor models *in vivo*. We show that AZD1152 (10-150 mg/kg/d, administered by s.c. osmotic mini-pump infusion over 48 h) induced time-dependent pharmacodynamic changes in tumors that were consistent with inhibition of Aurora B kinase *in vivo*, which led to significant inhibition of tumor xenograft growth. These data show that AZD1152 has the potential for activity against multiple tumor types and support investigation of this novel agent in cancer patients.

Materials and Methods

Reagents. AZD1152-HQPA and its prodrug AZD1152 were both synthesized by AstraZeneca Pharmaceuticals (12).

Cell lines. The human colorectal (SW620, Colo205, and HCT116), lung (A549 and Calu-6), and leukemia (HL-60) tumor cell lines were obtained from the American Type Culture Collection. Cells were maintained *in vitro* using L-15 (SW620) or RPMI 1640 (Colo205, HCT116, A549, Calu-6, and HL-60) culture medium (all media were from Sigma), supplemented with 10% heat-inactivated FCS (Life Technologies) and 1% glutamine (Sigma; except SW620). All cell cultures were maintained in 5% CO_2 at 37°C in a humidified incubator, with the exception of SW620, which were grown in the absence of CO_2.

[4] Submitted for publication.

In vitro studies. Phospho-histone H3 (PhH3) suppression was determined by high-content image analysis screening. SW620 cells, seeded in 96-well plates, were incubated with AZD1152-HQPA for 24 h before being fixed in 3.7% formaldehyde for 30 min. Cells were then washed with PBS, permeabilized with 0.5% Triton X-100 (Sigma), and stained with rabbit anti-PhH3 (Ser^{10}) antibodies (1:100; Upstate Cell

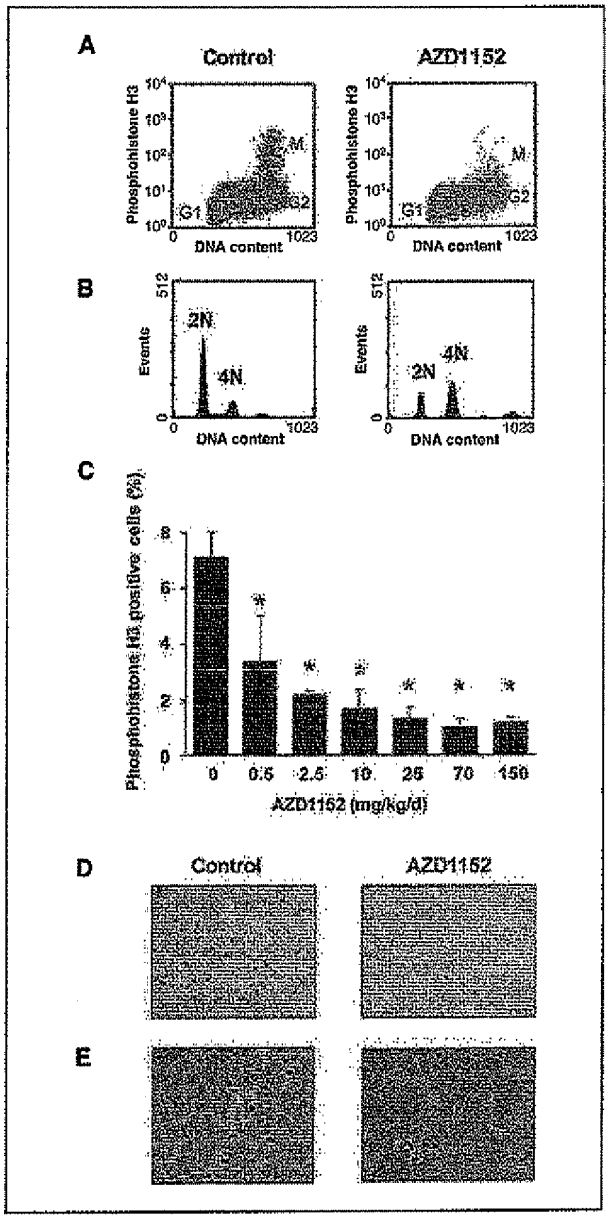

Fig. 2. AZD1152 blocks Aurora B activity in SW620 xenografts. Male nude mice were implanted subcutaneously with SW620 tumors. When tumors became palpable, animals (n = 4 per group) were dosed with either AZD1152 (0.5-150 mg/kg/d) or vehicle as a constant infusion for 48 h using a s.c. mini-pump. Following treatment, tumors were excised and analyzed for pharmacodynamic effects. Flow cytometric analysis of disaggregated tumors from animals treated with AZD1152 (70 mg/kg/d) or vehicle showing changes in PhH3 (*A*) and DNA content (*B*). Dose-response curve showing percentage PhH3-positive cells in SW620 tumors analyzed by flow cytometry. Columns, PhH3-positive cells (%); bars, SE; *, $P < 0.05$, (*C*). Representative sections of tumors treated with AZD1152 (70 mg/kg/d) or vehicle immunostained for PhH3 Ser^{10} (*D*) and H&E (*E*). Inset denotes polyploidic cell.

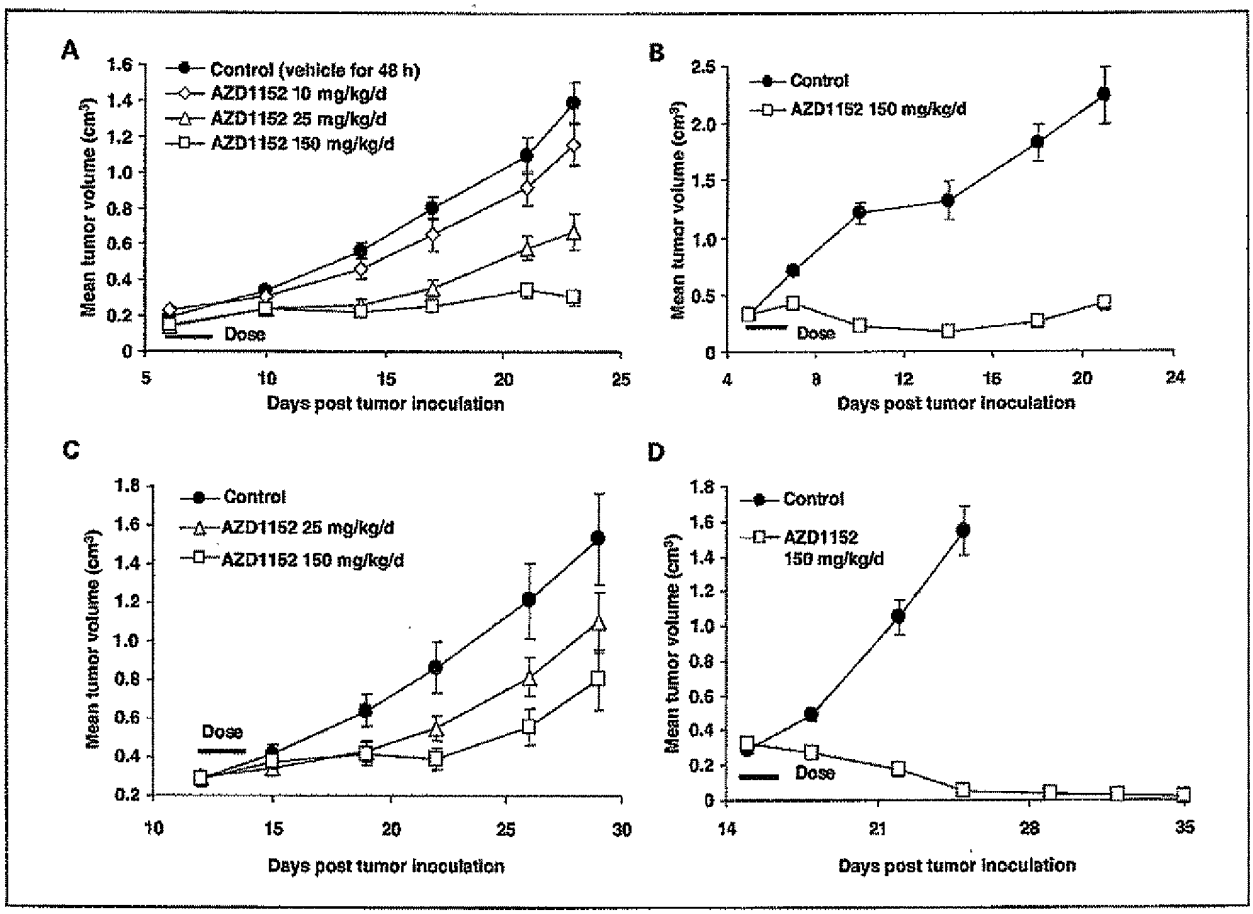

Fig. 3. AZD1152 inhibits growth in a panel of human tumor xenografts. Male nude mice bearing established SW620 (*A*), Colo205 (*B*), A549 (*C*), and HL-60 (*D*) human tumor xenografts were dosed s.c. at a constant infusion via an osmotic mini-pump for 48 h with either vehicle or AZD1152 (10-150 mg/kg/d). Mean tumor volume (cm^3) of 8 to 10 mice; vertical bars, SE; horizontal bars, duration of dosing.

Signaling Solutions) for 1 h at room temperature. After washing with PBS, cells were incubated with Alexa Fluor 488 goat anti-rabbit antibodies (1:200; Molecular Probes) and Hoechst stain (1:10,000; Molecular Probes) for 1 h at room temperature. Cellular levels of PhH3 were analyzed on the Array Scan II (Cellomics) using the Target Activation algorithm (Cellomics) to calculate the percentage of PhH3-positive cells. Individual IC_{50} values were calculated in Origin (version 7.5; OriginLab) and the data were summarized using the geometric mean (i.e., the average of the logarithmic values converted back to a base 10 number).

In vivo studies. Male Swiss nude (*nu/nu* genotype; AstraZeneca), SCID-bg mice (CB17/Icr.Cg.Prkdc^{SCID}Lyst^{bg}/Crl; Charles River), or nude rats (Nude:Hsd Han:RNU-rnu; AstraZeneca) were housed in negative pressure isolators (PFI Systems Ltd.) or in an individually ventilated cage system (Tecniplast Ltd.). Experiments were conducted on 8- to 12-week-old animals in full accordance with the United Kingdom Home Office Animal (Scientific Procedures) Act 1986. Human tumor xenografts were established by s.c. injecting 100 to 200 μL tumor cells (between 1×10^6 and 1×10^7 cells mixed 50:50 with Matrigel; Becton Dickinson) on the flank. Animals were randomized into treatment groups (n = 8-11 per group) when tumors reached a defined palpable size (0.2-0.3 cm^3 and 0.5-1 cm^3 for mice and rats, respectively). AZD1152 was prepared in Tris buffer (pH 9) and administered either as a bolus injection (i.v. or i.p.) or as a continuous 48-h infusion via s.c. implanted osmotic mini-pumps (two 24-h pumps implanted sequentially; model 2001D, Durect Corp.) in accordance with the manufacturer's instructions. Tumors were measured up to three times weekly with calipers, tumor volumes were calculated, and the data were plotted using the geometric mean for each group versus time. Tumor volume and tumor growth inhibition were calculated as described previously (14). Statistical analysis of any change in tumor volume was carried out using a Student's one-tailed t test (P value of <0.05 was considered to be statistically significant).

For pharmacodynamic time course studies, nude rats bearing established SW620 tumor xenografts received vehicle or AZD1152 (25 mg/kg/d) as a daily i.v. bolus dose for 4 consecutive days (days 1-4). At multiple time points after dosing (days 0, 5, 9, 12, 16, and 19), two subgroups (n = 3 per group) of either vehicle- or AZD1152-treated animals were humanely killed and tumor and normal proliferating tissues (including bone marrow) were excised and assessed for pharmacodynamic effects using flow cytometric, histologic, or immunohistochemical analysis.

Flow cytometry. For *in vitro* studies, SW620 cells in logarithmic growth phase were exposed to 50 nmol/L AZD1152-HQPA for 24 or 48 h and then fixed in 70% ethanol at −20°C overnight. Cells were rehydrated in PBS and resuspended in PBS containing 100 μg/mL RNase (Sigma) and 10 μg/mL propidium iodide (Sigma), and cellular DNA content was analyzed on a FACSCalibur flow cytometer (Becton Dickinson). A total of 15,000 cells were counted and phases of the cell cycle were assessed using CellQuest software (Becton Dickinson). For tumor samples, cell suspensions were prepared from the snap-frozen

tumors using an automated tissue disaggregation system (Medimachine, BD Biosystems) and fixed in 80% ethanol for a minimum of 24 h. Once fixed, disaggregated tumors were prepared for DNA content and PhH3 analysis by flow cytometry following a previously described immunofluorescent staining protocol (15) using propidium iodide and the same commercially available antibodies [PhH3, rabbit polyclonal IgG (Upstate Biotechnology) and fluorescein-conjugated goat anti-rabbit IgG (Jackson ImmunoResearch)].

Histology and immunohistochemistry. For histologic analyses, tumors and femurs were fixed in formalin for 24 to 48 h and then processed to paraffin wax blocks. Femurs were decalcified using 10% formic acid before being processed to paraffin blocks. Tissue sections (3-4 μm thick) were stained with H&E. For immunohistochemical studies, sections were stained with rabbit polyclonal antibodies directed against either PhH3 or cleaved caspase-3 (Cell Signaling Technology) followed by a one-step horseradish peroxidase-labeled polymer method (Envision; DakoCytomation). Sections were counterstained with Carazzi's hematoxylin. Analysis of immunostaining in tumor sections was done on a Zeiss KS400 image analysis system (version 3; Imaging Associates Ltd.) linked to a Leica DMRB microscope. The KS400 is a color space/morphologic image analyzer for which thresholds of hue, luminosity, and saturation were set relative to the brown chromagen used for the immunolocalization of cleaved caspase-3. Area of cleaved caspase-3 immunostaining was quantified using an in-house macro to calculate the average percentage area of brown staining per area of field of vision (six fields per evaluable tumor section; ×20 magnification).

Results

AZD1152-HQPA inhibits Aurora B kinase activity and prevents cell division. AZD1152-HQPA has been shown previously to be a highly potent inhibitor of Aurora kinase enzyme activity *in vitro*, with selectivity for Aurora B kinase (Aurora B-INCENP K_i of 0.36 nmol/L) versus Aurora A (K_i of 1,369 nmol/L) and Aurora C (Aurora C-INCENP K_i of 17 nmol/L; ref. 13).[4] Consistent with Aurora B kinase inhibition, exposure of human SW620 colorectal tumor cells to AZD1152-HQPA resulted in a dose-dependent inhibition of histone H3 phosphorylation on Ser^{10} (Fig. 1A) that led to an increase in polyploidy following a 48-h exposure (Fig. 1B).

AZD1152 administration leads to inhibition of Aurora B kinase activity in vivo. Pharmacokinetic studies confirmed that AZD1152 was rapidly converted to the active drug AZD1152-HQPA in mouse and rat following systemic administration (data not shown). To determine whether AZD1152 administration leads to inhibition of Aurora B kinase activity in human tumor xenografts, we first examined PhH3 and DNA ploidy in SW620 colon tumors (established in nude mice) following s.c. infusion (by osmotic mini-pump) of AZD1152 (0.5-150 mg/kg) or vehicle over 48 h. Flow cytometric analysis of disaggregated tumor xenografts showed that the proportion of PhH3-positive cells within the G_2-M phase of the cell cycle was markedly reduced in AZD1152-treated animals compared with those receiving vehicle (AZD1152 at 70 mg/kg/d; Fig. 2A). Significant suppression of PhH3 was evident following 48-h administration of AZD1152, at doses as low as 0.5 mg/kg/d (52% inhibition). This inhibition increased further with 2.5 mg/kg/d AZD1152 (to 69%), whereas doses of 10 to 150 mg/kg/d resulted in between 77% and 86% inhibition (Fig. 2C).

Flow cytometric analysis of the DNA content (2N, 4N, and >4N) of tumors indicated an increased proportion of cells with a 4N and >4N DNA content from animals that received AZD1152 (AZD1152 at 70 mg/kg/d; Fig. 2B). The proportion of 2N and 4N DNA content was 58% and 24%, respectively, in tumors from vehicle-treated mice, whereas in tumors retrieved from mice receiving AZD1152 (70 mg/kg/d) treatment, the proportions were reversed, with 35% of cells showing 2N and 56% of cells showing 4N DNA content. This accumulation of cells with 4N DNA content is consistent with failed cytokinesis and continued cell cycle progression following inhibition of Aurora kinase activity. These findings were supported by histologic data, which showed a reduction of PhH3 and an increase in large multinucleated cells in AZD1152-treated

Table 1. *In vivo* activity of AZD1152 against a range of human tumor xenograft models

Tumor model	Tumor origin	Dose (mg/kg/d)	Route (duration)	Inhibition of tumor volume (%)	
				Maximum	End of study
SW620	Human colon	150	S.c. mini-pump (48 h, days 7-9)	87* (day 23)	87* (day 23)
		25	S.c. mini-pump (48 h, days 7-9)	65† (day 14)	49† (day 23)
		10	S.c. mini-pump (48 h, days 7-9)	55‡ (day 10)	28‡ (day 23)
		25	I.p. bolus daily (4 d, days 6-9)	65† (day 13)	54* (day 24)
		25	I.v. bolus daily (3 d, days 6-8)	91* (day 13)	47† (day 24)
Colo205	Human colon	150	S.c. mini-pump (48 h, days 5-7)	>100* (day 18)	94* (day 21)
HCT116	Human colon	150	S.c. mini-pump (48 h, days 11-13)	93* (day 18)	74* (day 25)
A549	Human lung	150	S.c. mini-pump (48 h, days 13-15)	79† (day 26)	69† (day 29)
		25	S.c. mini-pump (48 h, days 13-15)	74‡ (day 15)	36‡ (day 29)
Calu-6	Human lung	150	S.c. mini-pump (48 h, days 20-22)	67† (day 29)	55* (day 41)
HL-60§	Human leukemia	150	S.c. mini-pump (48 h, days 16-18)	>100* (day 18)	>100* (day 35)

NOTE: Human tumor xenografts were established in the flank of male Swiss athymic mice (8-12 wks of age). Mice were randomized into treatment groups when tumors reached a mean volume of 0.2 to 0.5 cm^3 and then treated with a continuous infusion of AZD1152 or vehicle (0.3 mol/L Tris buffer) via a s.c. implanted mini-pump or as a once-daily i.p or i.v bolus. Percentage tumor growth inhibition was calculated as the difference between the change in control and AZD1152-treated tumor volumes during and following the treatment period. Statistical significance was calculated using a one-tailed *t* test. *P* value of <0.05 was considered to be statistically significant.

*$P < 0.0005$.

†$P < 0.005$.

‡$P < 0.05$.

§No palpable or measurable tumors in 8 of 11 animals following treatment with AZD1152.

tumors when compared with vehicle controls (AZD1152 at 70 mg/kg/d; Fig. 2D and E, respectively). These data indicate that the mechanism of action of AZD1152 *in vivo* recapitulates that observed with AZD1152-HQPA *in vitro* (13).[4]

AZD1152 inhibits the growth of human tumor xenografts. AZD1152 (10-150 mg/kg/d; s.c. mini-pump infusion over 48 h) exerted potent, dose-dependent inhibition of growth in s.c. implanted human colorectal (SW620, HCT116, and Colo205), lung (A549 and Calu-6), and hematologic (HL-60) tumor xenografts in immunodeficient mice. The inhibition of tumor growth in individual models ranged from 55% to ≥100% (all $P < 0.05$; Fig. 3A-D; Table 1). HL-60 tumor xenografts were the most responsive to AZD1152, with complete tumor regression (i.e., no measurable tumors) at the end of the study in 8 of 11 animals (Fig. 3D). Significant antitumor activity was also observed when AZD1152 was dosed episodically to mice using other parenteral routes (i.e., i.v. or i.p. bolus injections). For example, three consecutive daily bolus i.v. injections of AZD1152 (25 mg/kg/d) in SW620-bearing mice led to a maximal tumor volume inhibition of 91% ($P < 0.0005$; Table 1).

Temporal pharmacodynamic analysis of AZD1152-sensitive tumors. To analyze the molecular and cellular events that lead to tumor growth inhibition in xenograft models, we established an episodic AZD1152 dosing schedule (25 mg/kg i.v. bolus once daily from days 1 to 4) in nude rats bearing established SW620 tumor xenografts. Treatment with AZD1152 resulted in significant tumor growth inhibition that was maximal (93%) at 8 days after the final dose (Fig. 4A). Flow cytometry revealed that PhH3 was suppressed by ~40% to 50% during the dosing period (days 1-4), with levels returning to baseline by day 9. There was also a transient increase in the proportion of both 4N (30% in vehicle versus 60% in AZD1152 treated) and polyploid (≥8N; 23% in vehicle versus 67% in AZD1152 treated) tumor cells, which peaked between days 1 to 5 (Fig. 4B).

Histologic assessment of tumor cells obtained from vehicle-treated animals on day 5 (24 h after the final dose) displayed relative uniformity in cell size and morphology (Fig. 5A). In contrast, tumors from AZD1152-treated rats exhibited a high degree of pleomorphism and displayed morphologic characteristics that were indicative of apoptosis. Consistent with a failure of cell division, tumor cells from AZD1152-treated rats were larger than those from control animals receiving vehicle alone. Furthermore, even larger multinucleated tumor cells were evident by day 9 (5 days after the final dose of AZD1152). Staining and quantification of tumor samples for the apoptotic marker cleaved caspase-3 showed elevated levels following AZD1152 treatment compared with controls, particularly in the markedly enlarged cells observed at day 9 (Fig. 5B and D). This suggests that apoptosis is the final fate of cells exposed to AZD1152-HQPA during cell division (Fig. 5E).

Bone marrow tissue was used to study the effects of AZD1152 administration on a normal rapidly cycling cellular compartment. The bone marrow micrographs from vehicle-treated rats (day 5) were densely populated with hematopoietic cells and exhibited a normal histologic appearance (Fig. 5C). In comparison, the bone marrow micrographs from rats receiving AZD1152 and sampled on day 5 displayed signs of atrophy, with a marked reduction in total cellular content (Fig. 5C). However, the bone marrow had recovered markedly by day 9 (5 days after the last dose of AZD1152) and was repopulated with hematologic cells of a histologically normal appearance (Fig. 5C). Flow cytometric analysis of bone marrow and peripheral whole blood cells from the same animal groups also indicated transient AZD1152-induced myelosuppression, with neutrophils being the most affected leukocyte population (data not shown). AZD1152 was otherwise well tolerated at doses where antitumor efficacy was observed; compared with vehicle-treated animals, AZD1152-treated athymic rats had a mean maximal body weight loss of 5%, 24 h following 4 days of treatment (25 mg/kg/d i.v. daily for four consecutive days), and regained body weight thereafter.

Discussion

AZD1152, a specific Aurora kinase inhibitor with selectivity for Aurora B kinase, is a dihydrogen phosphate prodrug that is highly soluble in simple pH-adjusted aqueous vehicles, making it suitable for parenteral dosing. In mouse and rat, AZD1152 undergoes rapid systemic conversion to the active drug AZD1152-HQPA, which has pharmacokinetic properties that cause dose-dependent plasma exposure (12).

These data confirmed that AZD1152 was converted to the active drug AZD1152-HQPA *in vivo* and elicited pharmacodynamic effects consistent with inhibition of Aurora B kinase. We have shown that administering AZD1152 to animals

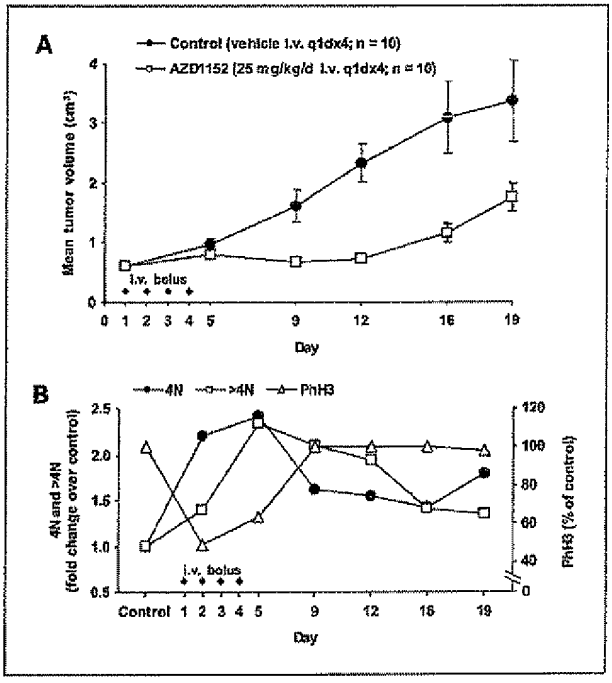

Fig. 4. Chronological characterization of AZD1152-induced antitumor responses. Male nude rats ($n = 28$ per group) bearing established SW620 tumor xenografts were dosed daily (once daily) with either vehicle or AZD1152 (i.v. bolus, 25 mg/kg) for 4 consecutive days. Subgroups of rats ($n = 3$ per group per time point) were removed during the experiment (days 0, 5, 9, 12, 16, and 19 from start of dosing) and tumor tissue was analyzed for pharmacodynamic effects using flow cytometry as described in Materials and Methods. *A*, tumor growth inhibition response. Mean tumor volume (cm^3; $n = 10$); bars, SE. *B*, flow cytometric analysis of disaggregated tumors showing PhH3 (expressed as percentage of control) and 4N DNA or polyploid (>4N) DNA content (expressed as fold increase over control) changes.

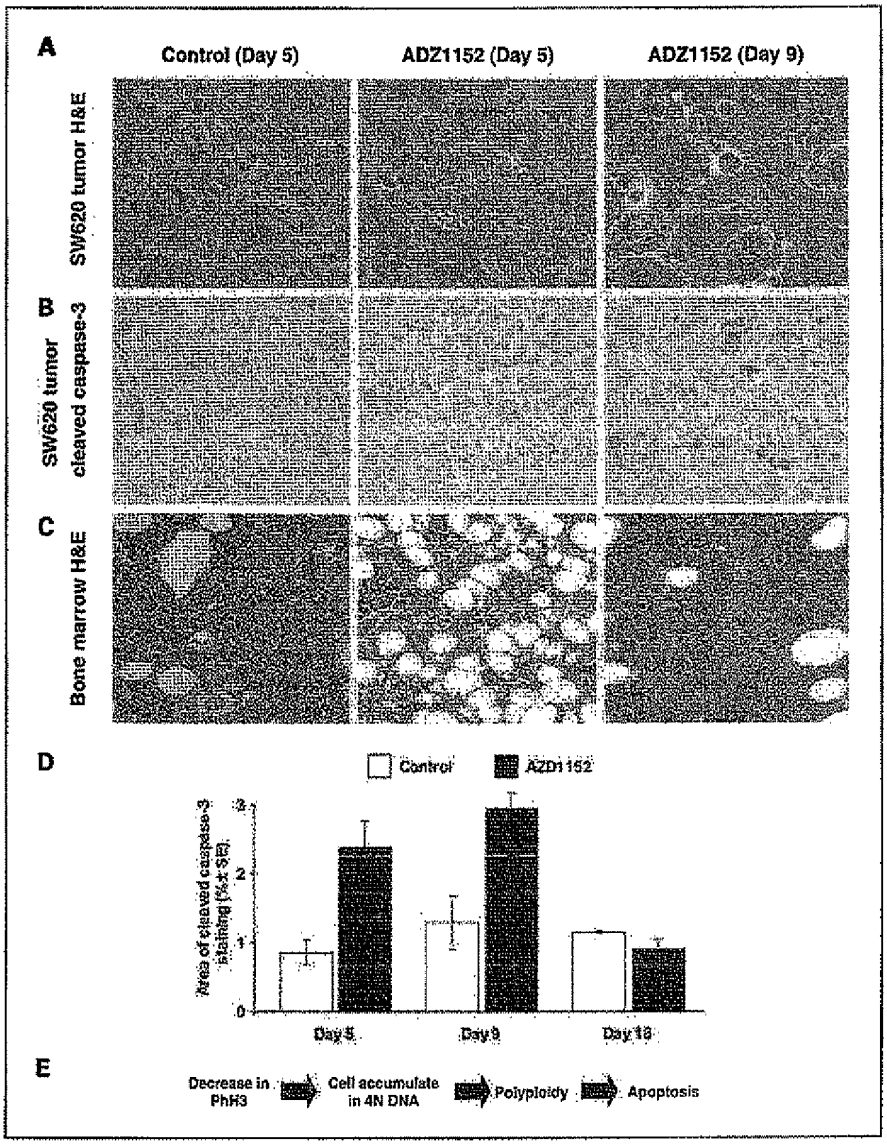

Fig. 5. AZD1152 treatment leads to phenotypic changes in tumor and hematologic tissue. Excised tissue derived from the antitumor study described in Fig. 4 also underwent histologic analyses (*A-C*). Representative sections of tumor (*A* and *B*) and bone marrow (*C*) taken on days 1 and 4 after the final dose of AZD1152 are shown (*middle* and *right*, respectively) and compared with corresponding sections from vehicle-treated animals taken on day 1 (*left*). Sections were stained with H&E (*A* and *C*) and immunoreactivity for cleaved caspase-3 (*B*). Magnification, ×40. *D*, quantitative analysis by scanning microscopy of cleaved caspase-3–immunostained tumors. Columns, mean of one experiment ($n = 3$ animals per group per time point, one tumor section per animal, six fields per tumor); bars, SE. *E*, the proposed sequence of events occurring in AZD1152-treated tumor tissue.

bearing human tumor xenografts leads to an inhibition of histone H3 phosphorylation followed by a failure of tumor cell division, endoreduplication, and an induction of tumor cell death by apoptosis. Moreover, these findings are consistent with the observed effects of AZD1152-HQPA *in vitro* (13)[4] and are distinct from the phenotype associated with antimitotic/anti-tubulin agents, such as paclitaxel (i.e., where cells usually arrest in mitosis; refs. 2, 16).

Parenteral administration of AZD1152 resulted in profound antitumor effects in each of the colorectal, lung, and acute myeloid leukemia human tumor xenograft models examined. This antitumor response persisted for a considerable time after the end of dosing. Furthermore, in the HL-60 acute myeloid leukemia model, durable regressions were observed over a 20-day period, with no palpable tumors observed in 8 of 11 animals. The responsiveness of HL-60 xenografts to Aurora kinase inhibitors has also been reported in two independent studies using the mixed Aurora (Aurora A/Aurora B) inhibitors VX-680 and PHA-680632 (9, 11): VX-680 (75 mg/kg administered twice daily by i.p. injection for 13 days) inhibited HL-60 tumor growth by 98% and PHA-680632 (45 mg/kg administered twice daily by i.v. injection for 5 days) inhibited growth by 85%. The effect of administering AZD1152 via different dosing schedules was investigated further in nude mice bearing colorectal tumor xenografts. Significant antitumor activity was observed in tumors following dosing of AZD1152 either at high doses for short durations (i.v. or i.p. bolus injections) or at lower doses for longer durations using s.c. osmotic minipumps. This suggests that examination of different clinical schedules may be warranted either as a monotherapy or in combination with existing therapeutic modalities.

Analyses of tissue from AZD1152-treated tumors showed a sequence of molecular/cellular events following the inhibition of Aurora B activity that was consistent with a failure of cell

division leading ultimately to apoptosis. Initial suppression of PhH3 was followed by a transient accumulation of 4N cells, with subsequent accumulation of polyploid cells. Histologic examination showed increased apoptosis in AZD1152-treated tumors compared with control, which reached a maximum over a time scale corresponding with the decline of polyploid cells observed by flow cytometry, and declined thereafter. These results support a mechanism by which induction of endoreduplication leads to polyploidy and eventual apoptosis. Previous studies investigating the effects of Aurora kinase inhibitors have proposed PhH3 as a surrogate marker of activity (9, 11). In the current study, PhH3 was found to be a sensitive and highly dynamic marker of Aurora kinase inhibition. The number of cells positive for PhH3 declined significantly after treatment across all AZD1152 concentrations tested and recovered rapidly after cessation of dosing. Interestingly, dose-dependent suppression of PhH3 occurred across a lower concentration range than dose-dependent inhibition of tumor growth. This difference may reflect the involvement of Aurora kinase substrates other than histone H3 in mediating effects on cytokinesis. Indeed, although PhH3 is widely used as a marker for Aurora kinase inhibition, its biological relevance to cytokinesis is not clear. Other putative Aurora B kinase substrates involved in cytokinesis include vimentin, GFAP, desmin, MgcRacGAP, and motorprotein MKlp1 (17–20). Considering all of the above, the dynamics of PhH3 suppression may be more predictive of therapeutic outcome when examined in conjunction with downstream phenotypic markers, such as tumor cell polyploidy and apoptosis.

There are several limitations with the currently available drugs that act by targeting mitosis. For example, agents that bind tubulin are associated with peripheral neuropathy (21). In this study, AZD1152 was well tolerated within the dose range required to elicit a potent and durable antitumor effect, with animals showing only transient loss of body weight. Bone marrow analyses revealed reversible myelosuppression in AZD1152-treated animals, with full recovery occurring within a week of cessation of dosing. Analysis of peripheral blood cells also indicated a reduction in WBC counts (mainly neutropenia) followed by full recovery. These findings suggest that intermittent dosing schedules at appropriate intervals can be used to repeatedly target tumor cells while allowing bone marrow to recover. One reason may be the difference in proliferative rates during hematopoiesis, with bone marrow stem cells and progenitor cells having relatively low frequency of division, compared with late-stage differentiating neutrophils (22). This may explain the rapid reduction in absolute neutrophil counts that is followed by fast recovery of the bone marrow after withdrawal of AZD1152. Furthermore, normal cells may be less susceptible to the induction of polyploidy due to the presence of functional p53 (23).

In conclusion, these data show that inhibition of Aurora B activity *in vivo* has profound effects on tumor growth and that AZD1152 has the potential for efficacy in multiple tumor types. Moreover, the pharmacodynamic and efficacy results indicate that the major effects of AZD1152-HQPA on tumor cells *in vitro* are recapitulated with AZD1152 *in vivo*. In addition, simultaneous tracking of time-dependent changes in PhH3, polyploidy, and apoptosis provided an important and useful insight into how the antitumor effects of AZD1152 are mediated. This may ultimately lead to a strategy for monitoring the biological consequences of Aurora B kinase inhibition in the clinic. AZD1152 is currently undergoing phase I clinical evaluation as a treatment for cancer.

Acknowledgments

We thank Sharon Barnett, Nicola Haupt, David Smith, Julie Humphreys, Keith Welsh, Darren Harrison, and Nigel Leake from the CDMG for technical assistance; Kerry Ratcliffe for histologic support; Julia Young, Joanne Wilson, and Mike Walker for pharmacokinetic support; Dereck Amakye and Andrew Hughes for translational science input; Chris Watson and Matthew Lewis of Mudskipper Bioscience for editorial support; and AZD1152 chemistry team for kindly providing compounds.

References

1. Andrews PD. Aurora kinases: shining lights on the therapeutic horizon? Oncogene 2005;24:5005–15.
2. Wood KW, Cornwell WD, Jackson JR. Past and future of the mitotic spindle as an oncology target. Curr Opin Pharmacol 2001;1:370–7.
3. Carmena M, Earnshaw WC. The cellular geography of aurora kinases. Nat Rev Mol Cell Biol 2003;4:842–54.
4. Ducat D, Zheng Y. Aurora kinases in spindle assembly and chromosome segregation. Exp Cell Res 2004;301:60–7.
5. Ditchfield C, Johnson VL, Tighe A, et al. Aurora B couples chromosome alignment with anaphase by targeting BubR1, Mad2, and Cenp-E to kinetochores. J Cell Biol 2003;161:267–80.
6. Yang H, Burke T, Dempsey J, et al. Mitotic requirement for aurora A kinase is bypassed in the absence of aurora B kinase. FEBS Lett 2005;579:3385–91.
7. Keen N, Taylor S. Aurora-kinase inhibitors as anticancer agents. Nat Rev Cancer 2004;4:927–36.
8. Hauf S, Cole RW, LaTerra S, et al. The small molecule Hesperadin reveals a role for Aurora B in correcting kinetochore-microtubule attachment and in maintaining the spindle assembly checkpoint. J Cell Biol 2003;161:281–94.
9. Harrington EA, Bebbington D, Moore J, et al. VX-680, a potent and selective small-molecule inhibitor of the Aurora kinases, suppresses tumor growth *in vivo*. Nat Med 2004;10:262–7.
10. Young MA, Shah NP, Chao LH, et al. Structure of the kinase domain of an imatinib-resistant Abl mutant in complex with the Aurora kinase inhibitor VX-680. Cancer Res 2006;66:1007–14.
11. Soncini C, Carpinelli P, Gianellini L, et al. PHA-680632, a novel Aurora kinase inhibitor with potent antitumoral activity. Clin Cancer Res 2006;12:4080–9.
12. Mortlock AA, Foote KM, Heron NM, et al. Discovery, synthesis and *in vivo* activity of a new class of pyrazoloquinazolines as selective inhibitors of aurora B kinase. J Med Chem 2007;50:2213–24.
13. Keen N, Brown E, Crafter C, et al. Biological characterisation of AZD1152, a highly potent and selective inhibitor of aurora kinase activity. Clin Cancer Res 2005;11:B220.
14. Wedge SR, Kendrew J, Hennequin LF, et al. AZD2171: a highly potent, orally bioavailable, vascular endothelial growth factor receptor-2 tyrosine kinase inhibitor for the treatment of cancer. Cancer Res 2005;65:4389–400.
15. Widrow RJ, Laird CD. Enrichment for submitotic cell populations using flow cytometry. Cytometry 2000;39:126–30.
16. Chen JG, Horwitz SB. Differential mitotic responses to microtubule-stabilizing and -destabilizing drugs. Cancer Res 2002;62:1935–8.
17. Goto H, Yasui Y, Kawajiri A, et al. Aurora-B regulates the cleavage furrow-specific vimentin phosphorylation in the cytokinetic process. J Biol Chem 2003;278:8526–30.
18. Kawajiri A, Yasui Y, Goto H, et al. Functional significance of the specific sites phosphorylated in desmin at cleavage furrow: Aurora-B may phosphorylate and regulate type III intermediate filaments during cytokinesis coordinatedly with Rho-kinase. Mol Biol Cell 2003;14:1489–500.
19. Minoshima Y, Kawashima T, Hirose K, et al. Phosphorylation by aurora B converts MgcRacGAP to a RhoGAP during cytokinesis. Dev Cell 2003;4:549–60.
20. Neef R, Klein UR, Kopajtich R, Barr FA. Cooperation between mitotic kinesins controls the late stages of cytokinesis. Curr Biol 2006;16:301–7.
21. Scuteri A, Nicolini G, Miloso M, et al. Paclitaxel toxicity in post-mitotic dorsal root ganglion (DRG) cells. Anticancer Res 2006;26:1065–70.
22. Kondo M, Wagers AJ, Manz MG, et al. Biology of hematopoietic stem cells and progenitors: implications for clinical application. Annu Rev Immunol 2003;21:759–806.
23. Margolis RL. Tetraploidy and tumor development. Cancer Cell 2005;8:353–4.

EXHIBIT D

PHA-680632, a Novel Aurora Kinase Inhibitor with Potent Antitumoral Activity

Chiara Soncini, Patrizia Carpinelli, Laura Gianellini, Daniele Fancelli, Paola Vianello, Luisa Rusconi, Paola Storici, Paola Zugnoni, Enrico Pesenti, Valter Croci, Roberta Ceruti, Maria Laura Giorgini, Paolo Cappella, Dario Ballinari, Francesco Sola, Mario Varasi, Rodrigo Bravo, and Jürgen Moll

Abstract **Purpose:** Aurora kinases play critical roles during mitosis in chromosome segregation and cell division. The aim of this study was to determine the preclinical profile of a novel, highly selective Aurora kinase inhibitor, PHA-680632, as a candidate for anticancer therapy.

Experimental Design: The activity of PHA-680632 was assayed in a biochemical ATP competitive kinase assay. A wide panel of cell lines was evaluated for antiproliferative activity. Cell cycle analysis, immunohistochemistry, Western blotting, and Array Scan were used to follow mechanism of action and biomarker modulation. Specific knockdown of the targets by small interfering RNA was followed to validate the observed phenotypes. Efficacy was determined in different xenograft models and in a transgenic animal model of breast cancer.

Results: PHA-680632 is active on a wide range of cancer cell lines and shows significant tumor growth inhibition in different animal tumor models at well-tolerated doses. The mechanism of action of PHA-680632 is in agreement with inhibition of Aurora kinases. Histone H3 phosphorylation in Ser^{10} is mediated by Aurora B kinase, and our kinetic studies on its inhibition by PHA-680632 *in vitro* and *in vivo* show that phosphorylation of histone H3 is a good biomarker to follow activity of PHA-680632.

Conclusions: PHA-680632 is the first representative of a new class of Aurora inhibitors with a high potential for further development as an anticancer therapeutic. On treatment, different cell lines respond differentially, suggesting the absence of critical cell cycle checkpoints that could be the basis for a favorable therapeutic window.

Mitosis is a highly dynamic phase of the cell cycle and any error can have dramatic consequences as seen in most tumors, which bear chromosomal anomalies and are often aneuploid. Due to its high complexity, mitosis needs stringent regulators, among which are the Aurora kinases. Aurora proteins belong to a small family of serine/threonine kinases that are key regulators of different steps in mitosis and meiosis (for review, see refs. 1, 2). In mammalians, the Aurora family consists of three members: Aurora A, Aurora B, and the less well characterized Aurora C, whereas in yeast only one Aurora kinase gene exists. All Aurora kinases bear a conserved COOH terminus that contains the typical catalytic subdomains of a serine/threonine kinase and a destruction box that might be important for protein degradation (3–6).

Authors' Affiliation: Nerviano Medical Sciences S.r.l.-Oncology, Milan, Italy
Received 9/7/05; revised 4/20/06; accepted 4/24/06.
The costs of publication of this article were defrayed in part by the payment of page charges. This article must therefore be hereby marked *advertisement* in accordance with 18 U.S.C. Section 1734 solely to indicate this fact.
Note: Supplementary data for this article are available at Clinical Cancer Research Online (http://clincancerres.aacrjournals.org/).
Requests for reprints: Jürgen Moll, Nerviano Medical Sciences S.r.l.-Oncology, Via Pasteur 10, I-20014 Nerviano, Milan, Italy. Phone: 39-331-58-1396; Fax: 39-331-58-1374; E-mail: jurgen.moll@nervianoms.com.

doi:10.1158/1078-0432.CCR-05-1964

Despite these similarities, the three mammalian Aurora kinases show differences in subcellular localizations, timing of activation, and functions during mitosis. For example, whereas Aurora A and B mRNA and protein levels as well as kinase activity increase during mitosis, the peak of Aurora A activity is seen during prometaphase, whereas Aurora B is most active from metaphase to telophase (7).

Aurora A localizes to centrosomes during interphase and moves to the spindle poles during early mitosis. In contrast, Aurora B is a chromosomal passenger protein, where it is in a complex with at least three other chromosomal passenger proteins: inner centromere protein, survivin, and the recently described Borealin (8).

Several studies in different organisms show a role of Aurora A in centrosome maturation and spindle assembly. On the contrary, Aurora B is part of the spindle checkpoint regulating chromosome cohesion and bipolar attachment of microtubules. In addition, Aurora B has been proposed to play a role in the control of cytokinesis (9–11). Aurora C has been reported to be localized at the centrosomes and to have a limited expression in testis and in some cancer cell lines (12). However, a recent publication indicates a novel role for Aurora C, more similar to Aurora B (13). Since their discovery, Aurora kinases have been implicated in cancer and tumorigenesis (14). Initially, Aurora A and B were found to be overexpressed in primary tumors of breast and colon. Further studies revealed Aurora A amplification or overexpression in many other tumor types (15–21).

Moreover, their genetic localizations (Aurora A, 20q13; Aurora B, 17q13) map to chromosomal loci frequently altered in tumors.

Aurora A has been shown to act as an oncogene because overexpression of wild-type Aurora A or of a constitutive active mutant transforms Rat1 and NIH 3T3 cells leading to colony formation in soft agar assays (7, 22). In addition, NIH 3T3 cells expressing constitutively active Aurora A can grow as solid tumors when injected into *nu/nu* mice (7). When Aurora A is overexpressed in the diploid human breast cell line MCF10A, centrosome abnormalities and aneuploidy are observed (22). A direct role of Aurora B or C in tumorigenesis is less well documented, although Aurora B is also overexpressed in many human tumors. Aurora kinases, by virtue of their roles in mitosis, have been implicated in the genetic instability of tumor cells by controlling chromosomal ploidy.

Some of the known substrates or interacting proteins of Aurora kinases, such as Ras-GAP (23), p53 (24–26), Cdc20 (27), or NM23-H1 (28), could be important mediators in malignant transformation.

These properties make the Aurora kinases attractive targets for anticancer therapy; indeed, the first inhibitors have entered the clinic (29). At present, there are three small molecules inhibiting Aurora kinases (for review, see ref. 30) described in more details in the literature [Hesperadin (31), ZM447439 (32, 33), and VX-680 (34)] and other compounds are in development.

We report here the characterization of a novel, highly selective Aurora kinase inhibitor, which is active on a wide range of cancer cell lines *in vitro* and shows significant tumor growth inhibition (TGI) in different animal tumor models. The molecular mechanism of action of our inhibitor is in agreement with inhibition of Aurora A and B kinases as has been shown *in vitro* and *in vivo*, monitoring phosphorylation of Aurora A as well as histone H3 and BubR1. The differences in cellular response of different cell lines (e.g., some tumor cells versus normal cells) observed after treatment with this inhibitor might be due to the absence of critical cell cycle checkpoints in some tumor cells and could form the basis for a favorable therapeutic window.

Materials and Methods

Cell cultures. HeLa cells (European Collection of Cell Culture, Salisbury, United Kingdom) were cultured in MEM supplemented with heat-inactivated 10% FCS. A2780 and HL60 cells (European Collection of Cell Culture) were maintained in RPMI with 10% FCS. HCT116 cells (American Type Culture Collection, Manassas, VA) were maintained in McCoy's medium with 10% FCS. U2OS cells (American Type Culture Collection) were grown in DMEM with 10% FCS. Normal human dermal fibroblasts (NHDF; Promocell, Heidelberg, Germany) were maintained in fibroblast basal medium supplemented with growth factors and with 10% FCS. Total WBC from peripheral or marrow blood of leukemia patients were purified by ACK lysis or Ficoll (Amersham Biosciences, Pittsburgh, PA) gradients and assayed for cell viability before treatment. These samples were used after patient consent. In all the experiments, cells were treated with PHA-680632 at the indicated concentrations and times, starting from a stock solution of 10 mmol/L in DMSO (Sigma, St. Louis, MO). Nocodazole (Sigma) was used at 75 ng/mL for 9 hours.

Recombinant protein production. The coding sequences of human Aurora kinases (A, B, and C) were amplified by PCR and introduced into plasmid pDONOR201 using Gateway Cloning Technology (Invitrogen, Carlsbad, CA) and subsequently cloned into the vector PVL1393 (PharMingen, San Diego, CA) that was modified by insertion of a glutathione *S*-transferase coding sequence and a PreScission Protease cleavage site upstream and in frame to the Aurora sequences. Recombinant viruses containing the different recombinant transfer vectors were produced following standard protocols (BaculoGold manual; Life Technologies, Inc., Rockville, MD). For protein production, High5 cells, grown in flasks at 27°C in ultimate serum-free medium (Invitrogen), were infected with each recombinant virus and treated with 500 nmol/L okadaic acid 3 hours before collection. Cells were then collected 42 hours after infection and resuspended in ice-cold lysis buffer [PBS (pH 7.4), 500 mmol/L NaCl, 10% glycerol, 0.2% CHAPS, 20 mmol/L DTT, 1 mmol/L orthovanadate, Complete protease inhibitor cocktail (Roche Diagnostics, Mannheim, Germany)]. After sonication, the protein extract was centrifuged at 33,000 × *g* for 45 minutes. The suspension was loaded onto a glutathione-Sepharose 4 fast flow column (Amersham Biosiences) that was preequilibrated in lysis buffer. Proteins were eluted by on-column cleavage with PreScission Protease according to the manufacturer's instructions (Amersham Biosciences). The purified proteins were stored in stabilizing buffer 50 mmol/L Tris (pH 7.6), 500 mmol/L NaCl, 20% glycerol, 1 mmol/L DTT, protease inhibitors, and 1 mmol/L orthovanadate.

*In vitro **kinase assays.*** Inhibition of kinase activity by PHA-680632 was assessed using a scintillation proximity assay format. In this assay, the biotinylated substrate is transphosphorylated by the kinase in presence of ATP traced with γ^{33}-ATP. The phosphorylated substrate is then captured using streptavidin-coated scintillation proximity assay beads and the extent of phosphorylation is evaluated by β-counter after a 4-hour rest for the floatation of the beads on a dense 5 mol/L CsCl solution. In particular a peptide derived from the Chocktide sequence (LRRWSLGL) was used as substrate for Aurora A, whereas the optimized peptide Auroratide[1] was employed for Aurora B and C. The assay was run in a robotized format on 96-well plates. The potency of the compound toward Aurora kinases and 29 additional kinases belonging to our Kinase Selectivity Screening panel (35) was evaluated and the relevant IC_{50}s were determined. For each Kinase Selectivity Screening enzyme, the K_ms for ATP and the specific substrate were initially determined and each assay was then run at optimized ATP ([$2K_m$]) and substrate ([$5K_m$]) concentrations. This setting enabled direct comparison of IC_{50}s of PHA-680632 across the Kinase Selectivity Screening panel for the evaluation of its biochemical selectivity.

Analysis of cell proliferation. Cells were seeded at different densities ranging from 5,000 to 15,000 cm^2 in 24-well plate with the appropriate complete medium. After 24 hours, plates were treated with compound and incubated for 72 hours at 37°C in 5% CO_2 atmosphere. At the end of incubation time, cells were detached from each plate and counted using a cell counter (Beckman Coulter, Fullerton, CA). IC_{50}s were calculated using percentage of growth versus untreated control.

Cell cycle analysis. All of the cells in the plates, including cells floating in the medium, were collected and analyzed. Adherent cells were released from the plastic by trypsin treatment and added to the tubes. Cells were washed in PBS and fixed in 70% ethanol in PBS, resuspended in PBS containing RNase A (2 μg/mL) and propidium iodide (5 μg/mL), and incubated for 30 minutes at 37°C. Samples were analyzed by flow cytometry with a FACScan (Becton Dickinson Biosciences, San Jose, CA). Data were analyzed with ModFit LT software (Verity Software House, Topham, ME).

The tumors were excised and minced and a cell suspension was prepared by passing the tumor thrice through a needle. The suspension was centrifuged and the cells were resuspended in CytoPerm and stained with anti-active caspase-3 (BD Biosciences, San Jose, CA) according to the manufacturer's protocol.

RNA interference. For small interfering RNA (siRNA) experiments, the following double-stranded RNA oligonucleotides were used: 5′-AUGCCCUGUCUUACUGUCA-3′ and 5′-GUCCCAGAUAGAAG-GAG-3′, specific for Aurora A and B, respectively. GL2 oligonucleotide

[1] L. Rusconi et al., in preparation.

(Dharmacon Research, Inc., Lafayette, CO), which targets the luciferase gene, was used as control. All of the siRNA duplexes were synthesized by Dharmacon and were transfected using Oligofectamine (Invitrogen) according to the manufacturer's recommendations. siRNAs were used at final concentrations of 100 nmol/L.

Immunoblotting. Cell or tissue extracts were prepared in 125 mmol/L Tris-HCl (pH 6.8) and 2% SDS. Samples were sonicated and heated for 5 minutes at 95°C. Protein extract (10 μg), as determined by BCA protein assay (Pierce, Rockford, IL) was loaded on SDS-PAGE. Immunoblot analysis was done using the following antibodies: anti-Aim1 and anti-Iak1 (BD Transduction Laboratories, Franklin Lakes, NJ), anti-phosphorylated histone H3 Ser^{10} (Upstate Biotechnology, Lake Placid, NY), anti-phospho-Aur2 (T288) (Cell Signaling, Danvers, MA), anti-BubR1 (a kind gift from Dr. T.J. Yen, Fox Chase Cancer Center, Philadelphia, PA), anti-active caspase-3 (Chemicon International, Temecula, CA), anti-active caspase-9 (Oncogene, San Diego, CA), anti-Cdk2 (Santa Cruz Biotechnology, Santa Cruz, CA), anti-histone H3 (Abcam, Cambridge, United Kingdom), and anti-γ-tubulin (Sigma). Immunoblotting was done according to standard methods. SuperSignal chemiluminescence kit (Pierce) was used for detection.

Array Scan IV. The Array Scan 4.0 system (Cellomics, Pittsburgh, PA) was used to analyze cells positive for phosphorylation of histone H3 in Ser^{10}. The Array Scan software mitotic index algorithm (Cellomics) was used to calculate the percentage of cells positive for phosphorylation of histone H3 in Ser^{10}. Plates (96 wells) were seeded with 8,000 U2OS cells per well, and on the day after, the cells were treated for 7 hours with 75 ng/mL nocodazole followed by different doses of PHA-680632 for 1.5 hours.

Cells were then fixed in 3.7% formaldehyde (Sigma) for 20 minutes, washed with PBS, and permeabilized with 0.5% Triton X-100 (Sigma) in PBS for 15 minutes. Phosphorylated histone H3 Ser^{10} (40 μL; Cell Signaling) was added to each well at the recommended dilution in PBS containing 1% bovine serum albumin and 0.3% Tween 20 (Sigma) for 1 hour at 37°C. An anti-rabbit primary Cy2-conjugated secondary antibody (Amersham Biosciences) was used for antigen detection.

Immunocytochemistry. Tumors were harvested, formalin-fixed, and paraffin-embedded. Paraffin sections (3 μm) were deparaffinized in xylene, rehydrated in graded ethanol, and transferred to PBS. Sections were placed in citrate buffer (pH 6.0) and thermally processed with two cycles in autoclave "2100 Retriever" (PickCell Laboratories, Amsterdam, the Netherlands). After washing with PBS, endogenous peroxidase was blocked using 3% hydrogen peroxide in PBS for 10 minutes. The tissues were washed with PBS plus 0.01% Tween 20 and incubated for 30 minutes at room temperature with a protein-blocking solution consisting of PBS containing 10% normal goat serum and 0.01% Tween 20. The sections were stained with an anti-phosphorylated histone H3 Ser^{10} polyclonal antibody (Upstate Biotechnology) diluted 1:800 in blocking solution and incubated for 1 hour at room temperature. The samples were rinsed twice with PBS plus 0.01% Tween 20, incubated for 30 minutes at room temperature with Envision rabbit (DAKO, Glastrup, Denmark), rinsed, and incubated for 3 minutes with 3,3'-Diaminobenzidine Plus (DAKO). The sections were then washed and counterstained with hematoxylin. For the bromodeoxyuridine labeling, 2 hours before mice were sacrificed, 100 mg/kg bromodeoxyuridine (Sigma) was injected i.p. Excised tumors were formalin-fixed for 24 hours and paraffin-embedded. The sections were processed as above and stained with a monoclonal antibody specific for bromodeoxyuridine (Becton Dickinson).

Animal efficacy studies. Female Hsd, athymic *nu/nu* mice, ages 5 to 6 weeks (20-22 g), and female severe combined immunodeficient mice were obtained from Harlan (San Pietro al Natisone, Italy). Mouse mammary tumor virus v-Ha-*ras* transgenic mice were originally obtained from Charles River Breeding Laboratories (Wilmington, MA) and maintained in a FVB background.

All animal studies were carried out in compliance with Italian Legislative Decree N.116 dated January 27, 1992 and the European Communities Council Directive N.86/609/EEC concerning the protection of animals used for experimental or other scientific purposes and according to Institutional Policy Regarding the Care and Use of Laboratory Animals. A2780 human ovarian carcinoma and HCT116 colon carcinoma cell lines (American Type Culture Collection) were transplanted s.c. into athymic mice. Mice bearing a palpable tumor (100-200 mm^3) were selected and randomized into control and treated groups. Treatments started 1 day after randomization.

In the HL60 study, female severe combined immunodeficient mice were injected s.c. with 5×10^6 leukemia cells. Treatments started, when tumors were 200 to 250 mm^3 in size.

In the study with mouse mammary tumor virus v-Ha-*ras* transgenic mice with established mammary tumors, compound administration began when mammary tumors had an average volume in the range of 300 to 500 mm^3. In all cases, tumor growth was measured approximately once weekly for 7 weeks and animal weight was measured twice weekly.

Dimensions of the tumors were measured regularly by caliper during the experiments and tumor masses were calculated as described (36). The TGI (%) was calculated according to the equation: % TGI = 100 − (mean tumor weight of treated group / mean tumor weight of control group) × 100. Toxicity was evaluated based on the body weight reduction. Mice were sacrificed when the tumors reached a volume that hampered them, and the gross autopsy findings were reported.

Results

PHA-680632 is a cell cycle inhibitor specific for Aurora kinases. PHA-680632 was identified by the combinatorial expansion of the 1,4,5,6-tetrahydropyrrolo[3,4-*c*]pyrazole scaffold as described previously (ref. 37; Fig. 1A). The specificity of this compound was tested *in vitro* against a broad panel of kinases representative of different kinase families. PHA-680632 was shown to be a potent inhibitor of all three Aurora kinases with IC_{50}s of 27, 135, and 120 nmol/L for Aurora A, B, and C, respectively. The selectivity of PHA-680632 for the Aurora kinases was tested over a panel of 29 additional kinases (Fig. 1B) and the compound was found to be inactive (IC_{50}, >10 μmol/L) on 22 of them. Six kinases in the panel (FLT3, LCK, PLK1, STLK2, VEGFR2, and VEGFR3; Fig. 1B) exhibited a 30- to 200-fold higher IC_{50} compared with Aurora A. The strongest cross-reactivity was seen with FGFR1, although PHA-680632 retained a ~15-fold selectivity for Aurora A (IC_{50} for FGFR1, 390 nmol/L).

We then evaluated the antiproliferative effects of PHA-680632. A panel of 35 exponentially growing cell lines from different tumor types and NHDF were treated for 72 hours with different concentrations of PHA-680632 (Fig. 1C; Supplementary Data 1). PHA-680632 has potent antiproliferative activity in a wide range of cell types with an IC_{50} in the range of 0.06 to 7.15 μmol/L. The antiproliferative effect of our inhibitor was determined by cell counting because inhibition of Aurora kinases induces endoreduplication and gives rise to cells with a DNA content higher than 4N accompanied by an increase of the cell diameter. Conventional standard assays used to measure proliferation [as 3-(4,5-dimethylthiazol-2-yl)-2,5-diphenyltetrazolium bromide, sulforhodamine B, or ATP level evaluation] give misleading results and direct cell count as a readout for Aurora kinase inhibition allows a more appropriate determination of IC_{50}s and comparison of compounds.

PHA-680632 can cause polyploidy in tumor cells. Inhibition of Aurora kinases has been shown to generate polyploid cells as a consequence of DNA synthesis in the absence of cytokinesis (32). We evaluated the effects of PHA-680632 on the cell cycle

A

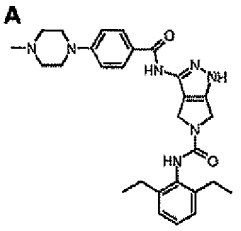

B

Kinase	IC_{50} (nM)
Aurora A	27
Aurora B	135
Aurora C	120
FGFR1	390
FLT3	820
LCK	1950
PLK1	780
STLK2	5500
VEGFR2	1920
VEGFR3	1000

C

Cell lines	IC_{50} (μM)
C33A	0.32
HeLa	0.41
HCT116	0.06
HT29	1.17
LOVO	0.56
A549	0.62
MCF7	0.29
A2780	0.11
U2OS	1.56
DU145	0.62
U937	0.07
HL60	0.13
NHDF	0.41

Fig. 1. PHA-680632 is a selective Aurora inhibitor that blocks proliferation of several tumor cell types. *A*, chemical structure of PHA-680632, a derivative of a 1,4,5,6-tetrahydropyrrolo[3,4-*c*]pyrazole scaffold. *B*, IC_{50}s of PHA-680632 against a panel of protein kinases. PHA-680632 was not active (IC_{50}, >10 μmol/L) against the following kinases: BUB1, CDC7, CDK2/CycA, CHK1, CK2, CMET, EGFR, ERK2, GSK3β, IGFR1, IKK1, IKK2, IR, LYN, MAPKAPK2, NIM1, PAK4, PKAα, PKBα, PKCβ, SULU1, and ZAP70. *C*, antiproliferative effect of PHA-680632 in a panel of human cell lines. The complete panel can be found in Supplementary Data 1. Mean of two or more independent dose-response curves.

by flow cytometry in NHDF as well as in several cancer cell lines, including HCT116, A2780, HL60, and HeLa cells. Cells were treated with increasing concentrations of PHA-680632 for 24, 48, and 72 hours (Fig. 2; Supplementary Data 2A). The cell lines respond with different kinetics and reach a saturation status at different doses. In Fig. 2A, we show comparison between HCT116 and NHDF treated for 24 hours. Whereas the tumor cell line HCT116 rapidly enters endoreduplication at low doses of PHA-680632, the NHDF require higher doses to accumulate in a 4N DNA content stage and do not reach polyploidy within the 24 hours of treatment. The increase in DNA content goes along with an increase in cell diameter (e.g., the percentage of HCT116 cells with a diameter between 15 and 25 μm increases from 14% in the control cells up to 90% in the treated cells). (The average diameter of HCT116 cells is 12 μm).

We then measured the effect of PHA-680632 over time to exclude the possibility that the differential responses seen are due to the different cycling time of the cells. The cell lines were followed for 24, 48, and 72 hours at different doses and Fig. 2B and Supplementary Data 2B show the profiles for each cell line tested at the dose for which saturation was reached in the titration experiment. The more sensitive cell lines, which displayed polyploidy already at 24 hours, do not change behavior, with the exception of HL60 cells that display massive cell death over time (Supplementary Data 2B). On the contrary, increasing the time, it was possible to see some polyploidy also in HeLa cells, whereas NHDF stayed blocked in the cell cycle even when treated at higher doses for 72 hours (Fig. 2B; Supplementary Data 2B). We then tested the ability of the cells to recover after drug washout (Fig. 2C). HCT116 cells and NHDF were treated with 0.5 μmol/L PHA-680632 for 40 hours, and cells were replated in drug-free medium and collected for analysis 6 days after the replating. As shown in Fig. 2C, after treatment, the majority of the HCT116 cells are in a polyploid stage, whereas NHDF are mainly in the G_2-M phase of the cell cycle. At 6 days after replating, the DNA profile shows that the NHDF are back to normality (with ~90% in cell number of the untreated cells), whereas for the tumor cells there is a very low number of cells (3% of the untreated), showing only partial recovery of cells associated with an abnormal DNA profile. These data strongly suggest a selective effect of PHA-680632 on different cell types spanning from induction of polyploidy to a 4N cell cycle block and may implicate that PHA-680632 might be selectively toxic to some tumor cells.

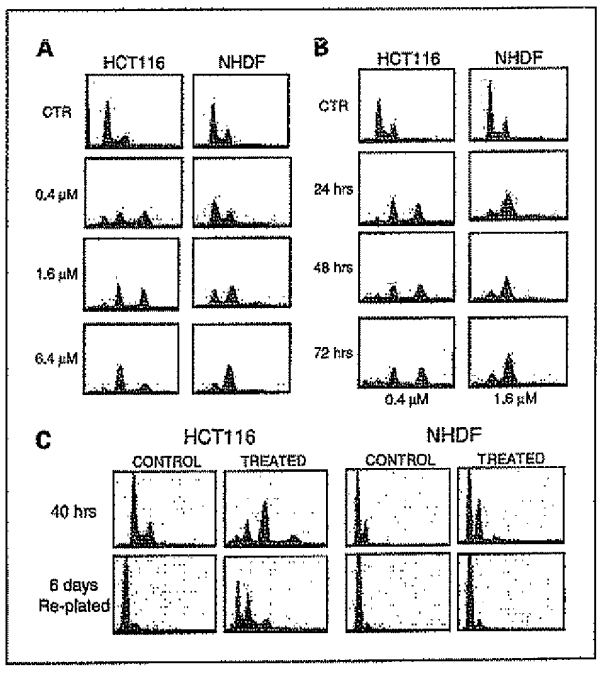

Fig. 2. Effect of PHA-680632 on the cell cycle and comparison between NHDF and a tumor cell line (HCT116). *A*, cells were treated for 24 hours with PHA-680632 at the indicated concentrations. After treatments, cells were collected and analyzed by flow cytometry. *B*, cell cycle analysis of HCT116 and NHDF treated with PHA-680632 at the indicated concentrations at 24, 48, and 72 hours of treatment. *C*, HCT116 and NHDF were treated with 0.5 μmol/L PHA-680632 for 40 hours. The remaining cells were collected and replated to follow regrowth up to 6 days. After treatments, cells were collected and analyzed by flow cytometry.

PHA-680632 cell treatment induces phenotypes similar to Aurora A or B depletion. To better explore the mechanism of action of PHA-680632, we compared the effect of the inhibitor on cells with siRNA down-regulating Aurora A or B. We designed several siRNA oligonucleotides corresponding to Aurora A and B and tested them for different times to choose the optimal conditions to reduce Aurora mRNA and protein. A typical result is shown in Fig. 3A, where HeLa cells were transfected with Aurora A or B oligonucleotides and after 48 hours showed a good reduction of the proteins in comparison with untreated cells or cells transfected with control siRNA oligonucleotides.

HeLa cells depleted either of Aurora A or B showed different phenotypes with cells accumulating with different DNA content. Aurora A siRNA promotes apoptosis as shown by an increase of the sub-G_1 cell population (Fig. 3B) and by the presence of active caspase-9 and caspase-3 measured by Western blot. Aurora A siRNA also does not inhibit histone H3 phosphorylation (Fig. 3A). On the contrary, depletion of Aurora B does not activate caspases but inhibits histone H3 phosphorylation. Moreover, Aurora B siRNA leads to an increase in 4N DNA content, and over the time, the percentage of cells with a DNA content higher than 4N is seen (Fig. 3B). Using the inhibitor, the morphologic effects on cells recall the ones obtained by depleting Aurora B as confirmed by phase-contrast microscopy (Fig. 3C). However, also at the molecular level, the induction of active caspase-9 and caspase-3 (Fig. 3A) is observed, which is compatible with Aurora A inactivation. This effect was measured also *in vivo* in tumor xenografts of treated mice (Fig. 4).

Inhibition of histone H3 phosphorylation due to Aurora B siRNA is in good agreement with the published data (38). All the reported Aurora inhibitors to date have shown modulation of histone H3 phosphorylation at Ser^{10}. Accordingly, HeLa cells treated with 2 μmol/L PHA-680632 for 24 hours also show a strong reduction of the phosphorylation of histone H3 in Ser^{10} (Fig. 3A), confirming the activity of our compound on Aurora B. Moreover, as shown in Fig. 3D, when HeLa cells are treated for 1 hour with PHA-680632 at concentrations ranging between 0.1 and 20 μmol/L, the compound clearly inhibits both Aurora A autophosphorylation at T288 (39) and Aurora B–mediated phosphorylation of histone H3 as expected for a dual Aurora kinase inhibitor (40).

A reduction in phosphorylation of BubR1, which is phosphorylated in response to spindle damage, was shown with siRNA experiments targeting Aurora B and also using Aurora kinase inhibitors (32, 40). In fact, upon treatment of HeLa cells with nocodazole, it is possible to observe a band shift of BubR1 due to phosphorylation (Fig. 3E, *arrow*). In the presence of PHA-680632, disappearance of the band corresponding to phospho-BubR1 is observed, suggesting that Aurora B–mediated phosphorylation of BubR1 is also inhibited (Fig. 3E). In summary, the drug-induced phenotypes are consistent with inhibition of Aurora A and B.

PHA-680632 suppresses tumor growth in animal models. The effect of PHA-680632 on tumor growth was evaluated in human tumor cell xenografts models and in syngeneic models in mouse and rat (Fig. 4; data not shown). PHA-680632 was initially evaluated in the HL60 human acute myelogenous leukemia xenograft model in a dose-finding study. After i.v. administration, at three dose levels (15, 30, and 45 mg/kg b.i.d. consecutively for 5 days), a significant TGI was observed as shown in Fig. 4A (*top*). The 45 mg/kg dose resulted in 85% of TGI without signs of toxicity. In the A2780 human ovarian carcinoma model (Fig. 4A, *middle*), the dose of 60 mg/kg i.v. b.i.d. for 5 days showed potent tumor inhibition, reaching 78% of TGI compared with the vehicle-treated controls. A more prolonged exposure to PHA-680632 was tested in the HCT116 colon carcinoma xenograft, administering the compound i.p. t.i.d. for 12 days. The treatments were also in this case well tolerated and TGI was 75% compared with controls (Fig. 4A, *bottom*).

PHA-680632 efficacy was then evaluated in a syngeneic breast cancer model where tumors arose through a transgenic oncogene. PHA-680632 inhibited growth of activated *ras*-driven mammary tumors in mouse mammary tumor virus v-Ha-*ras* transgenic mice, which exhibit many characteristics of human breast tumors, including spontaneous development and local invasiveness. PHA-680632 treatment of mice bearing established tumors resulted in complete tumor stabilization and partial regression (Fig. 4B). Comparable results were also obtained administering PHA-680632 to rats harboring 7,12-dimethylbenz(*a*)anthracene-induced mammary carcinomas (data not shown), showing the effectiveness of this agent against syngeneic models of mammary cancers arising from either oncogene overexpression or carcinogen exposure. Moreover, histologic analysis of A2780 xenografts at day 10 after treatment (30 mg/kg t.i.d) showed an increase in cellular and nuclear size and the appearance of multinucleated cells similar to the phenotype obtained with cell lines in tissue culture (Supplementary Data 3). Proliferation of tumor cells *in vivo* as measured by bromodeoxyuridine incorporation in the same xenograft model showed also a significant reduction after 5 days treatment with PHA-680632 (30 mg/kg b.i.d.). In HL60 xenografts, we observed in addition an ~3-fold increase in apoptosis as measured by caspase-3 staining (Supplementary Data 3). In summary, these observations *in vivo* confirm the effect of the compound observed *in vitro* and provide useful tools to follow activity of the inhibitor *in vivo*.

Phosphorylation of histone H3 at Ser^{10} is a biomarker that allows PHA-680632 activity to be monitored in vitro *and* in vivo. Inhibition of the phosphorylation of histone H3 at Ser^{10} caused by our Aurora inhibitor was confirmed in several cell lines. Using Array Scan 4.0 System, we were able to calculate an IC_{50} for this inhibition, which is 0.39 μmol/L in U2OS cells (Fig. 5A). U2OS are relatively resistant to polyploidy induction when treated with PHA-680632 for 24 hours with several doses of the inhibitor as shown by flow cytometry (Fig. 5B). Time-course experiments on U2OS cells treated with PHA-680632 showed that the inhibitory effect on the phosphorylation of the histone H3 is very fast: already after 15 minutes of treatment, it is possible to see the disappearance of the signal (Fig. 5C). This response makes histone H3 phosphorylation a fast and sensitive readout for targeting Aurora B. We tested whether this modulation can also be observed *in vivo* using tissues of mice treated with PHA-680632. Nude mice bearing A2780 xenografts were treated i.v. bolus with vehicle only or 60 mg/kg PHA-680632. Animals were sacrificed 30 minutes, 2 hours, 8 hours, and 24 hours after treatment. In bone marrow and tumors, phosphorylation of histone H3 was analyzed by immunohistochemistry and Western blot (Fig. 6A and B). In both tissues, it was possible to observe a strong reduction of

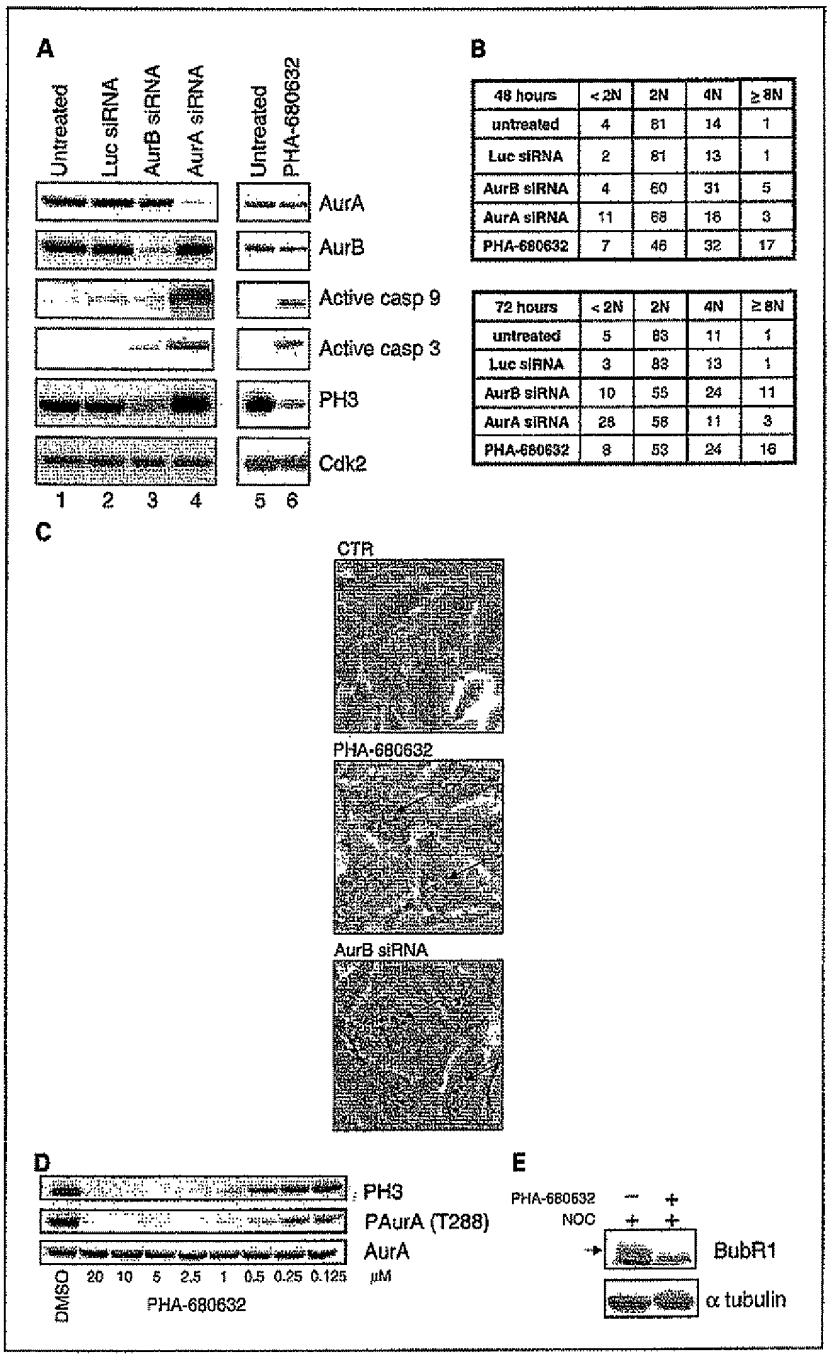

Fig. 3. Phenotype of down-regulating Aurora kinases by siRNA or treatment with PHA-680632. *A*, Western blot analysis of extracts prepared from HeLa cells 48 hours after transfection or after compound treatment. *Lanes 1* and *5*, nontransfected cells; *lane 2*, control siRNA; *lane 3*, Aurora B siRNA; *lane 4*, Aurora A siRNA; *lane 6*, 2 μmol/L PHA-680632. Membranes were blotted with the indicated antibodies. An antibody recognizing CDK2 was used as loading control. *B*, percentages of cells with different DNA content were calculated from cell cycle profiles of HeLa cells after transfection with Aurora A or B siRNA for 48 and 72 hours. *C*, phase-contrast microscopy of HeLa cells that were either untreated, treated with 2 μmol/L PHA-680632, or transfected for 72 hours with Aurora B siRNA. *Arrows*, examples of polynucleated cells (~10% of the total culture). *D*, Western blot analysis of HeLa cells treated for 1 hour with PHA-680632 at the indicated concentrations. Activity on Aurora A autophosphorylation (T288) and Aurora B–mediated phosphorylation on histone H3 (S^{10}). *E*, Western blot analysis of HeLa cells treated with nocodazole (9 hours at 75 ng/mL) in the absence (*left lane*) or presence (*right lane*) of 2 μmol/L PHA-680632 for the last 2 hours. Membranes were blotted with the indicated antibodies. *Arrow*, band shift associated with phosphorylation of BubR1.

this phosphorylation, although the kinetics were slightly different in the two organs possibly due to tissue penetration or retention of the compound. In both tissues, the effect starts to disappear 8 hours after treatment (Fig. 6), compatible with the half-life of the compound, which is ~70 minutes in mouse plasma. We are currently working on a pharmacokinetic/pharmacodynamic model to correlate efficacy with degree and time of biomarker modulation because the duration of the modulation is a critical factor for efficacy. Effects on histone H3 phosphorylation were also studied in human primary cells from leukemia patients. Total WBC from peripheral blood or bone marrow aspirates of patients with leukemia were purified. Cells were plated and treated with PHA-680632 or with nocodazole that was used as control to confirm that cells were cycling, because it blocks cells in G_2-M and gives a strong increase in the phosphorylation of histone H3. In 6 of 18 cases that responded to nocodazole treatment, we observed an inhibition of the phosphorylation of histone H3 when treated

with PHA-680632. An example of a responsive sample is shown in Fig. 6C. We also measured a massive cell death in the treated samples, but it was not possible to quantify the data considering the high ratio of spontaneous apoptosis in this type of cells once put into culture.

In summary, these data strongly indicate that phosphorylation of histone H3 at Ser^{10} is a good candidate as a biomarker for preclinical and clinical studies of an Aurora kinase inhibitor and to give an indication for plasma target concentrations to be reached in a clinical trial.

Discussion

PHA-680632 was developed as an ATP competitive compound with high activity on Aurora kinases. The compound showed minor cross-reactivity with other kinases tested. One of the cross-reactivities involves FGFR1 and its inhibition by PHA-680632 *in vivo* may contribute to the overall antitumor activity displayed by the compound. For example, the recently described Aurora inhibitor VX-680 (34) inhibits all the Aurora kinases and FLT3 tyrosine kinase [$K_{i(app)}$, 30 nmol/L], which is aberrantly expressed in a large percentage of acute myelogenous leukemia patients. However, for both compounds, the dominant cellular phenotype, as detected by the cell cycle profile, is compatible with an Aurora kinases mode of action (4N and polyploidy) and, in case of PHA-680632, not with inhibition of FGFR1.

Different cells were treated with PHA-680632 showing differences in the cellular response as reflected in the cell cycle profiles. We did not find a correlation between sensitivity of cells in the proliferation assay and the mRNA expression levels of the Aurora kinases within the cell lines analyzed thus far. Differences in sensitivity and type of response might rather be associated with different genetic backgrounds among the cell lines. For instance, HCT116 cells seem to be highly sensitive (IC_{50}, 60 nmol/L) and also readily go to polyploidy and cannot revert the phenotype after drug withdrawal (Fig. 2C). This could be explained considering the fact that HCT116 lack CHFR, a mitotic checkpoint protein (41) recently shown to be involved also in Aurora regulation (42). On the other hand, NHDF that are primary cells with intact checkpoints cannot be brought into polyploidization after treatment even at high doses and long exposures and they are able to return to the normal cell cycle after drug washout. Similar results were obtained with mouse embryo fibroblasts (data not shown).

An involvement of a cell cycle checkpoint in this type of response is supported by the work of Ditchfield et al. (32) describing the Aurora kinase inhibitor ZM447439. They showed different behavior of U2OS cells treated with the inhibitor, in the presence or absence of functional p53, suggesting that Aurora inhibitors might be selectively toxic to tumor cells lacking p53. Indeed, there are evident links between Aurora A and p53 that might correlate with tumor development. It was reported that p53 interacts with Aurora A and suppresses its oncogenic activity in a transactivation-independent manner (24). It was also shown that p53 is phosphorylated by Aurora A. This phosphorylation can promote degradation of p53 (Ser^{315}; ref. 25) or can cause suppression of p53 transcriptional activity (Ser^{215}; ref. 26). Moreover, Aurora A overexpression has been correlated with mutations in p53 in hepatocellular carcinomas and tumors

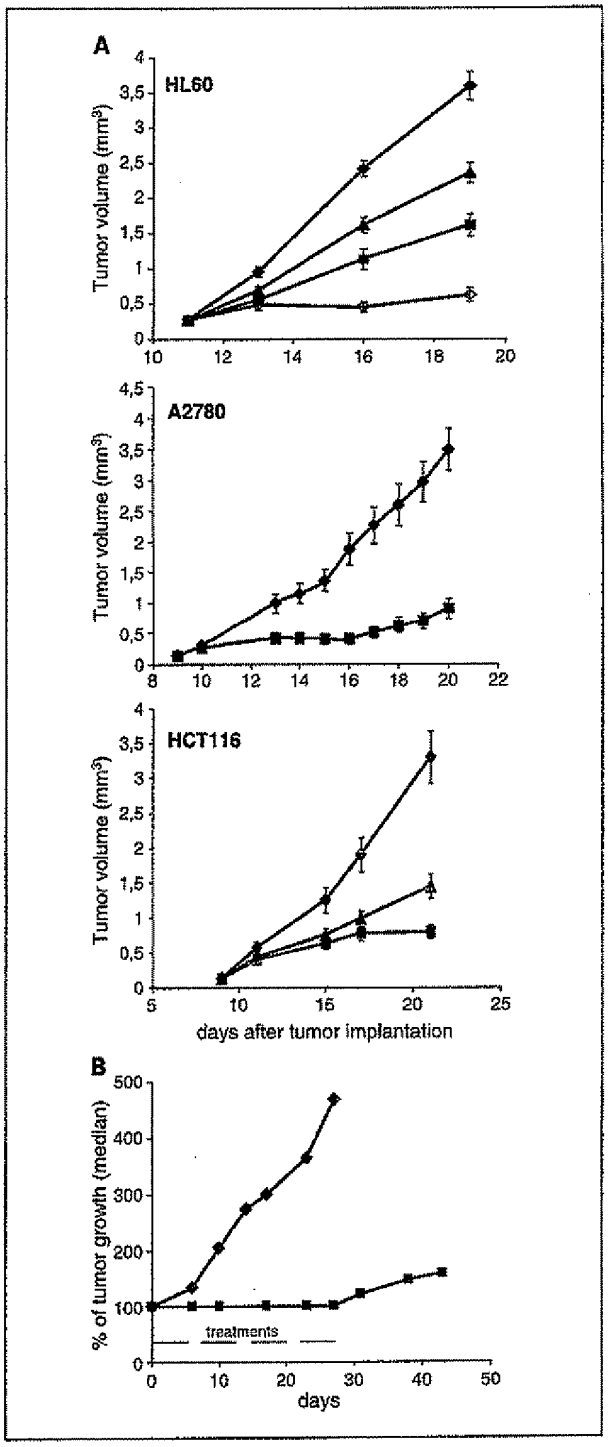

Fig. 4. PHA-680632 suppresses tumor growth in animal models. *A, top,* HL60 tumors were treated i.v. b.i.d. from days 11 to 15 with vehicle (◆) or PHA-680632 at 15 (▲), 30 (■), or 45 (◇) mg/kg. *Middle,* A2780 ovarian carcinoma tumors were treated i.v. b.i.d. from days 9 to 13 with vehicle (◆) or PHA-680632 at 60 mg/kg (■). *Bottom,* HCT116 colon carcinoma tumors were treated i.p. t.i.d. from days 9 to 20 with vehicle (◆) or PHA-680632 at 15 (▲) or 30 (■) mg/kg. *B,* mouse mammary tumor virus v-Ha-*ras* mammary carcinoma established tumors were treated i.p. t.i.d with vehicle (◆) or PHA-680632 at 45 mg/kg (■) followed by 2 days off treatment, repeated for four cycles.

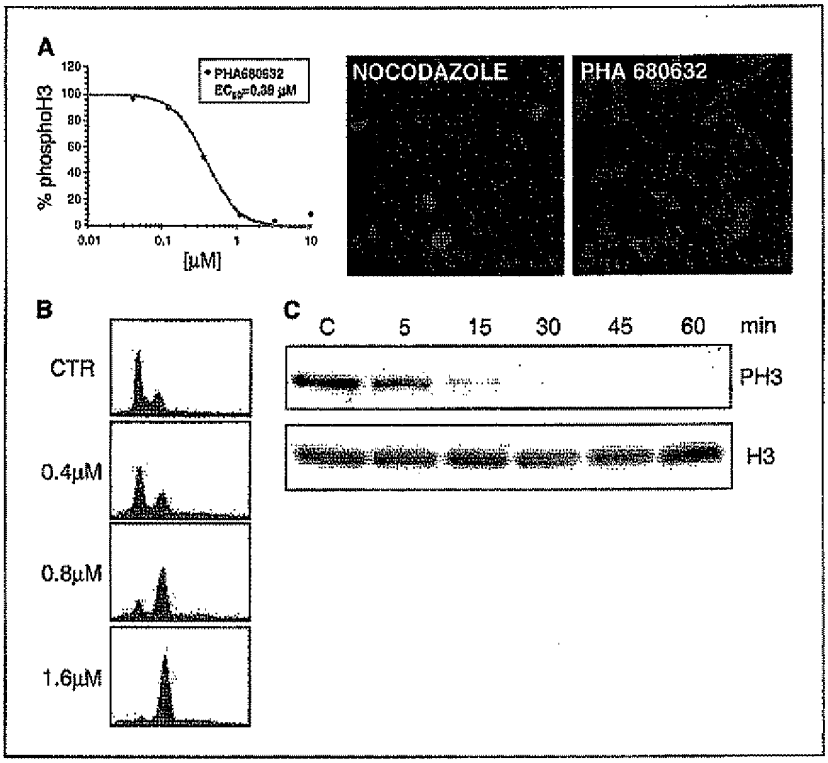

Fig. 5. Kinetics of inhibition of the phosphorylation of histone H3. *A*, Array Scan IV analysis of phosphorylation of histone H3 on U2OS cells treated for 7 hours with 75 ng/mL nocodazole followed by different doses of PHA-680632 for the last 1.5 hours. *B*, cell cycle profiles of U2OS cells treated for 24 hours at the indicated doses of PHA-680632. *C*, Western blot analysis of phosphorylated histone H3 of U2OS cells treated with 5 μmol/L PHA-680632 and collected at the indicated time points.

with both features had the worse prognosis (20), indicating a cooperative effect on tumor formation.

The thus far described Aurora inhibitors, which hit all Aurora kinases, induce a cellular phenotype comparable with the one described here for PHA-680632 and are identical to inactivation of Aurora B alone. This is supported by a recent publication (40), whereby siRNA experiments targeting simultaneously Aurora A and B, resulted in a phenotype comparable with Aurora B siRNA alone, suggesting that inactivation of Aurora B bypasses Aurora A functions in mitosis.

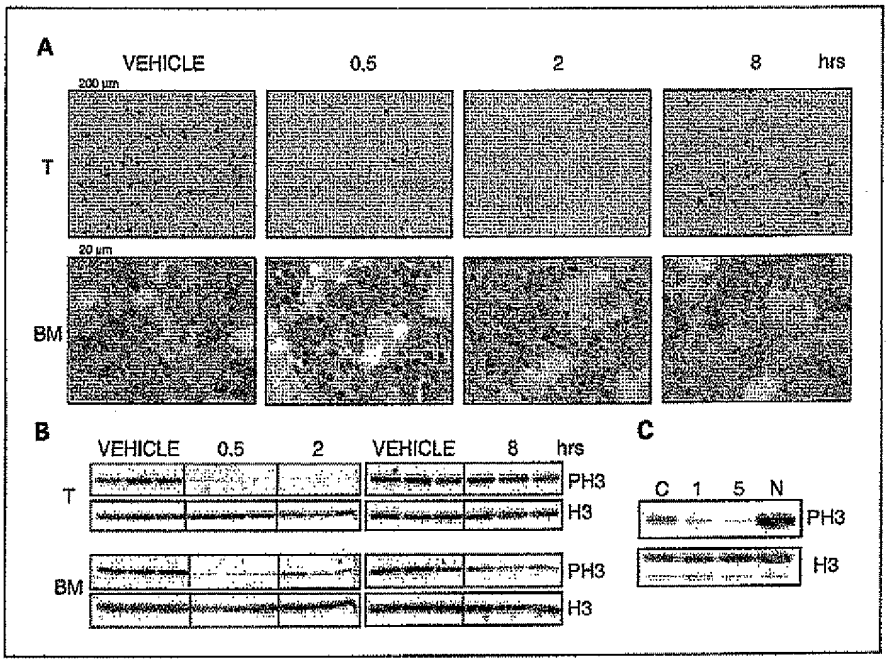

Fig. 6. *In vivo* evaluation of phosphorylated histone H3 modulation. *A*, immunohistochemical staining of phosphorylated histone H3 antigen in tumor (*T*) or bone marrow (*BM*) of mice bearing A2780 xenograft treated i.v. with vehicle only or 60 mg/kg PHA-680632. Animals were sacrificed after treatment at the indicated times. *B*, Western blot analysis of phosphorylated histone H3 (*PH3*) in the same sample described above. Results for three mice that are representative of a group of five. *C*, Western blot analysis of total WBC from an acute myelogenous leukemia patient treated *in vitro* with either nocodazole (75 ng/mL) or 1 μmol/L or 5 μmol/L PHA-680632 for 24 hours. C, control.

Originally, Aurora A and B kinases have been implicated in phosphorylation of histone H3 *in vitro* and *in vivo* (43), but Aurora B seems to be the preferential histone H3 kinase. This modification, which is conserved from yeast to vertebrates, is carried out by Ipl1 in budding yeast (44) and the Aurora B homologue in other organisms, such as *Caenorhabditis elegans* (44) and *Drosophila melanogaster* (45). PHA-680632 is a potent inhibitor of the phosphorylation of histone H3. We were able to measure modulation of the phosphorylation status of histone H3 *in vivo* in different tissues, including bone marrow (Fig. 6) and skin. This property suggests the use of histone H3 phosphorylation as a specific biomarker for a readout of Aurora kinase B in clinical samples. Effects on histone H3 phosphorylation were also seen in human primary cells derived from leukemia patients and we were able to see an inhibition of the phosphorylation of histone H3 when treated with PHA-680632. Interestingly, in a recent publication (46), it has been shown that phosphorylation of histone H3 at Ser^{10} might be required for inducing neoplastic cell transformation, suggesting that inhibition of this phosphorylation could be directly involved in the antitumoral activity that we observed.

A growing number of Aurora kinase inhibitors are in development and first compounds have entered the clinic (29). All the described inhibitors have similar effects on cells, typically mimicking genetic depletion of Aurora B, but they might differ in potency against all three Aurora kinases and specificity against other kinases. PHA-680632 shows the same features consistent with a potent Aurora B inhibitor, although we show also evidence for inhibition of Aurora A. We are currently undertaking experiments to better understand the mechanism of action of our compound during different stages of mitosis and to understand the molecular basis for the differential responses observed in different cell lines. The answer to whether it is better to inhibit Aurora A or B alone or in combination will become clearer once results on selective inhibitors are available. This will be important in a clinical context to minimize potential toxic effects and to identify the appropriate patient population to be treated. For this purpose, it will be useful to compare activities of single and multiple Aurora kinase inhibitors, because these compounds might have different cellular effects. For example, a specific inhibitor of Aurora A would be expected to give an arrest or delay in G_2-M associated with defects in centrosome number, spindle formation, and, consequently, an increase in apoptosis.

Acknowledgments

We thank our colleagues from the Cell Bank, Experimental Therapy Unit, and Toxicology Department of Nerviano Medical Sciences S.r.l. for their contributions and Drs. Porta and Bianchi (Institute of Internal Medicine and Medical Oncology, IRCCS Policlinico San Matteo, Pavia, Italy) and Drs. Brando and Longo (Laboratory of Transplant Immunology and Hematologic Diagnosis, Hospital Niguarda Ca' Granda, Milan, Italy) for providing patient samples.

References

1. Carmena M, Earnshaw WC. The cellular geography of aurora kinases. Nat Rev Mol Cell Biol 2003;4:842–54.
2. Andrews PD, Knatko E, Moore WJ, et al. Mitotic mechanics: the auroras come into view. Curr Opin Cell Biol 2003;15:672–83.
3. Castro A, Vigneron S, Bernis C, Labbe JC, Prigent C, Lorca T. The D-box-activating domain (DAD) is a new proteolysis signal that stimulates the silent D-box sequence of Aurora-A. EMBO Rep 2002;3:1209–14.
4. Littlepage LE, Ruderman JV. Identification of a new APC/C recognition domain, the A box, which is required for the Cdh1-dependent destruction of the kinase Aurora-A during mitotic exit. Genes Dev 2002;16:2274–85.
5. Castro A, Arlot-Bonnemains Y, Vigneron S, Labbe JC, Prigent C, Lorca T. APC/Fizzy-related targets Aurora-A kinase for proteolysis. EMBO Rep 2002;3:457–62.
6. Honda K, Mihara H, Kato Y, et al. Degradation of human Aurora2 protein kinase by the anaphase-promoting complex-ubiquitin-proteasome pathway. Oncogene 2000;19:2812–9.
7. Bischoff JR, Anderson L, Zhu Y, et al. A homologue of *Drosophila* aurora kinase is oncogenic and amplified in human colorectal cancers. EMBO J 1998;17:3052–65.
8. Gassmann R, Carvalho A, Henzing AJ, et al. Borealin: a novel chromosomal passenger required for stability of the bipolar mitotic spindle. J Cell Biol 2004;166:179–91.
9. Meraldi P, Honda R, Nigg EA. Aurora kinases link chromosome segregation and cell division to cancer susceptibility. Curr Opin Genet Dev 2004;14:29–36.
10. Ducat D, Zheng Y. Aurora kinases in spindle assembly and chromosome segregation. Exp Cell Res 2004;301:60–7.
11. Marumoto T, Zhang D, Saya H. Aurora-A—a guardian of poles. Nat Rev Cancer 2005;5:42–50.
12. Kimura M, Matsuda Y, Yoshioka T, Okano Y. Cell cycle-dependent expression and centrosome localization of a third human aurora/Ipl1-related protein kinase, AIK3. J Biol Chem 1999;274:7334–40.
13. Sasai K, Katayama H, Stenoien DL, et al. Aurora-C kinase is a novel chromosomal passenger protein that can complement Aurora-B kinase function in mitotic cells. Cell Motil Cytoskeleton 2004;59:249–63.
14. Katayama H, Brinkley WR, Sen S. The Aurora kinases: role in cell transformation and tumorigenesis. Cancer Metastasis Rev 2003;22:451–64.
15. Li D, Zhu J, Firozi PF, et al. Overexpression of oncogenic STK15/BTAK/Aurora A kinase in human pancreatic cancer. Clin Cancer Res 2003;9:991–7.
16. Katayama H, Ota T, Jisaki F, et al. Mitotic kinase expression and colorectal cancer progression. J Natl Cancer Inst 1999;91:160–2.
17. Gritsko TM, Coppola D, Paciga JE, et al. Activation and overexpression of centrosome kinase BTAK/Aurora-A in human ovarian cancer. Clin Cancer Res 2003;9:1420–6.
18. Sakakura C, Hagiwara A, Yasuoka R, et al. Tumour-amplified kinase BTAK is amplified and overexpressed in gastric cancers with possible involvement in aneuploid formation. Br J Cancer 2001;84:824–31.
19. Fraizer GC, Diaz MF, Lee IL, Grossman HB, Sen S. Aurora-A/STK15/BTAK enhances chromosomal instability in bladder cancer cells. Int J Oncol 2004;25:1631–9.
20. Jeng YM, Peng SY, Lin CY, Hsu HC. Overexpression and amplification of Aurora-A in hepatocellular carcinoma. Clin Cancer Res 2004;10:2065–71.
21. Tong T, Zhong Y, Kong J, et al. Overexpression of Aurora-A contributes to malignant development of human esophageal squamous cell carcinoma. Clin Cancer Res 2004;10:7304–10.
22. Zhou H, Kuang J, Zhong L, et al. Tumour amplified kinase STK15/BTAK induces centrosome amplification, aneuploidy and transformation. Nat Genet 1998;20:189–93.
23. Gigoux V, L'Hoste S, Raynaud F, Camonis J, Garbay C. Identification of Aurora kinases as RasGAP Src homology 3 domain-binding proteins. J Biol Chem 2002;277:23742–6.
24. Chen SS, Chang PC, Cheng YW, Tang FM, Lin YS. Suppression of the STK15 oncogenic activity requires a transactivation-independent p53 function. EMBO J 2002;21:4491–9.
25. Katayama H, Sasai K, Kawai H, et al. Phosphorylation by aurora kinase A induces Mdm2-mediated destabilization and inhibition of p53. Nat Genet 2004;36:55–62.
26. Liu Q, Kaneko S, Yang L, et al. Aurora-A abrogation of p53 DNA binding and transactivation activity by phosphorylation of serine 215. J Biol Chem 2004;279:52175–82.
27. Farruggio DC, Townsley FM, Ruderman JV. Cdc20 associates with the kinase aurora2/Aik. Proc Natl Acad Sci U S A 1999;96:7306–11.
28. Du J, Hannon GJ. The centrosomal kinase Aurora-A/STK15 interacts with a putative tumor suppressor NM23-1. Nucleic Acids Res 2002;30:5465–75.
29. Garber K. Divide and conquer: new generation of drugs targets mitosis. J Natl Cancer Inst 2005;97:874–6.
30. Keen N, Taylor S. Aurora-kinase inhibitors as anticancer agents. Nat Rev Cancer 2004;4:927–36.
31. Hauf S, Cole RW, LaTerra S, et al. The small molecule Hesperadin reveals a role for Aurora B in correcting kinetochore-microtubule attachment and in maintaining the spindle assembly checkpoint. J Cell Biol 2003;161:281–94.
32. Ditchfield C, Johnson VL, Tighe A, et al. Aurora B couples chromosome alignment with anaphase by targeting BubR1, Mad2, and Cenp-E to kinetochores. J Cell Biol 2003;161:267–80.
33. Gadea BB, Ruderman JV. Aurora kinase inhibitor ZM447439 blocks chromosome-induced spindle assembly, the completion of chromosome condensation, and the establishment of the spindle integrity checkpoint in *Xenopus* egg extracts. Mol Biol Cell 2005;16:1305–18.
34. Harrington EA, Bebbington D, Moore J, et al. VX-680, a potent and selective small-molecule inhibitor of the Aurora kinases, suppresses tumor growth *in vivo*. Nat Med 2004;10:262–7.
35. Pevarello P, Brasca MG, Amici R, et al. 3-Aminopyrazole inhibitors of CDK2/cyclin A as antitumor agents. 1. Lead finding. J Med Chem 2004;47:3367–80.

36. Simeoni M, Magni P, Cammia C, et al. Predictive pharmacokinetic-pharmacodynamic modeling of tumor growth kinetics in xenograft models after administration of anticancer agents. Cancer Res 2004;64:1094–101.
37. Fancelli D, Berta D, Bindi S, et al. Potent and selective aurora inhibitors identified by the expansion of a novel scaffold for protein kinase inhibition. J Med Chem 2005;48:3080–4.
38. Pascreau G, Arlot-Bonnemains Y, Prigent C. Phosphorylation of histone and histone-like proteins by aurora kinases during mitosis. Prog Cell Cycle Res 2003;5:369–74.
39. Bayliss R, Sardon T, Vernos I et al. Structural basis of Aurora-A activation by TPX2 at the mitotic spindle. Mol Cell 2003;12:851–62.
40. Yang H, Burke T, Dempsey J, et al. Mitotic requirement for aurora A kinase is bypassed in the absence of aurora B kinase. FEBS Lett 2005;579:3385–91.
41. Summers MK, Bothos J, Halazonetis TD. The CHFR mitotic checkpoint protein delays cell cycle progression by excluding cyclin B1 from the nucleus. Oncogene 2005;24:2589–98.
42. Yu X, Minter-Dykhouse K, Malureanu L, et al. Chfr is required for tumor suppression and Aurora A regulation. Nat Genet 2005;37:401–6.
43. Crosio C, Fimia GM, Loury R, et al. Mitotic phosphorylation of histone H3: spatio-temporal regulation by mammalian Aurora kinases. Mol Cell Biol 2002;22:874–85.
44. Hsu JY, Sun ZW, Li X, et al. Mitotic phosphorylation of histone H3 is governed by Ipl1/aurora kinase and Glc7/PP1 phosphatase in budding yeast and nematodes. Cell 2000;102:279–91.
45. Giet R, Glover DM. *Drosophila* aurora B kinase is required for histone H3 phosphorylation and condensin recruitment during chromosome condensation and to organize the central spindle during cytokinesis. J Cell Biol 2001;152:669–82.
46. Choi HS, Choi BY, Cho YY, et al. Phosphorylation of histone H3 at serine 10 is indispensable for neoplastic cell transformation. Cancer Res 2005;65:5818–27.

EXHIBIT E

nature medicine

VX-680, a potent and selective small-molecule inhibitor of the Aurora kinases, suppresses tumor growth *in vivo*

Elizabeth A Harrington[1], David Bebbington[1], Jeff Moore[1], Richele K Rasmussen[1], Abi O Ajose-Adeogun[1], Tomoko Nakayama[2], Joanne A Graham[1,4], Cecile Demur[3], Thierry Hercend[1,4], Anita Diu-Hercend[1,4], Michael Su[2], Julian M C Golec[1] & Karen M Miller[1]

The Aurora kinases are essential for the regulation of chromosome segregation and cytokinesis during mitosis. Aberrant expression and activity of these kinases occur in a wide range of human tumors, and lead to aneuploidy and tumorigenesis. Here we report the discovery of a highly potent and selective small-molecule inhibitor of Aurora kinases, VX-680, that blocks cell-cycle progression and induces apoptosis in a diverse range of human tumor types. This compound causes profound inhibition of tumor growth in a variety of *in vivo* xenograft models, leading to regression of leukemia, colon and pancreatic tumors at well-tolerated doses. Our data indicate that Aurora kinase inhibition provides a new approach for the treatment of multiple human malignancies.

The Aurora family of serine/threonine kinases is essential for mitotic progression[1–5]. Aurora-A has a crucial role in mitotic spindle formation and centrosome maturation, ensuring faithful segregation of chromosomes into daughter cells[1–6]. In mammalian cells, abrogation of Aurora-A kinase activity disrupts cell cycle progression. Microinjection of antibodies to Aurora-A or depletion of Aurora-A by RNA interference delays mitotic entry[7,8]. Very little is known, however, about the ultimate fate of the arrested cells. Aurora-B is a 'chromosomal passenger' protein that is essential for chromosomal congression and cytokinesis[1,5]. It is associated with centromeres during prometaphase, and with the spindle midzone during anaphase and telophase. Overexpression of kinase-inactive Aurora-B disrupts kinetochore–microtubule interactions, cleavage furrow formation and cytokinesis, leading to polyploidy[9–11]. This polyploid state may arrest cell-cycle progression through activation of a 'tetraploidy checkpoint'[12]. The function of Aurora-C remains unclear. In normal tissues, the expression of this centrosome-associated kinase is predominantly restricted to germ cells[13].

Expression and activity of the Aurora kinases are tightly regulated during the cell cycle. Activity of all three proteins peaks during the G2 and mitotic phases of the cell cycle, while expression is low or undetectable in resting cells[13,14]. A variety of Aurora substrates have been identified, the most well characterized being histone H3, a protein involved in chromosome condensation and mitotic entry[15,16]. Other substrates include CENP-A[17], myosin II regulatory light chain[18], protein phosphatase-1 (ref. 19), TPX-2 (ref. 20), INCENP[21,22], survivin[23,24], topoisomerase II alpha[25], vimentin[26], MBD-3 (ref. 27), MgcRacGAP[28], desmin[29], Ajuba[8], XiEg5 (in *Xenopus*)[30], Ndc10p (in budding yeast)[31] and D-TACC (in *Drosophila*)[32]. These proteins all have a role in cell division.

Since its discovery in 1997, the mammalian Aurora kinase family has been closely linked to tumorigenesis. Overexpression of Aurora-A transforms mammalian fibroblasts[14] and gives rise to aneuploid cells containing multiple centrosomes and multipolar spindles. The resulting genetic instability is likely to contribute to tumorigenesis. Indeed, amplification of the *AURKA* locus correlates with chromosomal instability in mammary and gastric tumors[33,34]. The Aurora kinases are overexpressed in a wide range of human tumors. Elevated expression of Aurora-A has been detected in over 50% of colorectal[14,35], ovarian[36] and gastric tumors[34], and in 94% of invasive duct adenocarcinomas of the breast[37]. In addition, amplification of the *AURKA* locus (20q13) correlates with poor prognosis for patients with node-negative breast cancer[38]. Aurora-B is highly expressed in multiple human tumor cell lines, and its levels increase as a function of Duke stage in primary colorectal cancers[39]. Aurora-C, which is normally only found in germ cells, is also overexpressed in a high percentage of primary colorectal cancers and in a variety of tumor cell lines[13,35].

The advent of targeted therapies for specific cancer phenotypes, such as Gleevec (imatinib) for chronic myelogenous leukemia, has resulted in a surge of optimism across the field of oncology. Gleevec is a small-molecule kinase inhibitor that targets BCR-ABL, c-Kit and platelet-derived growth factor receptor kinases[40]. The clinical success of Gleevec has increased confidence that small-molecule inhibitors of specific kinases may prove to be highly effective anticancer agents.

[1]Vertex Pharmaceuticals (Europe) Limited, 88 Milton Park, Abingdon, Oxfordshire, OX14 4RY, UK. [2]Vertex Pharmaceuticals Incorporated, 130 Waverly Street, Cambridge, Massachusetts 02139, USA. [3]INSERM E-9910, Institut Claudis Regaud, 20 Rue du Pont Saint-Pierre, 31052 Toulouse Cedex, France. [4]Present addresses: Decision Resources International, 50-51 Russell Square, London, WC1B 4HQ, UK (J.A.G.) and Aventis Pharma SA, Paris Research Center, 13 Quai Jules Guesde, F-94400 Vitry sur Seine, France (T.H. and A.D.-H.). Correspondence should be addressed to K.M.M. (karen_miller@vrtx.com).

Published online 22 February 2004; doi:10.1038/nm1003

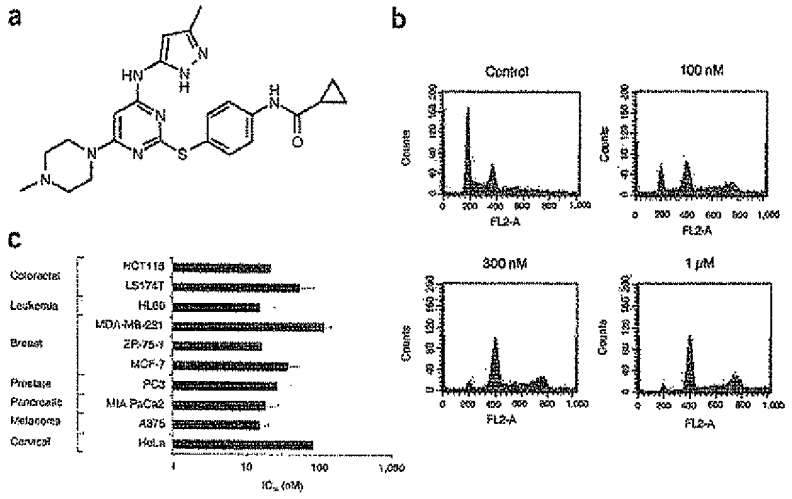

Figure 1 VX-680 is a potent and selective Aurora kinase inhibitor that blocks proliferation of multiple tumor cell types. (**a**) Chemical structure of VX-680 (cyclopropane carboxylic acid {4-[4-(4-methyl-piperazin-1-yl)-6-(5-methyl-2H-pyrazol-3-ylamino)-pyrimidin-2-ylsulphanyl]-phenyl}-amide). (**b**) VX-680 induces accumulation of cells with ≥4*N* DNA content. MCF-7 cells were treated with VX-680 for 48 h. DNA content was assessed by flow cytometric analysis of cells labeled with propidium iodide (FL2-A). (**c**) VX-680 blocks tumor cell proliferation. Proliferation of a panel of tumor cell lines was assessed by [^{3}H]thymidine incorporation after 96-h treatment with VX-680.

Based on the known function of the Aurora kinases, inhibition of their activity should disrupt the cell cycle and block proliferation. However, the impact of Aurora inhibition on tumor cell viability has not yet been explored. Here we describe the profile of VX-680, a potent and highly selective Aurora kinase inhibitor. In addition to its ability to disrupt the cell cycle and inhibit proliferation, it also induces apoptosis in a wide range of cancer cell types while noncycling cells remain unaffected. *In vivo*, VX-680 induces profound inhibition of tumor growth, resulting in regression at well-tolerated doses. These data provide compelling evidence that inhibition of the Aurora kinase family represents a new approach to pharmacological intervention in oncology.

RESULTS

Structure-based development of Aurora kinase inhibitors

Our aim was to generate highly potent, selective and reversible inhibitors by targeting the ATP-binding site of the Aurora kinases. The three human family members have identical ATP binding sites, and small molecules were not expected to differentiate between them. Crystal structures[41] identified several unique structural features in the Aurora kinases, compared with closely related enzymes such as Src and cyclin-dependent kinase-2. Such structural knowledge helped in the design of selective Aurora inhibitors, culminating in the synthesis of VX-680 (Fig. 1a).

VX-680 is a potent inhibitor of all three Aurora kinases, with apparent inhibition constant ($K_{i(app)}$) values of 0.6, 18 and 4.6 nM for Aurora-A, Aurora-B and Aurora-C, respectively. VX-680 shows greater than 100-fold selectivity for the Aurora-A kinase over 55 other kinases tested, the only exception being Fms-related tyrosine kinase-3 (FLT-3; $K_{i(app)}$ = 30 nM; Supplementary Table 1 online). The FLT-3 kinase has a role in hematopoiesis and is frequently mutated to a constitutively active form in patients with acute myelogenous leukemia. These mutations correlate with poor prognosis, thus making FLT-3 an attractive drug target in its own right[42].

Cellular consequences of Aurora inhibition

Because the Aurora kinases are essential for proliferation, we examined the effects of VX-680 on the cell-cycle profile of several human cell types by flow cytometry. VX-680 caused accumulation of cells with 4*N* DNA content (Fig. 1b) and potently inhibited the proliferation of a wide variety of tumor cell types with half-maximal inhibitory concentration (IC_{50}) values ranging from 15 to 113 nM (Fig. 1c). These data are consistent with the prediction that the Aurora kinases are crucial for cell-cycle progression, and with the finding that overexpression of kinase-inactive Aurora-B disrupts cell division[9,10].

Although the effects of VX-680 on the cell cycle and proliferation were in line with expectations, the consequences for cell viability could not be readily predicted. To address this, we examined the survival of a wide panel of tumor cell lines after VX-680 treatment. After cell cycle arrest, cell death followed in multiple tumor cell types. Leukemia, lymphoma and colorectal cancer cell lines were particularly sensitive (Fig. 2a). Using a variety of methods, including annexin-V binding, we showed that this cell death was attributable to apoptosis (Fig. 2b). The ability to induce cell death provides a mechanism whereby inhibitors

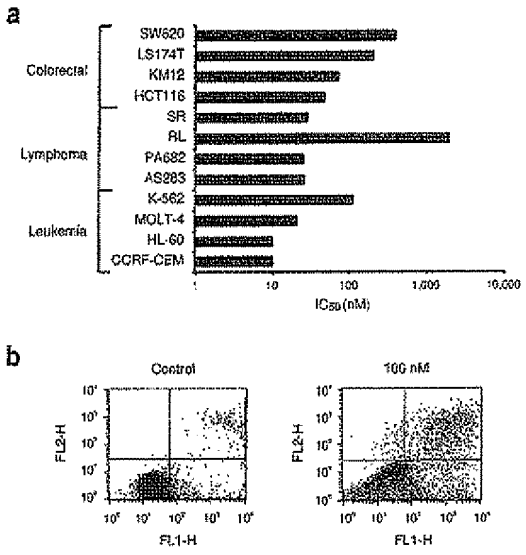

Figure 2 Inhibition of Aurora kinase activity induces tumor cell death. (**a**) Effect of VX-680 on viability of a panel of human tumor cell lines. Cells were incubated with VX-680 for 96 h, and viability was quantified by MTS assay (see Methods). (**b**) VX-680 induces apoptosis. COLO 205 colorectal tumor cells were treated with 100 nM VX-680 for 48 h. Apoptosis was assessed by flow cytometric analysis of cells labeled with annexin V (FL1-H) and propidium iodide (FL2-H).

of the Aurora kinase family may induce regression in a wide spectrum of tumor types.

In addition to testing the effects of Aurora kinase inhibitors on immortalized tumor cell lines, we studied the consequences of compound treatment on primary human tumor samples. VX-680 completely ablated colony formation of primary leukemic cells from patients with AML (CFU-L) who were refractory to standard therapies. VX-680 was extremely potent in this assay, with IC_{50} values in the range of 35–100 nM (Fig. 3). Encouragingly, VX-680 also abolished colony formation of primary leukemic cells possessing internal tandem duplication (ITD) mutations of *FLT3* (Fig. 3). These data indicate that VX-680 may be beneficial for the treatment of AML cases in which activating mutations of *FLT3* confer poor prognosis[42]. The combined inhibition of Aurora and FLT-3 by VX-680 may be of advantage in this setting, and this will be explored further.

Inhibition of Aurora-B activity is reported to generate polyploid cells as a result of repeated rounds of DNA synthesis in the absence of cytokinesis[9,10]. Consistent with this, VX-680 induced the accumulation of cells with greater than 4*N* DNA content before cell death (Fig. 1c). The generation of cells with >4*N* DNA content could occur by two distinct mechanisms. After completion of S phase, cells may rereplicate their DNA without entering mitosis. Alternatively, VX-680 treated cells may proceed through mitosis without dividing, and replicate their DNA in a subsequent S phase. To distinguish between these two possibilities, we examined the effects of VX-680 on cell-cycle progression in synchronized cells by determining DNA content and expression of cyclin B1, which peaks during mitosis (Fig. 4a,b). VX-680 treatment resulted in cells with high levels of cyclin B1 and 4*N* DNA 8–12 h after release from a G1/S block, suggesting that the cells were able to enter mitosis. However, the peak in cyclin B1 expression occurred later in VX-680-treated cells compared with control cultures, suggesting a delay in cell-cycle progression. Cyclin B1 expression subsequently decreased in both VX-680-treated and control cultures, indicating that the exit from mitosis was not blocked. After completion of mitosis, control cells divided to yield daughter cells with 2*N* DNA content. In contrast, VX-680 induced the accumulation of cells with 4*N* and ≥4*N* DNA content, suggesting that DNA replication could occur in the absence of cytokinesis. Additionally, Aurora-B localization was diffuse throughout the nucleus in nonsynchronized, VX-680-treated cells, with no cleavage furrow or midbody staining observed (data not shown). Taken together, these data suggest that VX-680-treated tumor cells enter mitosis and subsequently proceed through S phase in the absence of cell division. These findings are similar to the recently reported effects of Aurora inhibition on cell-cycle progression[43].

All available evidence points to a universal role for the Aurora proteins in mitosis. As expected, VX-680 inhibits the proliferation of

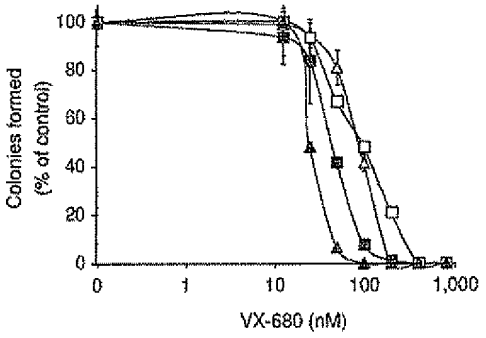

Figure 3 Aurora kinase inhibition ablates colony formation of primary AML cells. Clonogenic survival of AML samples from four different patients was assessed after 7 d of continuous exposure to VX-680. Two of the four samples (□,▲) were positive for the FLT-3 ITD mutation. Percentage of colonies formed in VX-680-treated cells relative to control cultures is shown.

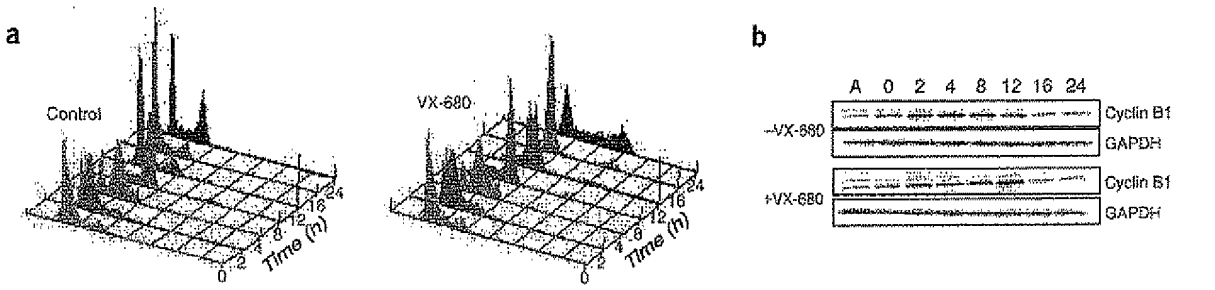

Figure 4 VX-680 causes accumulation of cells with ≥4*N* DNA content and inhibits histone H3 phosphorylation on Ser10. (a,b) HeLa cells were released from G1/S block in the presence of 300 nM VX-680 or DMSO. (a) DNA content of cells collected at the indicated time points was assessed by flow cytometric analysis of cells labeled with propidium iodide. (b) Cyclin B1 expression at these time points was assessed by Western blot analysis. A, asynchronous cell population. GAPDH was used as a loading control. Data shown is representative of three independent experiments. (c) MCF-7 cells were treated with VX-680 for 24 h. Histone H3 phosphorylation (top) was assessed by immunocytochemistry. Total cell population was visualized by DAPI staining (bottom).

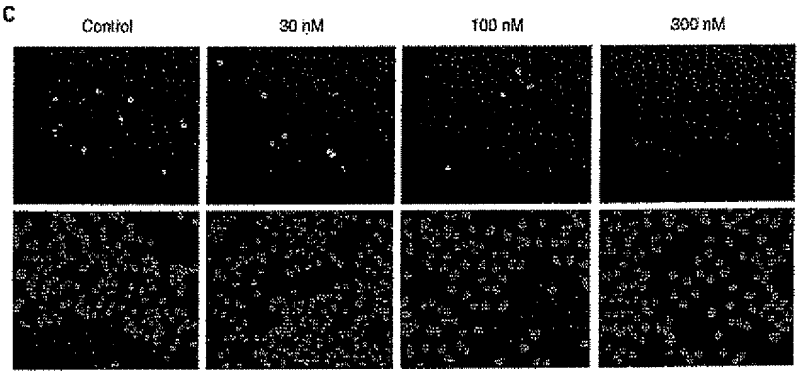

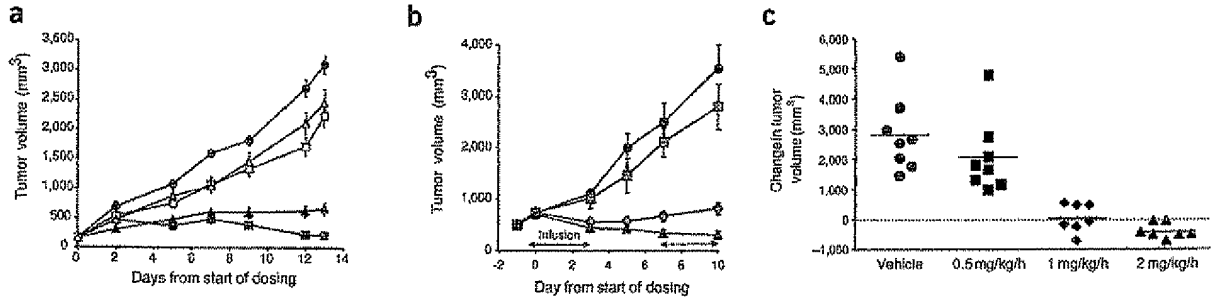

Figure 5 VX-680 induces regression of human HL-60 (AML) and HCT116 (colon) tumors in vivo. (**a**) Nude mice bearing established HL-60 tumors were treated i.p. b.i.d. with either vehicle control (●) or VX-680 at a dose of 12.5 mg/kg (△), 25 mg/kg (□), 50 mg/kg (▲) or 75 mg/kg (■). $n = 10$ per group. Mean tumor volumes ± s.e.m. are shown. (**b**) Nude rats bearing established HCT116 tumors were treated by i.v. infusion with either vehicle control (●) or VX-680 at a dose of 0.5 mg/kg/h (■), 1 mg/kg/h (◇) or 2 mg/kg/h (△), 3 d per week. $n = 8$ per group. Mean tumor volumes ± s.e.m. are shown. (**c**) Change in tumor volume for individual animals from day 0 to the end of the study (day 10).

phytohemagglutinin-stimulated primary human lymphocytes (IC_{50} = 79 nM). However, VX-680 had no effect on the viability of noncycling primary human cells (peripheral blood mononuclear cells) at concentrations as high as 10 μM (data not shown). This lack of toxicity in resting cells is consistent with the fact that the expression and activity of Aurora proteins is low or undetectable in noncycling cells, and supports our expectation that Aurora inhibition is a viable target for intervention in oncology.

To provide evidence that VX-680 is acting through Aurora inhibition in cells, we examined its effects on downstream signaling. Evidence suggests that histone H3 is a direct downstream target of the Aurora kinases[15,16]. Phosphorylation of a highly conserved serine residue (Ser10) in histone H3 is thought to be crucial for entry into mitosis. VX-680 suppressed histone H3 phosphorylation on Ser10 in human cells *in vitro* (Fig. 4c), indicating that Aurora kinases were inhibited.

In vivo modulation of Aurora kinase activity

To evaluate the role of Aurora kinases in tumor proliferation *in vivo*, we examined the ability of VX-680 to suppress the growth of human cancer cell xenografts in nude animals. VX-680 caused a marked reduction in tumor size in a human AML (HL-60) xenograft model. In nude mice treated with VX-680 at 75 mg/kg, twice a day intraperitoneally (b.i.d. i.p.) for 13 d, mean tumor volumes were reduced by 98% ($P < 0.001$) in comparison with the control group. In four of ten animals, the final tumor volume was lower than the initial volume before treatment. Tumor growth reduction was dose dependent and significant at a dose of 12.5 mg/kg b.i.d (% change in mean tumor volume for treatment group/change in mean tumor volume for control group (% T/C) = 78; $P < 0.05$; Fig. 5a). VX-680 was well tolerated, with a small decrease in body weight observed only at the highest dose (5% decrease at 75 mg/kg b.i.d.; $P < 0.001$). By comparison, cisplatin, dosed at 5.4 mg/kg every fourth day for a total of three doses (q.4.d. ×3) i.p. caused only a 9% inhibition in tumor growth (data not shown). VX-680 also induced tumor regression in pancreatic and colon xenograft models. In an established human pancreatic (MIA PaCa-2) xenograft model, VX-680 at 50 mg/kg b.i.d i.p. induced regression in seven of ten tumors, with a 22% decrease in mean tumor volume relative to initial tumor size before treatment ($P < 0.001$; data not shown). VX-680 was again well tolerated, with only a 7% decrease in body weight ($P < 0.001$). In comparison, 5-fluorouracil, administered intravenously (i.v.) q.4.d. at a maximum tolerated dose of 50 mg/kg, gave a % T/C of 77 ($P < 0.05$).

VX-680 also exhibited potent antitumor activity when infused i.v. in nude rats bearing established HCT116 (colon) tumors. Tumor regression in four of seven rats (mean % T/C = 3; $P < 0.001$) was achieved by administering VX-680 by i.v. infusion at 1 mg/kg/h, 3 d per week (Fig. 5b,c). A fall in neutrophil counts of 54% at the nadir was also observed. This was well tolerated, with no decrease in body weight, and neutrophil counts recovered to normal levels when treatment was stopped. A higher dose of VX-680 (2 mg/kg/h) showed improved efficacy, with a 56% decrease in mean tumor volume relative to initial tumor size before treatment. Mean body-weight loss in this group was only 6%. The higher dose was less well tolerated, however, resulting in the euthanization of one animal in this group. No signs of mechanism-independent toxicity of the compound were observed.

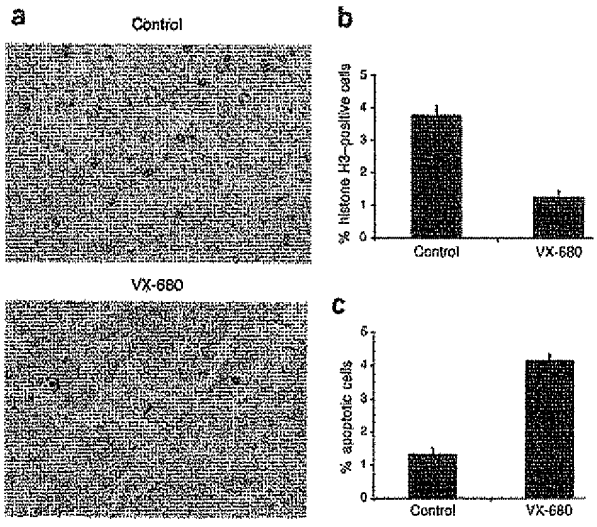

Figure 6 VX-680 inhibits histone H3 phosphorylation and induces apoptosis in tumors *in vivo*. Nude rats bearing established HCT116 tumors were treated with VX-680 (50 mg/kg) once a day i.p., 4 days per week. (**a**,**b**) Histone H3 phosphorylation in tumor tissue was assessed by immunohistochemistry. Percentage of histone H3–positive cells is shown in **b**. (**c**) Apoptosis was quantified by TUNEL assay. Percentage of apoptotic cells is shown.

Inhibition of tumor growth was paralleled by a reduction in histone H3 phosphorylation (Fig. 6a,b) and a significant increase in apoptosis, as measured by TUNEL staining of the tumor tissue (Fig. 6c). Taken together, the *in vivo* data for VX-680 provide a strong rationale for the further investigation of Aurora kinase inhibitors in oncology, and indicate that such compounds will not only inhibit cell proliferation but will also induce tumor cell death, with the potential of causing tumor regression.

DISCUSSION

Ten million cases of cancer were newly diagnosed worldwide in the year 2000. It is estimated that at least 6.2 million deaths per year are cancer related. There is a critical need for new therapies with improved efficacy over current treatments, especially against refractory tumors. Our discovery of highly potent, selective Aurora kinase inhibitors has enabled us to establish that blockade of Aurora kinase activity prevents proliferation of a diverse range of human tumor types. Although inhibition of individual Aurora family members has been reported to disrupt mitosis, the ultimate fate of cells lacking Aurora kinase activity has not been well documented. Our studies show that a selective inhibitor of all three Aurora kinases, such as VX-680, not only blocks cell proliferation but can also induce cell death by apoptosis in multiple tumor types, both *in vitro* and *in vivo*. Tumor regression was achieved in three tumor types—AML, pancreatic and colon—that are particularly difficult to treat in humans. Profound inhibition of tumor growth was achieved with VX-680 at well-tolerated doses, and no signs of mechanism-independent toxicity were observed. Targeting of the Aurora kinases is a new approach to cancer therapy, and therefore holds the potential to inhibit the growth of tumors that are refractory to conventional therapies. Encouragingly, we have shown that VX-680 can completely ablate colony formation of primary AML cells taken from patients who were refractory to the standard treatments.

As potent, selective kinase inhibitors reach the clinic, the ability to monitor target suppression in treated patients by surrogate markers will be important. In addition to the neutropenia caused by mechanism-based inhibition of normal cell proliferation, our small-molecule inhibitors block the phosphorylation of a direct downstream substrate of the Aurora kinases, histone H3, in tumor tissue *in vivo*. Determination of the phosphorylation status of histone H3 in proliferating cells may provide a specific, quantifiable measurement of Aurora kinase inhibition in the clinic.

In summary, our work provides strong evidence that inhibition of the Aurora kinases is a new approach to cancer therapy, holding the potential to induce regression of a diverse range of tumor types. VX-680 has attractive pharmacological properties and is now progressing into clinical development.

METHODS

In vitro kinase assays. Recombinant Aurora-1 (62-344), Aurora-2 (1-403) and Aurora-3 (1-309) were expressed as N-terminal, His_6-tagged fusion proteins using a baculovirus expression system (FastBac, Gibco BRL). The proteins were purified by affinity chromatography using Ni-NTA agarose, followed by size exclusion using a Superdex 200 26/60 column (Amersham Biosciences). Inhibition of kinase activity was assessed using a standard enzyme-coupled system or a radiometric, phosphocellulose-peptide capture assay as previously described[44–46].

Cell culture. Tumor cell lines were obtained from the European Collection of Animal Cell Cultures or the American Type Culture Collection, and were cultured according to the supplier's instructions. CFU-L cells were obtained from bone marrow aspirates from AML patients at diagnosis. These cells were cryopreserved after informed consent.

Cell-cycle analysis. Logarithmically growing MCF-7 cells were incubated with either VX-680 or DMSO for 48 h. Single-cell suspensions were fixed in 70% ethanol for 15 min, incubated with RNase (1 mg/ml) at 37 °C for 30 min, labeled with 400 µl propidium iodide (50 µg/ml) for at least 15 min at room temperature. Cell-cycle profiles were determined by flow cytometric analysis.

Cell synchronization. HeLa cells were synchronized using a double thymidine block as previously described[43]. Cells were released from the block in the presence of 300 nM VX-680 or compound diluent (DMSO), and collected at the indicated time points. The cell-cycle profile and DNA content of these cells were analyzed by flow cytometry (as above). Cyclin B1 expression was determined by immunoblotting with a monoclonal antibody to cyclin B1 (05-373, Upstate Biotechnology).

Analysis of cell proliferation and viability. Tumor cells were seeded in 96-well plates and incubated with VX-680 for 96 h. To measure DNA synthesis, 0.5 mCi of [^{3}H]thymidine was added to each well 3 h before the end of the experiment. Cells were then collected, and the incorporated radioactivity was counted on a Wallac microplate beta-counter. Cell viability was assessed using Promega CellTiter 96AQ to measure MTS (3-(4,5-dimethylthiazol-2-yl)-5-(3-carboxymethoxyphenyl)-2-(4-sulfophenyl)-2H-tetrazolium, inner salt) conversion.

Apoptosis analysis. COLO 205 cells were treated with VX-680 for 48 h. Apoptosis was assessed by flow cytometry using an annexin V–FITC apoptosis detection kit (PharMingen).

Colony formation analysis. CFU-L cells were resuspended in H44100 methylcellulose semisolid medium supplemented with 10% 5637-conditioned medium. VX-680 or DMSO was added, and the cells were incubated at 37 °C for 7 d. Colonies with >20 cells were scored using an inverted microscope.

Immunocytochemistry. MCF-7 cells were treated with VX-680 for 24 h. For analysis of histone H3 phosphorylation, the cells were fixed with 4% formaldehyde for 10 min at room temperature and then permeabilized with PBS containing 0.5% Triton X-100 for 10 min at room temperature. Cells were incubated with an antibody to Ser10-phosphorylated histone H3 (1:200; Upstate Biotechnology), followed by a FITC-conjugated antibody to rabbit IgG (1:300; Sigma), and then counterstained with DAPI (0.5 µg/ml).

Animal efficacy studies. Animal studies were carried out in the UK in accordance with the Animal (Scientific Procedures) Act, and in the US in accordance with the Institutional Animal Care and Use Committee of Southern Research Institute. For the HL-60 study, female athymic NCr-*nu* mice were inoculated subcutaneously with 10^7 HL-60(TB) leukemia cells into the right axillary area. Treatment was administered i.p. b.i.d. after tumors reached 150–200 mm^3. VX-680 was prepared in a vehicle of 50% PEG 300 in 50 mM phosphate buffer. Cisplatin, formulated in saline, was administered i.p. q.4.d. for a total of three injections, at a dose of 5.4 mg/kg. For the MIA PaCa-2 studies, female MF1 nude mice were inoculated with 10^7 MIA PaCa-2 cells into the dorsal flank. Treatment was administered i.p. b.i.d. after tumors reached 175 mm^3. VX-680 was prepared in a vehicle of 50% PEG 300 in 50 mM phosphate buffer. 5-fluorouracil, formulated in saline, was administered i.v. q.4.d. at a dose of 50 mg/kg. For the HCT116 study, female Hsd RH nu/nu rats were inoculated with 10^7 HCT116 cells into the right flank. Treatment was administered once the tumors reached 700–950mm^3. VX-680 was administered continuously through an indwelling femoral catheter, followed by a saline infusion for 4 d before repeating the dose cycle. For all studies, tumor volume was determined by caliper measurements three times a week.

For the analysis of histone H3 phosphorylation and apoptosis in tumor sections, female RH nude rats were inoculated with HCT116 cells. VX-680 was administered i.p. once a day for 4 d after tumors reached 300 mm^3, followed by 3 d of nontreatment and then a further 4 d of treatment with VX-680. Tumors were removed 30 min after the final dose, and histone H3 phosphorylation was determined in formalin-fixed tumor sections using an antibody to Ser10-phosphorylated histone H3 (Upstate Biotechnology). Apoptosis was quantified by TUNEL analysis.

Note: Supplementary information is available on the Nature Medicine website.

ACKNOWLEDGMENTS

We thank S. Renwick, J. Westcott, S. Gladwell, P. Weber, and the Aurora chemistry, crystallography, protein biochemistry, enzymology, DMPK and pharmacology teams for their contributions; and J. Boger, J. Thomson, M. Namchuk and M. Partridge for critical reading of the manuscript.

COMPETING INTERESTS STATEMENT

The authors declare competing financial interests (see the *Nature Medicine* website for details).

Received 9 December 2003; accepted 2 February 2004
Published online at http://www.nature.com/naturemedicine/

1. Carmena, M. & Earnshaw, W.C. The cellular geography of Aurora kinases. *Nat. Rev. Mol. Biol.* **4**, 842–854 (2003).
2. Bischoff, J.R. & Plowman, G.D. The Aurora/Ipl1p kinase family: regulators of chromosome segregation and cytokinesis. *Trends Cell Biol.* **9**, 454–459 (1999).
3. Giet, R. & Prigent, C. Aurora/Ipl1p-related kinases, a new oncogenic family of mitotic serine-threonine kinases. *J. Cell Sci.* **112**, 3591–3601 (1999).
4. Nigg, E.A. Mitotic kinases as regulators of cell division and its checkpoints. *Nat. Rev. Mol. Cell Biol.* **2**, 21–32 (2001).
5. Adams, R.R, Carmena, M. & Earnshaw, W.C. Chromosomal passengers and the (aurora) ABCs of mitosis. *Trends Cell Biol.* **11**, 49–54 (2001).
6. Dutertre, S., Descamps, S., & Prigent, P. On the role of aurora-A in centrosome function. *Oncogene* **21**, 6175–6183 (2002).
7. Marumoto, T. *et al.* Roles of aurora-A kinase in mitotic entry and G2 checkpoint in mammalian cells. *Genes Cells* **7**, 1173–1182 (2002).
8. Hirota, T. *et al.* Aurora-A and an interacting activator, the LIM protein Ajuba, are required for mitotic commitment in human cells. *Cell* **114**, 585–598 (2003).
9. Terada, T. *et al.* AIM-1: a mammalian midbody-associated protein required for cytokinesis. *EMBO J.* **17**, 667–676 (1998).
10. Kawasaki, K. *et al.* Downregulation of an AIM-1 kinase couples with megakaryocytic polyploidization of human hematopoietic cells. *J. Cell Biol.* **152**, 275–287 (2001).
11. Murata-Hori, M. & Wang, Y. The kinase activity of Aurora B is required for kinetochore-microtubule interactions during mitosis. *Curr. Biol.* **12**, 894–899 (2002).
12. Andreassen, P.R., Lohez, O.D., Lacroix, F.B. & Margolis, R.L. Tetraploid state induces p53-dependent arrest of nontransformed mammalian cells in G1. *Mol. Biol. Cell* **12**, 1315–1328 (2001).
13. Kimura, M., Matsuda, Y., Yoshioka, T. & Okano, Y. Cell cycle-dependent expression and centrosomal localization of a third human Aurora/Ipl1-related protein kinase, AIK3. *J. Biol. Chem.* **274**, 7334–7340 (1999).
14. Bischoff, J.R., *et al.* A homologue of *Drosophila aurora* kinase is oncogenic and amplified in human colorectal cancers. *EMBO J.* **17**, 3052–3065 (1998).
15. Hsu, J. *et al.* Mitotic phosphorylation of histone H3 is governed by Ipl1/aurora kinase and Glc7/PP1 phosphatase in budding yeast and nematodes. *Cell* **102**, 279–291 (2000).
16. Crosio, C. *et al.* Mitotic phosphorylation of histone H3: spatio-temporal regulation by mammalian aurora kinases. *Mol. Cell. Biol.* **22**, 874–885 (2002).
17. Zeitlin, S.G., Shelby, R.D. & Sullivan, K.F. CENP-A is phosphorylated by Aurora B kinase and plays an unexpected role in completion of cytokinesis. *J. Cell Biol.* **155**, 1147–1157 (2001).
18. Murata-Hori, M. *et al.* Myosin II regulatory light chain as a novel substrate for AIM-1, an Aurora/Ipl1p-related kinase from rat. *J. Biochem.* **128**, 903–907 (2000).
19. Katayama, H., Zhou, H., Li, Q., Tatsuka, M. & Sen, S. Interaction and feedback regulation between STK15/BTAK/Aurora-A kinase and protein phosphatase 1 through mitotic cell division cycle. *J. Biol. Chem.* **276**, 46219–46224 (2001).
20. Kufer, T. *et al.* Human TPX2 is required for targeting Aurora-A kinase to the spindle. *J. Cell Biol.* **158**, 617–623 (2002).
21. Bishop, J.D. & Schumacher, J.M. Phosphorylation of the carboxyl terminus of inner centromere protein (INCENP) by the Aurora B kinase stimulates Aurora B kinase activity. *J. Biol. Chem.* **277**, 27577–27580 (2002).
22. Honda, R., Korner, R. & Nigg E.A. Exploring the function interactions between Aurora B, INCENP, and survivin in mitosis. *Mol. Biol. Cell* **14**, 3325–3341 (2003).
23. Wheatley, S.P., Henzing A.J., Dodson H., Khaled, W. & Earnshaw, W.C. Aurora-B phosphorylation *in vitro* identifies a residue of survivin that is essential for its localization and binding to INCENP *in vivo*. *J. Biol. Chem.* (in the press).
24. Tien, A.C. *et al.* Identification of the substrates and interaction proteins of Aurora kinases from a protein-protein interaction model. *Mol. Cell. Proteomics* **3**, 93–104 (2004).
25. Morrison, C. *et al.* Proteomic analysis of human metaphase chromosomes reveals topoisomerase II alpha as an Aurora B substrate. *Nucleic Acids Res.* **30**, 5318–5327 (2002).
26. Goto, H. *et al.* Aurora-B regulates the cleavage furrow-specific vimentin phosphorylation in the cytokinetic process. *J. Biol. Chem.* **278**, 8526–8530 (2003).
27. Sakai, H. *et al.* MBD3 and HDAC1, two components of the NuRD complex, are localized at Aurora-A-positive centrosomes in M phase. *J. Biol. Chem.* **277**, 48714–48723 (2002).
28. Minoshima, Y. *et al.* Phosphorylation by Aurora B converts MgcRacGAP to a RhoGAP during cytokinesis. *Dev. Cell* **4**, 549–560 (2003).
29. Kawajiri, A. *et al.* Functional significance of the specific sites phosphorylated in desmin at cleavage furrow: Aurora-B may phosphorylate and regulate type III intermediate filaments during cytokinesis co-ordinately with Rho-kinase. *Mol. Biol. Cell* **14**, 1489–1500 (2003).
30. Giet, R., Uzbekov, R., Cubizolles, F., LeGuellec, K. & Prigent, C. The *Xenopus laevis* Aurora-related protein kinase pEg2 associates with and phosphorylates the kinesin-related protein XlEg5. *J. Biol. Chem.* **274**, 15005–15013 (1999).
31. Biggins, S. *et al.* The conserved protein kinase Ipl1p regulates microtubule binding to kinetochores in budding yeast. *Genes Dev.* **13**, 532–544 (1999).
32. Giet, R. *et al. Drosophila* Aurora A kinase is required to localize D-TACC to centrosomes and to regulate astral microtubules. *J. Cell Biol.* **156**, 437–451 (2002).
33. Miyoshi, Y., Iwao, K., Egawa, C. & Noguchi, S. Association of centrosomal kinase STK15/BTAK mRNA expression with chromosomal instability in human breast cancers. *Int. J. Cancer* **92**, 370–373 (2001).
34. Sakakura, C. *et al.* Tumor-amplified kinase BTAK is amplified and overexpressed in gastric cancers with possible involvement in aneuploid formation. *Br. J. Cancer* **84**, 824–831 (2001).
35. Takahashi, T. *et al.* Centrosomal kinases, HsAIRK1 and HsAIRK3, are overexpressed in primary colorectal cancers. *Jpn. J. Cancer Res.* **91**, 1007–1014 (2000).
36. Gritsko, T.M. *et al.* Activation and overexpression of centrosome kinase BTAK/Aurora-A in human ovarian cancer. *Clin. Cancer Res.* **9**, 1420–1426 (2003).
37. Tanaka, T. *et al.* Centrosomal kinase AIK1 is overexpressed in invasive ductal carcinoma of the breast. *Cancer Res.* **59**, 2041–2044 (1999).
38. Isola, J.J. *et al.* Genetic aberrations detected by comparative genomic hybridization predict outcome in node-negative breast cancer. *Am. J. Pathol.* **147**, 905–911 (1995).
39. Katayama, H. *et al.* Mitotic kinase expression and colorectal cancer progression. *J. Natl. Cancer Inst.* **91**, 1160–1162 (1999).
40. Capdeville, R., Buchdunger, E., Zimmerman, J. & Matter, A. Glivec (STI571, imatinib), a rationally developed, targeted anticancer drug. *Nat. Rev. Drug Discov.* **1**, 493–502 (2002).
41. Cheetham, G.M.T. *et al.* Crystal structure of Aurora-2 an oncogenic serine/threonine kinase. *J. Biol. Chem.* **277**, 42419–42422 (2002).
42. Sawyers, C.L. Finding the next Gleevec: FLT3 targeted kinase inhibitor therapy for acute myeloid leukaemia. *Cancer Cell* **3**, 413–415 (2002).
43. Ditchfield, C. *et al.* Aurora B couples chromosome alignment with anaphase by targeting BubR1, Mad2, and Cenp-E to kinetochores. *J. Cell Biol.* **161**, 267–280 (2003).
44. Fox, T. *et al.* A single amino acid substitution makes ERK2 susceptible to pyridinyl imidazole inhibitors of p38 MAP kinase. *Protein Sci.* **7**, 2249–2255 (1998).
45. Pitt, A.M. & Lee, C. High throughput screening protein kinase assays optimized for reaction, binding, and detection totally within a 96-well plate. *J. Biomol. Screening* **1**, 47–51 (1996).
46. Ling, Y.-H. *et al.* Phosphorylation of Bcl-2 is a marker of M phase events and not a determinant of apoptosis. *J. Biol. Chem.* **273**, 18984–18991 (1998).

EXHIBIT F

The *In vitro* and *In vivo* Effects of JNJ-7706621: A Dual Inhibitor of Cyclin-Dependent Kinases and Aurora Kinases

Stuart Emanuel,[1] Catherine A. Rugg,[1] Robert H. Gruninger,[1] Ronghui Lin,[1] Angel Fuentes-Pesquera,[1] Peter J. Connolly,[1] Steven K. Wetter,[1] Beth Hollister,[2] Walter W. Kruger,[2] Cheryl Napier,[2] Linda Jolliffe,[1] and Steven A. Middleton[1]

[1]Cancer Therapeutics Research, Johnson & Johnson Pharmaceutical Research & Development, LLC, Raritan, New Jersey and [2]Piedmont Research Center, Morrisville, North Carolina

Abstract

Modulation of aberrant cell cycle regulation is a potential therapeutic strategy applicable to a wide range of tumor types. JNJ-7706621 is a novel cell cycle inhibitor that showed potent inhibition of several cyclin-dependent kinases (CDK) and Aurora kinases and selectively blocked proliferation of tumor cells of various origins but was about 10-fold less effective at inhibiting normal human cell growth *in vitro*. In human cancer cells, treatment with JNJ-7706621 inhibited cell growth independent of p53, retinoblastoma, or P-glycoprotein status; activated apoptosis; and reduced colony formation. At low concentrations, JNJ-7706621 slowed the growth of cells and at higher concentrations induced cytotoxicity. Inhibition of CDK1 kinase activity, altered CDK1 phosphorylation status, and interference with downstream substrates such as retinoblastoma were also shown in human tumor cells following drug treatment. Flow cytometric analysis of DNA content showed that JNJ-7706621 delayed progression through G_1 and arrested the cell cycle at the G_2-M phase. Additional cellular effects due to inhibition of Aurora kinases included endoreduplication and inhibition of histone H3 phosphorylation. In a human tumor xenograft model, several intermittent dosing schedules were identified that produced significant antitumor activity. There was a direct correlation between total cumulative dose given and antitumor effect regardless of the dosing schedule. These results show the therapeutic potential of this novel cell cycle inhibitor and support clinical evaluation of JNJ-7706621. (Cancer Res 2005; 65(19): 9038-46)

Introduction

Under normal growth conditions, cell proliferation is tightly regulated in response to diverse intracellular and extracellular signals. In the eukaryotic cell cycle, a key role is played by the cyclin-dependent kinases (CDK). The combination of catalytic kinase subunits (such as CDK1, CDK2, CDK4, or CDK6) with regulatory cyclin subunits (such as cyclin A, B, D1, D2, D3, or E) results in the assembly of functionally distinct kinase complexes. Coordinated activation of these complexes at specific times drives cells through the cell cycle and ensures the fidelity of cell division (1). Complexes of CDK4 and D-type cyclins govern the early G_1 phase of the cell cycle; the activity of the CDK2/cyclin E complex is rate limiting for the G_1-to-S phase transition (2), and CDK2/Cyclin A kinase regulates progression through the S phase (3). Biochemical and genetic evidence have shown that the activity of the CDK1/cyclin B complex is required for passage from the G_2 phase of the cell cycle into the M phase and for successful completion of mitosis (4, 5). CDK1 phosphorylates a number of proteins including histone H1, DNA polymerase α, RNA polymerase II, retinoblastoma, p53, nucleolin, cAbl, and lamin A (6, 7). CDKs, their substrates, and regulatory proteins are the target of genetic alteration or overexpression in many human cancers (8, 9) and cell lines (10). Alterations in components of cell cycle signaling pathways are present in ~90% of human cancers (11, 12).

The Aurora kinases have a critical role in controlling chromosome movement and organization. Aurora-A contributes to formation of the mitotic spindle apparatus that guarantees accurate segregation of chromosomes into daughter cells; Aurora-B is required for cytokinesis and proper chromosome architecture during mitosis (13). These kinases are frequently overexpressed and amplified in many human tumors (14).

Accordingly, small-molecule inhibitors of CDK or Aurora activity should prevent the continuous, proliferative growth of cancer cells and provide a way of controlling abnormal mitosis, which would be applicable to a wide range of tumor types (15). A number of small-molecule inhibitors of CDKs have been described (reviewed in ref. 16) and several are currently under evaluation in clinical trials including Flavopiridol, UCN-01, CYC202, and BMS-387032 (17). Recently, relatively selective inhibitors of Aurora kinases have also been reported including ZM447439 (18) and VX-680 (19). In this report, we describe the identification of JNJ-7706621, a [1,2,4]triazole-3,5-diamine dual CDK and Aurora inhibitor with a unique inhibition profile of cell cycle regulatory kinases.

Materials and Methods

Reagents. JNJ-7706621 (Fig. 1A) was synthesized by the Cancer Therapeutics Research team (J&J Pharmaceutical Research & Development). Chemicals were obtained from Sigma (St. Louis, MO) and radioisotopes were from Perkin-Elmer (Boston, MA).

Cell culture. Human umbilical vascular endothelial cell, HASMC, and HMVEC were obtained from Cascade Biologicals (Portland, OR). MRC-5 human lung fibroblasts and all other cells were from the American Type Culture Collection (Manassas, VA). Cell culture reagents were obtained from Life Technologies, Inc. (Grand Island, NY). Cells were incubated at 37°C plus 5% CO_2 and all cell lines were maintained as exponentially growing cultures in the recommended medium.

***In vitro* kinase and cell proliferation assays.** To identify compounds that inhibited CDK1 kinase activity, a screening method was developed using the CDK1/cyclin B complex purified from baculovirus (NEB, Boston, MA) to phosphorylate a biotinylated peptide substrate containing the consensus phosphorylation site for histone H1, which is phosphorylated

Requests for reprints: Stuart Emanuel, Johnson & Johnson Pharmaceutical Research & Development, LLC, 1000 Route 202, Raritan, NJ 08869. Phone: 908-704-5815; Fax: 908-704-4996; E-mail: semanuel@prdus.jnj.com.

doi:10.1158/0008-5472.CAN-05-0882

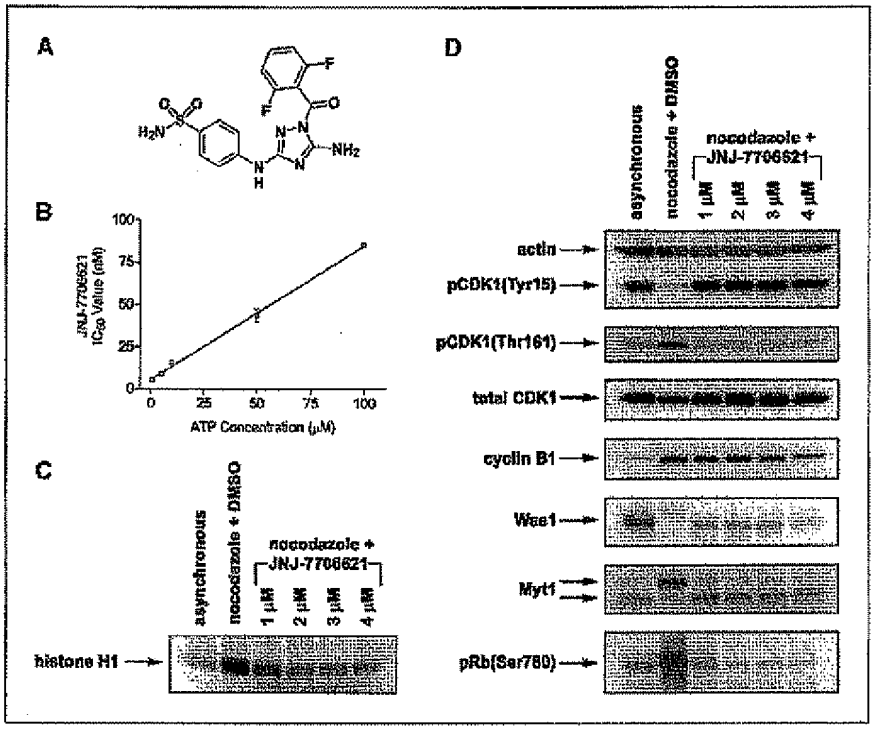

Figure 1. JNJ-7706621 inhibits CDK1 kinase activity in cells. *A*, chemical structure of JNJ-7706621 (4-[5-amino-1-(2,6-difluorobenzoyl)-1*H*-[1,2,4]triazol-3-ylamino]-benzenesulfonamide). *B*, IC_{50} value for inhibition of recombinant human CDK1/Cyclin B by JNJ-7706621 was calculated at increasing concentrations of ATP and produced a linear relationship relative to total ATP concentration. All groups were set up with $n = 3$; *bars*, SD. *C*, lysates were prepared from asynchronous HeLa cells and HeLa cells synchronized with nocodazole and treated with either vehicle (0.04% DMSO) or 1 to 4 μmol/L JNJ-7706621. Active CDK1 kinase was immunoprecipitated from lysates and evaluated for CDK1 kinase activity with histone H1 protein as substrate. The phosphorylated histone H1 was separated by SDS-PAGE and the extent of incorporation of ^{33}P-γ-ATP into histone H1 was quantified on a Storm 860 phosphorimager (Molecular Devices, Sunnyvale, CA). *D*, the same cell lysates used to measure kinase activity were subjected to immunoblot analysis to evaluate the effects of JNJ-7706621 on CDK1 phosphorylation and cell cycle regulatory proteins. Membranes were probed with antibodies to phospho-CDK1 (Tyr^{15}), phospho-CDK1 (Thr^{161}), total CDK1, total cyclin B1, total Wee1, total Myt1, and phospho-retinoblastoma (Ser^{780}). Each membrane was also probed with an antibody to β-actin as an internal control [only shown for the phospho-CDK1 (Tyr^{15}) blot].

in vivo by CDK1 (20). Inhibition of CDK1 activity was measured by observing a reduced amount of ^{33}P-γ-ATP incorporation into the immobilized substrate in streptavidin-coated 96-well scintillating microplates (NEN, Boston, MA). CDK1 enzyme was diluted in 50 mmol/L Tris-HCl (pH 8), 10 mmol/L $MgCl_2$, 0.1 mmol/L Na_3VO_4, 1 mmol/L DTT, 1% DMSO, 0.25 μmol/L peptide, 0.1 μCi per well ^{33}P-γ-ATP (2,000-3,000 Ci/mmol), and 5 μmol/L ATP in the presence or absence of various concentrations of test compound and incubated at 30°C for 1 hour. The reaction was terminated by washing with PBS containing 100 mmol/L EDTA and plates were counted in a scintillation counter. Linear regression analysis of the percent inhibition by test compound was used to determine IC_{50} values (GraphPad Prism 3, GraphPad Software, San Diego, CA). The Aurora kinase assays were done with 10 μmol/L ATP and a peptide containing a dual repeat of the kemptide phosphorylation motif. Assays for inhibition of additional kinases were done as described (21). Antiproliferative activity was assessed in a cell proliferation assay measuring ^{14}C-thymidine incorporation into cellular DNA as described (21).

Cell cycle analysis. Cells were stained with propidium iodide for analysis of nuclear DNA content using the CycleTEST PLUS DNA Reagent Kit (Becton Dickinson, San Jose, CA). Stained cells were run on a FACSCalibur (Becton Dickinson) with an excitation wavelength of 488 nm and an emission wavelength of 585 nm. Histograms were analyzed using ModFit (Verity Software House, Topsham, ME) to determine cell cycle distribution.

Cell synchronization. A modified mitotic shake method was used to synchronize cells in G_1 (22). Asynchronous cells were tapped to dislodge mitotic cells and the dislodged cells were collected and incubated in fresh medium. Adherent cells were harvested after 4 hours. Cell cycle analysis showed that >93% of the resulting population of cells were in G_1 (data not shown). To synchronize cells in G_2-M, the microtubule depolymerizing drug nocodazole was used (23). Treatment with 200 nmol/L nocodazole for 16 hours synchronized 98% of the population in G_2-M as determined by cell cycle analysis (data not shown).

CDK1 kinase activity in HeLa cell lysates. To eliminate variations in CDK1 kinase activity due to cell cycle position, the cell population was first synchronized in G_2-M. Synchronized cells were then treated for 8 hours with either 200 nmol/L nocodazole plus vehicle or 200 nmol/L nocodazole plus 1 to 4 μmol/L JNJ-7706621 and cell cycle analysis was done to confirm that cells remained in G_2-M arrest. Immunocomplexes were recovered from 1 mg of total cell lysate by incubation overnight with agarose conjugated total CDK1 antibody (Santa Cruz Biotechnology, Santa Cruz, CA) and evaluated for CDK1 kinase activity with 1.5 μg of histone H1 substrate (Upstate Biotechnology, Lake Placid, NY) as described (24).

Immunoblot analysis. Lysates of asynchronous HeLa cells or cells synchronized in G_2-M and treated with either nocodazole plus JNJ-7706621 or nocodazole plus vehicle, were separated by SDS-PAGE, transferred to nitrocellulose, and probed with the following antibodies: Wee1 (Santa Cruz Biotechnology); total CDK1, phospho-CDK1 (Thr^{161}), phospho-CDK1 (Tyr^{15}), Myt1, and phospho-retinoblastoma (Ser^{780}) (Cell Signaling, Beverly, MA); cyclin B1 (BD PharMingen, San Diego, CA); phospho-Histone H3 (Ser^{10}) (Upstate Biotechnology); and actin (Sigma). Secondary antibodies and enhanced chemiluminescence detection reagents were from Amersham Biosciences (Piscataway, NJ).

Colony formation assay. HeLa cells were plated at various densities in 90-mm diameter Petri dishes and exposed to JNJ-7706621 for 48 hours. Cells were then washed in PBS and incubated an additional 7 days in drug-free medium. Cells were fixed in 95% ethanol, stained with 0.5% crystal violet, and colonies containing >50 cells manually counted.

Apoptosis analysis. Detection of externalized phosphatidylserine on cell membranes and assessment of cell viability was done by dual staining with Annexin V and propidium iodide. U937 cells were treated with vehicle alone or JNJ-7706621 for 24 hours. Cells (5×10^5) were stained with Annexin V-FITC conjugate (Oncogene, San Diego, CA) for 15 minutes followed by propidium iodide and immediately analyzed flow cytometrically.

Human tumor xenograft studies. The effect of JNJ-7706621 on the growth of tumors in female *nu/nu* mice was done as previously reported (21). Briefly, animals were implanted s.c. with 1 mm^3 A375 tumor fragments in the hindflank. After tumors reached 62 to 126 mg, groups were pair matched. Animals were given JNJ-7706621 or vehicle control starting on day 1. The tumor growth delay method was followed where each animal was euthanized when its neoplasm reached a predetermined size of 2.0 g. All statistical analyses were conducted using unpaired *t* tests at a *P* level of 0.05 (two tailed).

Results

Inhibition of cell cycle kinase activity *in vitro*. JNJ-7706621 (Fig. 1*A*) is a pan-CDK kinase inhibitor with highest potency on CDK1 and CDK2 but also exhibits activity towards CDK3, CDK4, and CDK6 (Table 1). For the *in vitro* CDK1 kinase assay, a K_m for ATP of 17.12 ± 1.03 μmol/L was determined (data not shown) and the assay was carried out with 5 μmol/L total ATP. The IC_{50} value for inhibition of CDK1 by JNJ-7706621 at increasing concentrations of ATP was calculated and a linear relationship relative to the concentration of ATP present in the reaction was observed (Fig. 1*B*). This result is consistent with an ATP-competitive mode of inhibition of CDK1. In addition, JNJ-7706621 showed inhibition of Aurora-A and Aurora-B but had no activity at the highest concentration tested on the Plk1 or Wee1 serine/threonine kinases (Table 1). Therefore, its antiproliferative effects are likely attributable to the inhibition of a unique subset of kinases with important regulatory roles in cell growth and cell division.

Kinase selectivity profile. When assayed against a panel of representative tyrosine and serine/threonine kinases, JNJ-7706621 showed some inhibition of the VEGF-R2 and FGF-R2 tyrosine kinase receptors and also inhibition of GSK3β (Table 1). It was less potent but still exhibited submicromolar inhibition of the VEGF-R3, Tie2, and FGF-R1 receptor tyrosine kinases and was relatively inactive on the remainder of the kinases profiled.

Effects of JNJ-7706621 on cell proliferation. JNJ-7706621 showed potent growth inhibition *in vitro* on all human cancer cell types examined with IC_{50} values ranging from 112 to 514 nmol/L (Table 1). The compound was several fold less potent at inhibiting growth of normal cell types, including fibroblast, smooth muscle, and endothelial cells, where IC_{50} values ranged from 3.67 to 5.42 μmol/L (Table 1). The IC_{50} for JNJ-7706621 was nearly identical in both the sensitive MES-SA and the P-glycoprotein overexpressing MES-SA/Dx5 cell line (25), indicating that the antiproliferative effect of this compound was not modulated by P-glycoprotein overexpression (Table 1).

Inhibition of CDK1 kinase activity in cells. The ability of JNJ-7706621 to inhibit CDK1 activity in cells is shown in Fig. 1*C*. Asynchronous cells had a low level of CDK1 kinase activity. Cells synchronized in G_2-M and treated with vehicle alone exhibited a high level of CDK1 kinase activity, likely resulting from being growth arrested in G_2-M and not due to microtubule depolymerization or direct modulation of CDK1 kinase activity by nocodazole (26). G_2-M synchronized cells treated with JNJ-7706621 showed

Table 1. *In vitro* kinase and cell proliferation assays IC_{50} (μmol/L)

In vitro kinase assays

Cell cycle kinases		Other kinases	
CDK1/Cyclin B	0.009 ± 0.004	VEGF-R1	6.4 ± 0.141
CDK2/Cyclin A	0.004 ± 0.003	VEGF-R2	0.154 ± 0.052
CDK2/Cyclin E	0.003 ± 0.001	VEGF-R3	0.735 ± 0.120
CDK3/Cyclin E	0.058 ± 0.007	Tie2	0.465 ± 0.064
CDK4/Cyclin D1	0.253 ± 0.010	FGF-R1	0.575 ± 0.078
CDK6/Cyclin D1	0.175 ± 0.007	FGF-R2	0.226 ± 0.005
Aurora-A	0.011 ± 0.001	GSK3β	0.254 ± 0.042
Aurora-B	0.015 ± 0.004	RET	3.05 ± 0.354
Wee1, Plk1	>100	HER2	1.39 ± 0.320
		Casein kinase-1	9.73 ± 2.04
		PDGF-Rβ, Calmodulin kinase-2, ERK2, EGF-R, Casein kinase-2, Protein kinase-A, Protein kinase-Cβ2, Insulin-R kinaseβ, FLT3	>10

In vitro cell proliferation assays

Cell line (origin)		Normal cell type (origin)	
HeLa (cervical)	0.286 ± 0.072	MRC-5 (lung fibroblast)	3.67 ± 0.713
HCT-116 (colon)	0.189 ± 0.042	HASMC (aortic smooth muscle)	4.06 ± 0.650
SK-OV-3 (ovarian)	0.410 ± 0.075	HUVEC (umbilical vein endothelial)	4.57 ± 0.935
PC3 (prostate)	0.112 ± 0.012	HMVEC (microvascular endothelial)	5.42 ± 1.56
A375 (melanoma)	0.416 ± 0.054		
MDA-MB-231 (breast)	0.514 ± 0.063		
DU145 (prostate)	0.263 ± 0.113		
MES-SA (uterine drug sensitive)	0.413 ± 0.004		
MES-SA/Dx5 (uterine drug resistant)	0.433 ± 0.001		

NOTE: Inhibition of kinase activity was determined *in vitro* with human recombinant enzymes except for Calmodulin kinase and Casein kinase-1, which were rat isoforms; Protein kinase-A was of bovine origin and GSK3β was rabbit. Data represent the mean ± SE of at least two separate experiments carried out in duplicate.

a dose-responsive decrease in CDK1 kinase activity with >50% inhibition from 1 μmol/L treatment.

Effects of JNJ-7706621 on CDK1 regulation in cells. The effects of JNJ-7706621 treatment on CDK1 phosphorylation status and cell cycle regulatory proteins were characterized by immunoblot analysis. CDK1 activity is positively regulated by an activating phosphorylation at Thr^{161} (27) and is maintained in an inactive state by inhibitory phosphorylations on Tyr^{15} and Thr^{14} mediated by Wee1 and Myt1. In the asynchronous HeLa cell population, most of the CDK1 was inactive with Tyr^{15} in the phosphorylated state (Fig. 1*D*). Cells synchronized in G_2-M and treated with vehicle alone had a very low level of Tyr^{15} phosphorylation with most of the CDK1 exhibiting the activating Thr^{161} phosphorylation (Fig. 1*D*). G_2-M synchronized cells treated with JNJ-7706621 showed low levels of the activating Thr^{161} and high levels of the inhibitory Tyr^{15} phosphorylation (Fig. 1*D*). These results are consistent with the reduction in CDK1 kinase activity observed after JNJ-7706621 treatment (Fig. 1*C*). The amount of total CDK1 protein did not change following nocodazole synchronization or drug treatment (Fig. 1*D*). Cyclin B1 levels were low in the asynchronous cell population and elevated in cells treated with nocodazole (Fig. 1*D*) as expected for cells arrested in G_2-M (3). Wee1 protein levels were lower in nocodazole synchronized cells than in asynchronous cells (Fig. 1*D*). Expression of Wee1 is regulated by CDK1 and Plk1 catalyzed phosphorylation during mitosis, which targets it for ubiquitin-mediated degradation (28). A slower migrating species in nocodazole-arrested cells (Fig. 1*D*) is presumably hyperphosphorylated Wee1. Cells treated with JNJ-7706621 had higher levels of Wee1 and no hyperphosphorylated Wee1 compared with cells treated with vehicle alone (Fig. 1*D*), possibly as a result of inhibition of CDK1 kinase activity as has been described for the CDK inhibitor butyrolactone (28). Plk1 function is not affected by JNJ-7706621 treatment (Table 1); thus, the mechanism of targeting Wee1 for degradation is only partially inhibited. Myt1 kinase is also involved in the negative regulation of CDK1 by catalyzing the Tyr^{15} and Thr^{14} inhibitory phosphorylations, and during mitosis, Myt1 is inactivated by hyperphosphorylation (29). In asynchronous cells, Myt1 was present in an unphosphorylated faster migrating form (Fig. 1*D*). Cells synchronized in G_2-M and treated with vehicle alone have Myt1 in its slower migrating hyperphosphorylated form, whereas cells synchronized in G_2-M and treated with JNJ-7706621 express Myt1 in its active state where CDK1 kinase activity is inhibited (Fig. 1*D*). Retinoblastoma was found to be essentially unphosphorylated in asynchronous cultures of HeLa cells and highly hyperphosphorylated in the nocodazole-arrested cells (Fig. 1*D*). The hyperphosphorylation of retinoblastoma was prevented in JNJ-7706621-treated cells, which may result not only from inhibition of CDK1/cyclin B, the principal retinoblastoma kinase in mitotic cells (7), but also due to inhibition of other CDK isoforms by this compound given that inhibition of retinoblastoma phosphorylation at multiple residues was also indicated by the reduction of a wide band to a uniform single band following drug treatment.

JNJ-7706621 can induce a cytostatic or cytotoxic effect in HeLa cells. HeLa cells treated with 0.5 μmol/L JNJ-7706621 for 72 hours continued to proliferate at a reduced rate (Fig. 2*A*, ▽). Cells treated with 1 μmol/L JNJ-7706621 maintained a cytostatic growth profile (no net growth; Fig. 2*A*, △). Cells treated with 2 or 3 μmol/L JNJ-7706621 also maintained a cytostatic growth profile to 24 hours and thereafter viable cell numbers decreased below the number originally plated indicating a cytotoxic effect (Fig. 2*A*, ○ and □).

Reversibility of growth effects of JNJ-7706621 is concentration dependent. To investigate the reversibility of growth effects following exposure to JNJ-7706621, HeLa cells were exposed to either a cytostatic (1 μmol/L) or cytotoxic (3 μmol/L) dose of JNJ-7706621 for 48 hours (Fig. 2*A*). Cells were then washed twice with PBS (Fig. 2*B*, *arrow*) and maintained in the presence of either 1 or 3 μmol/L JNJ-7706621 or vehicle alone (Fig. 2*B*). Washed cells maintained in the presence of 1 μmol/L drug showed no net growth up to 144 hours (Fig. 2*B*, △), whereas those maintained in

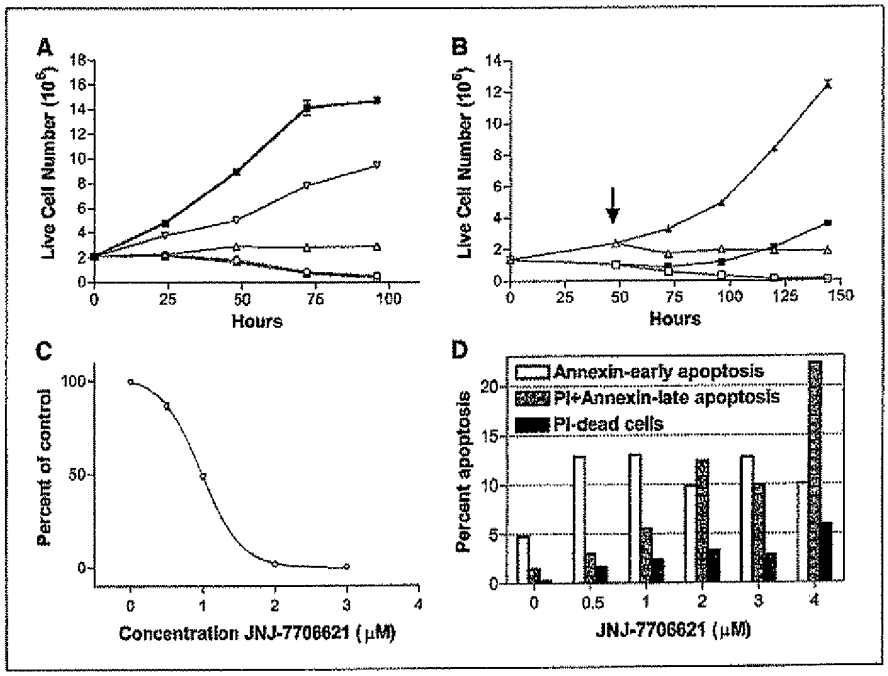

Figure 2. JNJ-7706621 inhibits cell growth and induces apoptosis. *A*, exponentially growing HeLa cells were treated with DMSO only (■) or with 0.5 μmol/L (▽), 1 μmol/L (△), 2 μmol/L (○), or 3 μmol/L (□) JNJ-7706621 in DMSO. Cells were harvested by trypsinization at the indicated times and live cell number determined with trypan blue staining. Total cell population (monolayer cells and cells in the medium) was counted. All groups were set up with $n = 3$; *bars*, SD. *B*, exponentially growing HeLa cells were treated with 1 μmol/L (△ and ▲) or 3 μmol/L (□ and ■) JNJ-7706621 for 48 hours. Cells (monolayer cells and cells in medium) were then washed twice in PBS (*arrow*), refed, and maintained in the presence of either 1 μmol/L (△) JNJ-7706621, 3 μmol/L (□) JNJ-7706621, or 0.03% DMSO (▲ and ■). Live cell numbers of the total population were determined as described above. All groups were set up with $n = 3$; n SD. *C*, colony formation in HeLa cells exposed to JNJ-7706621 for 48 hours and then incubated an additional 7 days in drug-free medium. All groups were set up with $n = 3$; *bars*, SD. *D*, U937 cells were exposed to JNJ-7706621 for 24 hours, stained with Annexin V-FITC and propidium iodide (*PI*), and analyzed flow cytometrically.

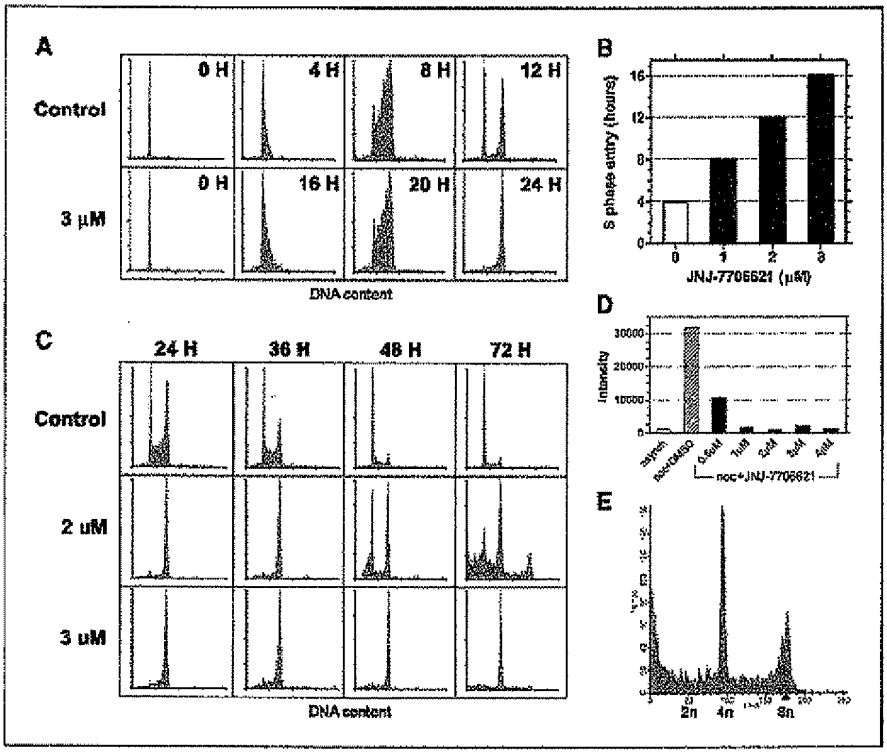

Figure 3. JNJ-7706621 delays exit from G_1, arrests cells in G_2-M, and induces endoreduplication. *A*, HeLa cells were synchronized in G_1 by mitotic shake and treated with JNJ-7706621. Cell cycle analysis showed that control cells (exposed to vehicle alone) began to enter the S phase 4 hours after G_1 synchronization. Cells treated with 3 μmol/L JNJ-7706621 did not enter the S phase until 16 hours after G_1 synchronization. S-phase transit time was identical in both control cells and drug treated cells. *B*, in G_1 synchronized cells, JNJ-7706621 delayed S-phase entry in a dose-dependent manner. *C*, cell cycle analysis showed that G_1 synchronized cells exposed to 2 or 3 μmol/L drug were predominantly in G_2-M phase after 24 hours of treatment. Cells exposed to 2 μmol/L JNJ-7706621 began to move out of G_2-M between 36 and 48 hours and an 8N population emerged by 72 hours. Cells exposed to 3 μmol/L JNJ-7706621 remained arrested in G_2-M out to 72 hours. *D*, level of histone H3 phosphorylation on Ser^{10} was analyzed by Western blotting in lysates of asynchronous HeLa cells and HeLa cells synchronized with nocodazole and treated with either vehicle or JNJ-7706621. Band intensity was quantified on a Lumi-Imager F1 (Roche Diagnostics, Indianapolis, IN) and normalized to the level of β-actin. *E*, HeLa cells were synchronized in G_2-M with nocodazole and exposed to nocodazole plus 0.5 μmol/L JNJ-7706621 for an additional 24 hours. Cell cycle analysis showed a large population of cells with DNA contents >4N. Cells exposed to nocodazole plus vehicle alone were maintained in G_2-M with no emergence of DNA polyploidy (data not shown).

the presence of 3 μmol/L drug continued to die, and by the 144-hour time point, almost all the cells were dead (Fig. 2*B*, □). When cells treated with 1 μmol/L drug for 48 hours were washed and placed in fresh medium containing vehicle alone, they resumed exponential growth (Fig. 2*B*, ▲). When cells treated with 3 μmol/L drug for 48 hours were washed and placed in fresh medium containing vehicle alone, they experienced a lag period of 48 hours before resuming exponential growth (Fig. 2*B*, ■). These results indicate the reversibility of the effects of JNJ-7706621 on cell growth is dependent on the concentration of the initial exposure and JNJ-7706621 can have a lasting effect on cells *in vitro*.

Inhibition of colony formation in HeLa cells. To determine the effects of JNJ-7706621 on long-term survival, the ability of HeLa cells to form colonies after drug exposure was evaluated. A 48-hour exposure to 1 μmol/L JNJ-7706621 inhibited colony formation by 50% and a 48-hour exposure to 3 μmol/L drug inhibited colony formation by 95.5% (Fig. 2*C*).

Induction of apoptosis in human cancer cells. To investigate if JNJ-7706621 treatment induces apoptosis, U937 cells were examined for alterations in the membrane phospholipid, phosphatidylserine. In cells treated with vehicle alone, only a small percentage of the population was in early or late apoptosis (Fig. 2*D*). When cells were treated with 0.5 or 1 μmol/L drug for 24 hours, an increase in the numbers of early and late apoptotic cells was observed along with an increase in dead cells (Fig. 2*D*). Cells exposed to higher concentrations of drug (2-4 μmol/L) for 24 hours showed greater increases in both late apoptotic and dead cells (Fig. 2*D*). These data show that the extent of apoptosis induced in cells exposed to JNJ-770662 depends on drug concentration and length of exposure.

JNJ-7706621 delays exit from G_1, arrests cells in G_2-M, and induces endoreduplication. To more precisely define the cell cycle effects of JNJ-7706621, HeLa cells were synchronized in G_1 by mitotic shake and treated with various concentrations of compound. Cells were harvested at specific times after drug treatment and cell cycle analysis done. Control cells (treated with DMSO only) entered the S phase 4 hours after G_1 synchronization (Fig. 3*A*). However, cells treated with 3 μmol/L JNJ-7706621 did not enter the S phase until 16 hours after G_1 synchronization (Fig. 3*A*). Figure 3*B* depicts time of S-phase entry of cells treated with various concentrations of drug and shows that JNJ-7706621 delayed entry of cells into the S phase in a dose-dependent manner. The time to complete the S phase was ~8 hours in both control cells and 3 μmol/L drug-treated cells (Fig. 3*A*). A total S-phase transition time of 8 hours was also seen in cells treated with 1 and 2 μmol/L drug (data not shown). Therefore, JNJ-7706621 has no effect on

S-phase progression in HeLa cells. As shown in Fig. 3C, JNJ-7706621 arrests cells in G_2-M. Cells synchronized in G_1 are arrested in G_2-M after 24 hours of drug treatment. At 3 μmol/L drug, cells were still arrested in G_2-M after 72 hours of drug exposure, whereas at 2 μmol/L drug, cells began to move out of G_2-M between 36 and 48 hours and a population of cells with a >4N DNA content emerged at 72 hours. The observed endoreduplication suggests that JNJ-7706621 also has an effect on Aurora kinase activity (18, 19).

Inhibition of Aurora kinases by JNJ-7706621. To provide evidence that JNJ-7706621 inhibited Aurora activity in cells, the effect on histone H3, a direct downstream target of the Aurora kinases, was evaluated. Histone H3 is involved in chromosome condensation and phosphorylation on Ser^{10} by Aurora-B kinase is thought to be crucial for proper chromosome alignment and cytokinesis (18, 30). Lysates of asynchronous HeLa cells and cells synchronized in G_2-M and treated for 8 hours with either JNJ-7706621 or vehicle were evaluated for levels of phospho-histone H3 (Ser^{10}) by immunoblotting. Nocodazole-synchronized cells exhibited a high level of histone H3 phosphorylation relative to untreated asynchronous cells. Cells synchronized with nocodazole and treated with 0.5 μmol/L JNJ-7706621 exhibited ~60% inhibition of histone H3 phosphorylation and cells exposed to higher amounts of drug had levels equivalent to asynchronous cells (Fig. 3D). These results show that JNJ-7706621 suppressed histone H3 phosphorylation on Ser^{10} *in vitro* indicating that Aurora-B kinase was inhibited. Aurora kinase inhibitors have been reported to compromise nocodazole-induced spindle checkpoint activation; cells arrested with nocodazole for prolonged periods have been shown to exit G_2-M when treated with the Aurora inhibitor, ZM447439 (18). To test whether JNJ-7706621 had a similar effect on arrested cells, HeLa cells were treated with nocodazole for 16 hours and then treated for an additional 24 hours with either nocodazole plus JNJ-7706621 or nocodazole plus vehicle. Cells were exposed to 0.5 μmol/L JNJ-7706621 as this concentration does not induce a cell cycle arrest (data not shown) but has a significant effect on histone H3 phosphorylation (Fig. 3D). In cells treated with nocodazole plus vehicle, cell cycle analysis showed that G_2-M arrest was maintained throughout the 40-hour treatment period (data not shown). In cells treated with nocodazole plus 0.5 μmol/L JNJ-7706621, significant numbers of cells were released from G_2-M arrest and endoreduplicated resulting in ~33% of the population with DNA contents >4N (Fig. 3E). These results show that JNJ-7706621 can compromise checkpoint arrest induced by nocodazole and suggest that the compound has an inhibitory effect on Aurora-B kinase.

Human tumor xenograft studies with intermittent dosing. The antitumor efficacy of JNJ-7706621 was examined in an A375 melanoma human tumor xenograft model. Two dose levels, 100 and 125 mg/kg, were evaluated and mean tumor size was calculated from six animals per group. Figure 4A shows tumor sizes for the 125 mg/kg dose under various schedules. Daily dosing was the most efficacious and caused tumor regression; however, this schedule could only be tolerated for 22 days before toxicity emerged (Table 2). There were five treatment-related deaths in this dose group; all occurred between days 22 and 39 and were not preceded by detectable weight loss. The 7 on/7 off schedule was nearly as effective as the daily dosing regimen with 93% tumor growth inhibition (TGI) and all animals survived to the end of the study (Fig. 4A; Table 2). The next most effective schedule at 125 mg/kg was 7 on/14 off (88% TGI) followed by Q3D and Q4D, with 69% and 43% TGI, respectively, and all these schedules were well tolerated (Fig. 4A; Table 2). Identical dosing schedules were applied to evaluate the 100 mg/kg dose and the same pattern of efficacy was observed (Table 2). Several schedules and dose combinations resulted in equivalent efficacy. For example, the 125 mg/kg 7 on/7 off schedule and the 100 mg/kg QD schedule produced identical TGI values of 93% (Fig. 4B; Table 2). Figure 4C compares two different dosing schedules at the same dose level. Tumor growth was nearly flat under the QD regimen (○), whereas under the 7 on/7 off schedule, a pattern of

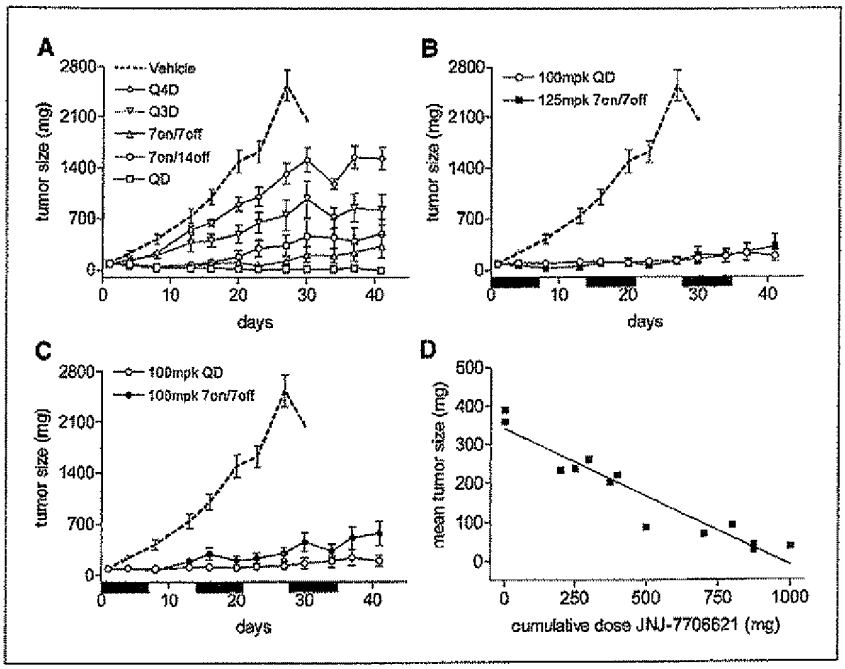

Figure 4. JNJ-7706621 is efficacious in a human tumor xenograft model under intermittent dosing regimens. *A*, JNJ-7706621 was given i.p. formulated in a nanocrystal suspension at 125 mg/kg under various schedules as indicated and tumor growth was measured over a 42-day period. Control animals were treated with vehicle alone (*dotted line*). *B*, several schedules and dose combinations resulted in equivalent efficacy. JNJ-7706621 given daily at 100 mg/kg (○) showed equivalent activity to compound dosed at 125 mg/kg on a 7 on/7 off schedule (■). Solid bars on the *x*-axis indicate periods of dosing for the 125 mg/kg 7 on/7 off regimen and gaps show dosing holidays. *C*, compound given at 100 mg/kg showed greater efficacy in groups receiving daily doses (○) than in groups on a 7 on/7 off schedule (●). A pattern of tumor inhibition during periods of dosing and tumor regrowth during nondosing was observed in the 7 on/7 off schedule. Solid bars on the *x*-axis indicate periods of dosing for the 100 mg/kg 7 on/7 off regimen and gaps show dosing holidays. *D*, when total cumulative dose was plotted against mean tumor size, there was a linear correlation between total amount of compound given and the size of the tumors regardless of the schedule of administration. Data from day 11 of the study is shown where $r^2 = 0.913$, but the trend continued throughout the study. For all treatment groups ($n = 6$) and for control group ($n = 10$).

tumor inhibition and regrowth was observed (●). A reduction in tumor size was apparent during periods of dosing (days 1-7, 14-21, and 29-35), and tumor regrowth was observed during periods of nondosing (days 8-14, 22-28, and 36-41). However, at a slightly higher dose level of 125 mg/kg but under the same schedule of 7 on/7 off, there was a persistent effect evident during dosing holidays with very little tumor regrowth (Fig. 4*B*). Analysis of the relationship between tumor size and dose indicates that the amount of inhibition of tumor growth was proportional to the total cumulative dose, regardless of the schedule. Figure 4*D* shows the average tumor size versus the total cumulative dose calculated on day 11 of the study. This relationship held true for analysis done at any time during the study (data not shown). These results identify suitable dosing regimens that could be applied in clinical trials.

Discussion

JNJ-7706621 is a promising antitumor agent that inhibits cell growth, activates apoptosis, and induces cytotoxicity in human cancer cells. This activity is a result of potent inhibition of several CDKs and Aurora kinases. When IC_{50} values for JNJ-7706621 are compared with published values for other CDK inhibitors, JNJ-7706621 is a more potent inhibitor of CDK1, CDK2, and CDK4 than BMS-387032 (31) and exhibits superior potency to Flavopiridol on CDK1 and CDK2 but shows less activity towards CDK4 and CDK6 than Flavopiridol (17). JNJ-7706621 showed moderate inhibition of several receptor tyrosine kinases involved in angiogenesis including VEGF-R2, FGF-R2, VEGF-R3, Tie2, and FGF-R1 that may contribute to its antitumor activity, especially in the A375 melanoma model as this cell type expresses VEGF-R2 and secretes the vascular endothelial growth factor (VEGF) ligand (32). The GSK3 kinases are phylogenetically most closely related to the CDKs and consequently, most CDK inhibitors have been found to be good inhibitors of GSK3β due to the similarity of the ATP binding domain in the GSK family. In fact, both UCN-01 and Flavopiridol inhibit GSK3β with nearly equal potency to CDK1 (33). In contrast, JNJ-7706621 is markedly more potent towards CDK1 than it is to GSK3β.

JNJ-7706621 shows potent antiproliferative activity in all cancer cell types evaluated, regardless of p53, retinoblastoma status, or P-glycoprotein expression level, and is several fold less potent at inhibiting normal cell growth. The *in vitro* potency of JNJ-7706621 against various human cancer cell types is comparable with Flavopiridol and BMS-387032 (17, 31). The differential antiproliferative activity on normal cells relative to human cancer cell lines could be partially due to the longer cycling time of the primary cell types. The population doubling time of human umbilical vascular endothelial cell cells has been reported to be 92 hours (34), HASMC cells 70 to 85 hours (35), HMVEC cells 72 hours (36), and MRC-5 cells 51 hours (37). The cancer cell lines cycle much faster, with doubling times of 18 to 19 hours in HeLa cells (38), 16 to 18 hours for HCT116 (39), and 16 hours for A375 (40). This ability to target rapidly cycling cells may translate to a wider therapeutic index in the clinic. *In vivo*, there may be even less of an effect on endothelial and other cell types that are not actively cycling. The antiproliferative activity of the compound was not affected by P-glycoprotein overexpression and resulted in nearly identical IC_{50} values in genetically matched drug-sensitive and drug-resistant cells. In contrast, BMS-387032 has been reported to act as a substrate of P-glycoprotein (41).

In cells, 1 μmol/L JNJ-7706621 reduced kinase activity of CDK1 immunocomplexes >50% and to baseline levels at ≥2 μmol/L. The difference observed between cellular potency and *in vitro* potency is not surprising for an ATP-competitive kinase inhibitor. In the *in vitro* kinase assay, JNJ-7706621 exhibited an IC_{50} of 5 nmol/L at 1 μmol/L ATP and 85 nmol/L at 100 μmol/L ATP (Fig. 1*B*) and would be expected to be less potent in cells where ATP concentrations can reach 1 mmol/L. When cells were treated with JNJ-7706621, the CDK1 protein displayed high levels of the inhibitory

Table 2. *In vivo* activity of JNJ-7706621 in A375 melanoma human tumor xenograft model under intermittent dosing regimens

Schedule and dose (i.p.)*	% Tumor growth inhibition†	*P*‡	Treatment-related deaths	Maximum % body weight loss (day)
125 mpk, QD X 41	99	0.001	5	−0.8 (d 23)
100 mpk, QD X 41	93	0.001	0	−3.2 (d 41)
125 mpk, 3on/4off to end	91	0.0004	3	−2.7 (d 4)
100 mpk, 3on/4off to end	78	0.008	0	—
125 mpk, Q3D to end	69	0.04	0	−3.4 (d 41)
100 mpk, Q3D to end	52	0.08	0	−10.3 (d 41)
125 mpk, Q4D to end	43	0.1	0	−11.3 (d 34)
100 mpk, Q4D to end	56	0.004	1	−10.9 (d 34)
125 mpk, 7 on/7 off to end	93	0.004	0	−1.8 (d 37)
100 mpk, 7 on/7 off to end	87	0.004	1	−2.7 (d 37)
125 mpk, 7 on/14 off to end	88	0.008	0	—
100 mpk, 7 on/14 off to end	80	0.01	0	−1.7 (d 37)

*All dosing was i.p. in groups of six mice with JNJ-7706621 formulated as a nanocrystal suspension in 1.5% pluronic acid F108. QD, once a day, 3 on/4 off, 3 d of dosing followed by 4 d of rest (no dosing); Q3D, every third day; Q4D, every fourth day, 7 on/7 off, 7 d of dosing followed by 7 d of rest, 14 on/14 off, 14 d of dosing followed by 14 d of rest. For all treatment groups ($n = 6$) and for control group ($n = 10$).

† The percentage of tumor growth inhibition was calculated as the difference between the change in control and drug-treated tumor volumes (T/C) on the last day that all animals were alive in both treatment and control groups.

‡ Statistical significance was evaluated by comparing the mean tumor size of vehicle-treated groups to drug-treated groups using a two-tailed Student's *t* test.

Tyr^{15} phosphorylation and low levels of the activating Thr^{161} phosphorylation. The cdc25C phosphatase which is responsible for removing the Thr^{14} and Tyr^{15} phosphates is activated in the M phase by phosphorylation of its NH_2-terminal regulatory domain by CDK1 (27); thus, its ability to dephosphorylate these residues may be compromised in drug-treated cells. Similarly, this compound may interfere with CDK7 directly or through a feedback loop to influence Thr^{161} phosphorylation. Wee1 protein stability is reportedly regulated by feedback from CDK1 and also by other kinases such as Plk1. The degradation of Wee1 is likely not as complete in cells treated with JNJ-7706621 due to CDK1 inhibition. CDK1 is able to catalyze phosphate addition on both serine and threonine residues of Myt1, and although this does not directly reduce its kinase activity (29), Myt1 hyperphosphorylation could be blocked as a result of CDK1 inhibition. The inhibition of retinoblastoma hyperphosphorylation in nocodazole-arrested and JNJ-7706621-treated cells likely occurs through inhibition of multiple CDKs. Although the Ser^{780} residue has been shown to be phosphorylated by CDK4 (42), the retinoblastoma protein detected by this phospho-specific antibody also seems to be phosphorylated at several additional residues, which is catalyzed by other CDKs (43).

The principal effects of this compound on cells stem from its ability to delay transit through the cell cycle and induce a G_2-M arrest. These effects are consistent with JNJ-7706621 acting primarily as a CDK inhibitor, although additional mechanisms are also functioning such as inhibition of Aurora kinases. Potent inhibition of CDK1/Cyclin B results in the expected mitotic arrest phenotype, but the delay of G_1-phase progression observed in G_1 synchronized cells reflects inhibition of other CDK family members that control G_1 and S phases (CDK2/Cyclin E or CDK4, CDK3 and CDK6/Cyclin D). The inhibition of GSK3β may be another factor in the G_1-S delay as this kinase has been reported to be involved in Cyclin D1 degradation (44). JNJ-7706621 shows significant inhibition of Aurora-A, which is required for activation of CDK1/CyclinB in mitosis and is essential for recruitment of CDK1/Cyclin B to centrosomes (45), as well as Aurora-B. It should be noted that the DNA polyploidy expected to occur as a result of Aurora-B inhibition may not be apparent at all drug concentrations due to CDK inhibition which takes place upstream from Aurora-mediated functions and precludes endoreduplication events. Endoreduplication was observed in cells treated with 2 μmol/L but not 3 μmol/L JNJ-7706621 and only after incubations of ≥72 hours presumably because cells were released from G_2-M arrest following exposure to 2 μmol/L compound but were held in G_2-M in the presence of 3 μmol/L compound thus masking any effects on chromosome segregation due to Aurora-B inhibition. However, when cells were first treated with nocodazole to arrest the population in G_2-M and then treated with concentrations of JNJ-7706621 that did not induce G_2-M arrest, a large proportion of the cells underwent endoreduplication. This shows that JNJ-7706621 can compromise nocodazole-induced spindle checkpoint activation. Furthermore, the phosphorylation of histone H3 on Ser^{10} was inhibited by drug treatment. This phosphorylation event and the phenotype of compromised spindle checkpoint function is mediated through Aurora-B (18, 30); thus, this effect could be attributed to Aurora-B inhibition by JNJ-7706621.

Tumor xenograft studies showed that efficacy improved as dose and frequency of administration increased. However, tolerability issues limited the doses and schedules that could be applied in rodents. By manipulating the dose and schedule, equivalent activity could be achieved while minimizing adverse effects of the compound. From these studies, the optimal schedule to follow can be selected and used as a starting point for clinical trials.

We have described a novel kinase inhibitor that shows activity against multiple CDK family members and Aurora kinases. In preclinical models, the effects on cell cycle progression, modulation of CDK and Aurora regulatory pathways, and induction of apoptosis indicate the profile of a promising antineoplastic agent. These findings support further clinical investigation to determine the therapeutic potential of this compound.

Acknowledgments

Received 3/16/2005; revised 7/20/2005; accepted 7/22/2005.

The costs of publication of this article were defrayed in part by the payment of page charges. This article must therefore be hereby marked *advertisement* in accordance with 18 U.S.C. Section 1734 solely to indicate this fact.

References

1. Draetta G. Cell cycle control in eukaryotes: molecular mechanisms of cdc2 activation. Trends Biochem Sci 1990;15:378–82.
2. Sherr CJ. G_1 phase progression: cycling on cue. Cell 1994;79:551–5.
3. Sherr CJ. Mammalian G_1 cyclins. Cell 1993;73:1059–65.
4. Lee M, Nurse P. Cell cycle control genes in fission yeast and mammalian cells. Trends Genet 1988;4:289–90.
5. Dunphy WG, Brizuela L, Beach D, Newport J. The *Xenopus* cdc2 protein is a component of MPF, a cytoplasmic regulator of mitosis. Cell 1988;54:423–31.
6. Nurse P. Universal control mechanism regulating onset of M-phase. Nature 1990;344:503–8.
7. Lin BTY, Wang JYJ. Cell cycle regulation of retinoblastoma protein phosphorylation. Ciba Found Symp 1992; 170:227–43.
8. Motokura T, Arnold A. Cyclins and oncogenesis. Biochim Biophys Acta 1993;1155:63–78.
9. Yasui W, Ayhan A, Kitadai Y, et al. Increased expression of p34cdc2 and its kinase activity in human gastric and colonic carcinomas. Int J Cancer 1993;53:36–41.
10. Hinds PW, Dowdy SF, Eaton EN, Arnold A, Weinberg RA. Function of a human cyclin gene as an oncogene. Proc Natl Acad Sci U S A 1994;91:709–13.
11. Hall M, Peters G. Genetic alterations of cyclins, cyclin-dependent kinases, and Cdk inhibitors in human cancer. Adv Cancer Res 1996;68:67–108.
12. Sherr CJ. Cancer cell cycles. Science 1996;274: 1672–7.
13. Adams RR, Carmena M, Earnshaw WC. Chromosomal passengers and the (aurora) ABCs of mitosis. Trends Cell Biol 2001;11:49–54.
14. Zhou H, Kuang J, Zhong L, et al. Tumour amplified kinase STK15/BTAK induces centrosome amplification, aneuploidy and transformation. Nat Genet 1998;20: 189–93.
15. Meijer L. Chemical inhibitors of cyclin dependent kinases. Prog Cell Cycle Res 1995;1:351–63.
16. Knockaert M, Greengard P, Meijer L. Pharmacological inhibitors of cyclin-dependent kinases. Trends Pharmacol Sci 2002;23:417–25.
17. Fischer PM, Gianella-Borradori A. CDK inhibitors in clinical development for the treatment of cancer. Exp Opin Invest Drugs 2003;12:955–70.
18. Ditchfield C, Johnson VL, Tighe A, et al. Aurora B couples chromosome alignment with anaphase by targeting BubR1, Mad2, and Cenp-E to kinetochores. J Cell Biol 2003;161:267–80.
19. Harrington EA, Bebbington D, Moore J, et al. VX-680, a potent and selective small-molecule inhibitor of the Aurora kinases, suppresses tumor growth *in vivo*. Nat Med 2004;10:262–7.
20. Lew J, Beaudette K, Litwin CME, Wang JH. Purification and characterization of a novel proline-directed protein kinase from bovine brain. J Biol Chem 1992; 267:13383–90.
21. Emanuel S, Gruninger R, Fuentes-Pesquera A, et al. A VEGF-R2 kinase inhibitor potentiates the activity of the conventional chemotherapeutic agents paclitaxel and doxorubicin in tumor xenograft models. Mol Pharmacol 2004;66:1–13.
22. Lundgren E, Roos G. Cell surface changes in HeLa cells as an indication of cell cycle events. Cancer Res 1976;36:4044–51.
23. De Brabander MJ, Van de Veire RML, Aerts FEM, Borgers M, Janssen PAJ. The effects of methyl [5-(2-thienyl-carbonyl)-1*H*-benzimidazol-2-yl] carbamate, (R 17934; NSC 238159), a new synthetic antitumoral drug interfering with microtubules, on mammalian cells cultured *in vitro*. Cancer Res 1976; 36:905–16.
24. Emanuel S, Chamberlin H, Cohen D. Antimitotic drugs cause increased tumorigenicity of multidrug resistant cells. Int J Oncol 1999;14:487–94.
25. Harker WG, Sikic BI. Multidrug (pleiotropic) resistance in doxorubicin-selected variants of the

human sarcoma cell line MES-SA. Cancer Res 1985; 45:4091–6.
26. Draetta G, Beach D. Activation of cdc2 protein kinase during mitosis in human cells: cell cycle-dependent phosphorylation and subunit rearrangement. Cell 1988; 54:17–26.
27. Hunter T. Protein kinases and phosphatases: the yin and yang of protein phosphorylation and signaling. Cell 1995;80:225–36.
28. Watanabe N, Arai H, Nishihara Y, et al. M-phase kinases induce phospho-dependent ubiquination of somatic Wee1 by $SCF^{\beta\text{-TrCP}}$. Proc Natl Acad Sci U S A 2004;101:4419–24.
29. Booher RN, Holman PS, Fattaey A. Human Myt1 is a cell cycle-regulated kinase that inhibits Cdc2 but not Cdk2 activity. J Biol Chem 1997;272:22300–6.
30. Adams RR, Maiato H, Earnshaw WC, Carmena M. Essential roles of *Drosophila* inner centromere protein (INCENP) and aurora B in histone H3 phosphorylation, metaphase chromosome alignment, kinetochore disjunction, and chromosome segregation. J Cell Biol 2001; 153:865–79.
31. Wong TW, Kimball D, Misra RN, et al. BMS-387032, a potent and selective inhibitor of cyclin-dependent kinase 2 (CDK2), induces cell cycle arrest and apoptosis in human tumor cells. Proc Am Assoc Cancer Res 2003; 44:620.
32. Liu B, Earl HM, Baban D, et al. Melanoma cell lines express VEGF receptor KDR and respond to exogenously added VEGF. Biochem Biophys Res Commun 1995; 217:721–7.
33. Leclerc S, Garnier M, Hoessel R, et al. Indirubins inhibit glycogen synthase kinase-3b and CDK5/P25, two protein kinases involved in abnormal tau phosphorylation in Alzheimer's disease. A property common to most cyclin dependent kinase inhibitors? J Biol Chem 2001; 261:251–60.
34. Jaffe EA, Nachman RL, Becker CG, Minick R. Culture of human endothelial cells derived from umbilical veins. Identification by morphologic and immunologic criteria. J Clin Invest 1973;52:2745–56.
35. Kirschenlohr HL, Metcalfe JC, Weissberg PL, Grainger DJ. Adult human aortic smooth muscle cells in culture produce active TGF-β. Am J Physiol 1993; 265:C571–6.
36. Romero LI, Zhang D-N, Cooke JP, et al. Differential expression of nitric oxide by dermal microvascular endothelial cells from patients with scleroderma. Vasc Med 2000;5:147–58.
37. Upchurch S, Gabridge MG. Differential cytopathogenicity accompanying *Mycoplasma pneumoniae* infection of human lung fibroblasts maintained in newborn bovine serum or fetal bovine serum. In Vitro 1983; 19:203–9.
38. Tamm I. HeLa cell RNA and protein syntheses. Effects of long-term treatment with 5,6-dichloro-1-β-D-ribofuranosylbenzimidazole (DRB). Biochem Pharmacol 1984;33:551–7.
39. Zhou Y, Gwadry FG, Reinhold WC, et al. Transcriptional regulation of mitotic genes by camptothecin-induced DNA damage: microarray analysis of dose-and time-dependent effects. Cancer Res 2002;62: 1688–95.
40. Krasagakis K, Fimmel S, Genten D, et al. Lack of protein kinase C (PKC)-β and low PKC-α,-δ,-ε, and-ζ isozyme levels in proliferating human melanoma cells. Int J Oncol 2002;20:865–71.
41. Kamath AV, Chong S, Chang M, Marathe PH. P-glycoprotein plays a role in the oral absorption of BMS-387032, a potent cyclin-dependent kinase 2 inhibitor, in rats. Cancer Chemother Pharmacol 2004;55:110–6.
42. Kitigawa M, Higashi H, Jung II-K, et al. The consensus motif for phosphorylation by cyclin D1-Cdk4 is different from that for phosphorylation by cyclin A/E-Cdk2. EMBO J 1996;15:7060–9.
43. Lundberg AS, Weinberg RA. Functional inactivation of the retinoblastoma protein requires sequential modification by at least two distinct cyclin-cdk complexes. Mol Cell Biol 1998;18:753–61.
44. Diehl JA, Cheng M, Roussel MF, Sherr CJ. Glycogen synthase kinase-3β regulates cyclin D1 proteolysis and subcellular localization. Genes Dev 1998;12:3499–511.
45. Hirota T, Kunitoku N, Sasayama T, et al. Aurora-A and an interacting activator, the LIM protein ajuba, are required for mitotic commitment in human cells. Cell 2003;114:585–98.